

POLITECNICO DI TORINO

Master's Degree in Aerospace Engineering



Master's Degree Thesis

SPACE DRONES

Design and Control of UAVs for
planetary exploration

Supervisors

Prof. FABRIZIO DABBENE

Dr. ELISA CAPELLO

Dr. MARTINA MAMMARELLA

Candidate

FRANCESCA FORINO

JULY 2020

Summary

The study of the application of drones for planetary exploration dates back to the early 70s, since then the interest in this field has gradually intensified thanks to the numerous advantages highlighted during the studies. The main objective of this work is the development of a dynamic model for a drone operating in a planetary environment. Moreover, control laws for the nonlinear system are designed, including sources of disturbances acting on the aerobot.

Venus, Titan and Mars emerge among the planets and bodies present in our Solar System suitable for such applications. The various types of designs proposed for all three bodies were analysed, and finally the study focused on applications relating to the Martian environment, as a strong research interest, highlighting the advantages and disadvantages of each proposal. Among the various designs, the Y4-Tilt Rotor (Y4-TR) developed by the Surrey Space Center (SSC) has been identified as the object of this study, since this tilt-rotor drone can be used as rotorcraft and fixed-wing system.

Starting from SSC's work, the aerodynamics of the aerobot body and the performance of the rotors have been investigated through the XROTOR software and the Blade Element Theory for tilt-rotors and CROTOR for coaxial rotors; finally, the nonlinear six degree of freedom (6-DOF) dynamic model for the drone has been developed. Then, the study has been focused on the Martian environment and the analysis of disturbances that could affect the Y4-TR's behaviour, identifying the presence of wind and any oscillations respect to the average value as the main source of disturbance.

For a preliminary study phase, it was decided to linearize the dynamic model around the equilibrium conditions relating to the nominal operating phase, i.e. horizontal straight flight, neglecting the initial phase of take-off and the transition from hovering to horizontal phases. Taking into account the disturbances and assigning a hypothetical trajectory, an LQR (Linear Quadratic Regulator) control law has been designed for the LTI model. The results show that, in the presence of the implemented disturbances, the implemented controller manages satisfactorily the aerobot, which is capable of correctly following the assigned trajectory.

Summary

Il forte sviluppo tecnologico degli ultimi anni ha favorito la progettazione di missioni robotiche per l'esplorazione planetaria. L'obiettivo dei sistemi robotici è quello di estendere la presenza umana nello spazio, andando a supportare le future missioni con equipaggio. Inoltre, tali sistemi possono fornire informazioni utili per comprendere meglio i pianeti e i corpi che si desidera esplorare e per preparare il pianeta target all'arrivo dell'uomo, svolgendo missioni di esplorazione remota e in-situ per rilevare dati e identificare i siti di atterraggio ideali. Per svolgere questi compiti, sono necessari progressi nel rilevamento e nella percezione robotica, così come nella mobilità autonoma senza l'aiuto del supporto umano.

Negli ultimi due decenni gli studi si sono concentrati sull'applicazione di piattaforme aeree per esplorazione planetaria, dal momento che queste possono fornire una possono esplorare superfici più ampie indipendentemente dalla topografia. Tali sistemi funzioneranno in ambienti estremamente pericolosi e devono essere in grado di gestire la presenza di possibili disturbi in un ambiente imprevedibile e senza supporto da Terra. Diverse agenzie e centri di ricerca si sono concentrati sullo studio del controllo di tali piattaforme. In particolare, le prime fasi preliminari di design hanno coinvolto applicazioni di leggi di controllo LQR o PID su modelli semplificati, mentre recentemente sono state proposte leggi di controllo non lineari per sistemi non lineari.

Questo lavoro è volto allo sviluppo di un modello dinamico di un drone operante in ambiente planetario. Viene, inoltre, implementata una legge di controllo di tipo LQR per il sistema lineare tenendo in considerazione le possibili fonti di disturbo che agiscono sul drone.

Il Capitolo 1 si concentra sui progressi compiuti nell'esplorazione di Pianeti e altri corpi del Sistema Solare tramite droni. Vengono analizzati i design per i tre corpi del Sistema Solare di maggiore interesse (Venere, Titano, Marte), concentrandosi sulle proposte recenti, sulle loro possibili applicazioni e sfide. Lo studio del background delle applicazioni di piattaforme aeree per le esplorazioni spaziali

ha portato alla scelta di Marte come oggetto di studio del presente lavoro. Da un'analisi delle principali proposte di design per droni marziani l'Y4-TR sviluppato dall'SSC è stato scelto come prototipo da implementare.

Nel Capitolo 2 le caratteristiche di design, di missione e strategia di controllo dell'Y4-TR sono riportate e analizzate, così come, una volta introdotti gli opportuni sistemi di riferimento, le descrizioni dei suoi modelli di massa e inerzia.

Nel Capitolo 3 viene presentata la modellazione matematica dell'aerobot Y4-TR. Vengono analizzate le sue caratteristiche aerodinamiche ed introdotti i modelli di atmosfera e campo gravitazionale marziano. Sono poi stimate anche le prestazioni dei motori utilizzando i software XROTOR e CROTOR. I risultati ottenuti da tali analisi risultano coerenti con quelli forniti da Collins, e vengono quindi implementati nel Simulatore. Infine, viene presentato il modello dinamico completo non-lineare del drone. Tale modello completo può essere semplificato considerando le condizioni di volo orizzontale e di hover. In particolare, nel caso di volo rettilineo uniforme l'aerobot si comporta come un velivolo ad ala fissa propulso ad elica. Pertanto, per analizzare la fase di crociera che risulta essere quella di maggiore durata per l'Y4-TR, è possibile utilizzare le equazioni in forma semplificata.

Il Capitolo 4 presenta una panoramica generale sia del simulatore dinamico completo che di quello semplificato, sviluppati entrambi utilizzando Matlab/Simulink. Una volta determinate le variabili di trim per volo orizzontale ed hover, entrambi in modelli sono stati testati in ambedue le condizioni e risultano essere stabili nelle condizioni assegnate.

Per un primo studio si è deciso di linearizzare le equazioni del modello semplificato, introdotto nel Capitolo 3, considerando come condizione di equilibrio la fase operativa nominale di crociera, ovvero volo orizzontale rettilineo. Nel capitolo 5 il modello matematico del drone è espresso in forma LTI e vettori di stato e controllo vengono richiamati ed esplicitati. Si è, infine, condotta un'analisi dei disturbi marziani che potrebbero influenzare il volo nell'atmosfera di Marte. La presenza del vento e di eventuali oscillazioni rispetto al valore medio è stata identificata come fonte principale. È stato poi costruito un modello matematico dei disturbi sfruttando i dati ricavabili dal Mars Climate Database, che è poi stato introdotto nel simulatore.

Nel Capitolo 6 viene eseguito uno studio preliminare sulla progettazione di un controller LQR per il modello lineare semplificato di Y4-TR. Infine, la legge di controllo progettata viene testata per una traiettoria assegnata, che è stata stimata considerando il sito di atterraggio della missione MARS2020 ed i risultati mostrano

che il controllore implementato gestisce in modo soddisfacente l'aerobot, che è in grado di seguire correttamente la traiettoria assegnata. Tuttavia, in futuro la legge di controllo implementata dovrebbe essere testata anche sul modello non lineare e si dovrebbero andare a considerare fonti di disturbo più forti al fine di tener conto dell'elevata incertezza ambientale marziana. Inoltre, è necessaria un'analisi aerodinamica più dettagliata per l'intero inviluppo di volo e uno studio delle fasi di transizione per caratterizzare pienamente il comportamento Y4-TR in ambiente marziano.

Table of Contents

List of Tables	X
List of Figures	XI
Acronyms	XIV
1 Introduction	1
1.1 Research Motivation and Objective	1
1.2 Thesis Outline	3
1.3 Drone Applications Progressing in Space Exploration	4
1.4 Target Planets	5
1.4.1 Titan	5
1.4.2 Venus	9
1.4.3 Mars	11
1.5 Mars Drones Background	12
1.5.1 Mars Helicopters	13
1.5.2 Tilt-rotor Concepts	15
2 Y4-TR Martian Aerobot Design	17
2.1 Introduction	17
2.1.1 Mission Location and Objective	19
2.2 General Layout	19
2.2.1 Center of Mass location	21
2.2.2 Mass Model	22
2.3 Reference Frames	22
2.3.1 Inertial Frame	22
2.3.2 Body Frame	22
2.3.3 Tilt-Rotor Frame	23
2.3.4 Local Rotor Frame	24
2.3.5 Stability Frame	24
2.3.6 Inertia Model	25

2.4	Y4-TR Control Strategy	27
2.5	Tilt-Rotor Control Designs	29
3	Modelling	30
3.1	Introduction	30
3.2	Mars Environment Models	30
3.2.1	Atmosphere Model	32
3.2.2	Gravity Model	32
3.3	Aerobot Aerodynamics Models	33
3.3.1	Main Body Aerodynamics Coefficients Estimation	33
3.3.2	Aerodynamics Forces and Moments in the Body Frame	38
3.4	Rotors Performances Estimation	40
3.4.1	Tilt-Rotor Analysis	40
3.4.2	Coaxial Rotor Analysis	44
3.4.3	Results	44
3.5	Equations of Motion	45
3.5.1	Newton's Second Law	45
3.5.2	Euler's Rigid Body Equations	47
3.5.3	Kinematics Equations	53
3.5.4	Flight Path Equations	53
3.6	Simplified Equations	53
4	Development of the Y4-TR Martian Aerobot Dynamics Simulator	55
4.1	Introduction	55
4.2	General Simulator Structure	56
4.3	Trim Conditions Determination	59
4.3.1	Horizontal flight conditions	59
4.3.2	Hover Flight Conditions	62
4.4	Simulink Models	64
4.4.1	Y4_TR Model	64
4.4.2	CFME Model	65
4.5	Test and Results	65
4.5.1	Test in Horizontal Straight Flight	68
4.5.2	Test in Hover Flight	69
5	System Linearization and Disturbances Modelling	70
5.1	LTI System	70
5.1.1	Linearized Dynamics Equations	70
5.1.2	Perturbations of the Weight Components	71
5.1.3	Linearized Kinematics Equations	72

5.1.4	State Space Representation	72
5.2	Martian Disturbances Analysis	74
5.2.1	Atmospheric tides	74
5.2.2	Gravity field variation	76
5.2.3	Topography	76
5.2.4	Wind	77
5.2.5	Wind Disturbances Model	78
6	Controller Design	81
6.1	Hybrid UAVs Control Laws Classification	81
6.2	Linear Quadratic Regulator	83
6.3	Overall Control Architecture	84
6.3.1	References Settings	86
6.3.2	LQR Tuning	86
6.4	Test and Results	88
6.4.1	Gust Step	88
6.4.2	Trajectory	90
6.4.3	Trajectory and Wind Disturbances	93
7	Conclusion and Future Work	95
7.1	Conclusion	95
7.2	Future Work	96
A	Rotor Blades Features	98
A.1	Rotors Geometries	99
A.2	Rotor Blades discretization	102
A.3	XROTOR and CROTOR Input	105
A.3.1	Tilt-Rotor	105
A.3.2	Top Coaxial Rotor	106
A.3.3	Bottom Coaxial Rotor	107
B	Aerobot Features	108
B.1	Aerobot Longitudinal Derivatives	108
B.2	Aerobot Lateral Derivatives	109
B.3	Aerobot Body Geometry	111
C	State Space Matrices	112
C.1	Longitudinal Dynamics	112
C.2	Lateral Dynamics	113
	Bibliography	115

List of Tables

1.1	Titan LTA Concepts [24] - Figure 1.1	6
1.2	Mars Exploration Program, Science Goals	12
2.1	Rotors Masses and absolute values of radial position components relative to the aerobot's center of mass (CoM)	20
2.2	Inertia Tensor Values [$kg.m^2$]	27
2.3	Previous Tilt-Rotors Control Design	29
3.1	Martian Aerobot Coefficients Estimation	36
3.2	Martian Aerobot zero pitching moment coefficient estimation	38
3.3	Tilt-Rotor performances analysis in horizontal flight	44
3.4	Tilt-Rotor performances analysis in hover flight condition	45
3.5	Coaxial-Rotor Hover Flight performances analysis	45
4.1	Matlab Subroutines implemented in the Aerobot Simulator	56
4.2	Variables Initialization for Horizontal Straight Flight	68
4.3	Control Input Settings - Trim in Horizontal Conditions	68
4.4	Variables Initialization for Flight in Hover	69
4.5	Control Input Settings - Trim in Hover Conditions	69
6.1	Yaw Step Sequence	91

List of Figures

1.1	Overview of Aerial platform design to Explore Titan. Figure Credits to Malaska (2014)	7
1.2	Dragonfly: A Dual-Quadrotor Lander Concept for Exploration at Titan. Image Credit:Johns Hopkins APL.	8
1.3	Wind speeds and cloud layers of Venus (Copyright 2010 Professor Kenneth R. Lang, Tufts University)	9
1.4	Venus Solar powered aircraft design by Landis (2006) [2]. The mission defined by Landis was composed of a solar powered drone designed to fly in the middle atmosphere powered by a nuclear isotope with a lifetime of 50 days to perform on the surface of Venus [2]	10
1.5	Future Mars Human Mission Concept	11
1.6	Mars Helicopter Design Characteristic	14
1.7	Previous SSC Tilt-Rotors	15
1.8	Mars Tilt-rotor Rotor Radii Size Estimates ($Mass = 10kg$) and Y4-TR stored into the aeroshell	16
2.1	Overall Y4-TR Design and Assumed Location of Aerobot Subsystems	17
2.2	Mars Aerobot Mission Profile	18
2.3	Basic Aerobot Dimensions	19
2.4	Tilt and Coaxial Rotors Design	20
2.5	Martian Aerobot Rotor Geometries by Collins	21
2.6	Forces acting on the Aerobot in Hover	21
2.7	Y4-TR References Systems	22
2.8	Stability Frame	24
2.9	Controls for Hover	28
2.10	Controls for Hover	28
2.11	Controls for Hover	29
3.1	MCD Atmospheric Characteristics during a summer day at 1000 m of altitude	31

3.2	MCD Average Wind Characteristics in a martian summer day . . .	31
3.3	Martian Aerobot Polar in closed configuration [3].	34
3.4	Martian Aerobot Pressure Distribution $\alpha = 4^\circ$ estimated with 3DP [3].	34
3.5	Martian Aerobot Polar	36
3.6	Pitching Moment Behaviour	37
3.7	BET-Rotor blade subdivision	41
3.8	Blade parameters description	42
4.1	Martian Aerobot Simulator Flow Chart	58
4.2	Forces acting on the Aerobot in the Horizontal Flight conditions . .	59
4.3	Trim Conditions in Horizontal Flight - Flow Chart	62
4.4	Y4_TR Simulink Model	66
4.5	CFME Simulink Model	67
5.1	State Space Representation	73
5.2	Martian Seasons and Solar Longitude	75
5.3	Global Gravity Map of Mars [35]	76
5.4	Isidis Planitia	77
5.5	Daily Wind Speeds and Solar Insolation for Isidis Planitia During Summer, Winter, and Dust Storm Conditions	77
5.6	Wind Components in Spring and Summer	78
5.7	Wind Disturbance Model	79
5.8	Wind Disturbance Model (Longitudinal and Vertical Components) .	80
6.1	Overall Control Architecture	85
6.2	U response at gust step of $5m/s$	88
6.3	H response for a gust step of $5m/s$ of U	89
6.4	Left: Selected Mission Site - Jazero Crater, inside the Isidis Basin. Right: Assigned Trajectory	90
6.5	Trajectory definition	91
6.6	P, Q, R, Φ	92
6.7	Trajectory without disturbances	93
6.8	Results for $LS = 0^\circ$	94
6.9	Results for $LS = 90^\circ$	94

Acronyms

6DoF

Six Degree of Freedom

3DP

3D Panel Method

CoM

Center of Mass

EoM

Equations of Motion

JHU APL

Johns Hopkins University Applied Physics Laboratory

HTA

Heavier Than Air

LQR

Linear Quadratic Regulator

LS

Solar Longitude

LTA

Lighter than air

LLT

Lifting Line Theory

MA

Martian Aerobot

NAS

National Accademy of Science

PAV

Planetary Air Vehicle

PID

Proportional Integrative Derivative

SSC

Surrey Space Center

SDRE

State-Dependent Riccati Equation

VLM

Vortex Lattice Method

Y4-TR

Y4-Tilt Rotor

Chapter 1

Introduction

1.1 Research Motivation and Objective

In recent years, the strong technological development has led to increment of robotic missions design for planetary exploration. The goal of robotics and autonomous systems is to expand human planetary access, extend its presence into space supporting future crewed mission [1]. Moreover, they can provide useful information to better understand Solar bodies and to prepare planets for human arrival, performing remote and in-situ exploration missions in order to collect environments data and to identify the ideal landing site for future manned missions[1]. To accomplish these tasks, advancements in robotic sensing and perception, mobility and manipulation, onboard and ground base-autonomous capabilities are required [1].

In the past two decades space community focused on aerial platforms [2], because they can provide longer range and greater coverage of planetary surfaces regardless of the topography [1]. Such systems operate in extreme hazardous environments and would be able to deal with the presence of possible disturbances in a planetary environment without human control.

Several agencies and research centers have focused on the aerial platforms control studying since that drones need to be provided of robust control systems, in order to perform autonomously and safely their missions tasks. Preliminary studies involved Linear Quadratic Regulator (LQR) or Proportional-Integrative-Derivative (PID) control laws applications on simplified models, while recently nonlinear control laws for nonlinear system have been proposed [3] [4].

Mars, Titan and Venus are the Solar bodies indicated as the target planets, because they present suitable condition for UAVs applications. Mars represents

the most attractive candidate to test aerial robotic systems and its human colonization is a primary goal for space exploration advancements. Analyzing different martian drone designs [2] [5], the tilt rotors configuration has been indicated as a possible 'long term candidate' [5] [6], since they could be used as rotorcraft and fixed-wing system and they would the advantages of both configurations. The Y4-Tilt Rotor proposed by Nathan Collins [3] is chosen as the target drone to be implemented. The dynamic model of the Y4-TR is presented by introducing the rotational and translational dynamics of the aerobot [3]. The complete system of equations describing the drone motion in the Martian atmosphere is obtained by adding the Kinematics and Flight Path Equations to the dynamics equations[3]. The Y4-TR aerodynamics parameters and the rotors performances are estimated starting from the data provided by Collins [3] and a rotor performances estimation analysis is conducted through the XROTOR/CROTOR software [7] [8]. The tilt rotors performances are analyzed using the Blade Element Theory [9] too and the obtained results are consistent at data provided by Collins [3].

The Y4-TR Mission Profile reports the mission phases duration and the cruise operating phase is identified as the relevant one [3]. The VTOL (Vertical Take off and Landing) phases of and the transition phase from hover to horizontal flight have been neglected for a preliminary study. Only the horizontal straight flight is analyzed; in these considered conditions the Equations of Motion (EoM) can be simplified and a classical set of flight mechanics equations has been obtained [10]. Since the EoM simplify also in hovering, this flight condition is considered too within the drone dynamics analysis.

This work is intended to develop a dynamic model of a drone operating in a planetary environment. Moreover, control laws for the nonlinear system are designed, including sources of disturbances acting on the aerobot. For this preliminary study it was decided to exploit a simplified model obtained linearizing the complete one around the equilibrium condition in the nominal operating phase, i.e. horizontal straight flight; for this model, assigned a possible trajectory to follow and in the presence of disturbances, an LQR control is developed. The trajectory has been estimated considering the Jazero Crater, the selected MARS 2020 Mission landing site [11] inside the Isidis Basin that is ideal mission location for the Y4-TR Martian Aerobot [3]. The possible disturbances that can affect drone flight are identified analyzing Mars environment and determining the atmospheric parameters with the Mars Climate Database [12]. This analysis has conducted to identify the presence of the wind and the oscillations from its average value as the main disturbances sources. The result shows that the implemented controller manages satisfactorily the aerobot, which is capable of properly following the assigned trajectory.

1.2 Thesis Outline

Chapter 1 focuses on the studies concerning the progresses on Planets and Other Solar System Bodies exploration via drones [2]. A designs review is conducted for the three Solar System Bodies of major interests (Venus,Titan,Mars), focusing on recent proposals, their possible application and challenges. The study of drone applications background for the space explorations led to choice Mars as the present work target planet [13] [6] [1]

Chapter 2 presents the Y4-TR developed by the SSC. Its mission and design characteristics are reported and analyzed, as also its mass and inertia models descriptions basing on Collins' work [3]. Moreover, the reference system used to model Y4-TR dynamics are introduced.

Chapter 3 concerns the Y4_TR aerobot mathematical modeling with referring to the introduced References System, as well as the aerodynamic characteristics of the drone once the Mars atmosphere models are introduced [3] [14]. Moreover, the rotor performances are estimated using XROTOR and CROTOR software [7] [8]. The obtained results coincide with ones provided by Collins [3] and then implemented in the Simulator.

Chapter 4 presents a general overview of the complete dynamic simulator for the Y4-TR aerobot, developed using Matlab/Simulink. Moreover, the simplified model is implemented too and the trim variables are determinated for the two flight condition cases.

In Chapter 5 the system is expressed in the LTI form and the state and control vectors are determined analyzing Y4_TR control strategies [3]. Then, an analysis on the martian disturbances that could affect atmospheric martian flight is conducted, and the presence of wind and any oscillations respect to the average value is identified as the main source. The disturbances mathematically model is built by recovering winds data from the Mars Climate Database [12] and introduced in the simulator.

In Chapter 6 a preliminary study on a LQR controller design for the simplified linear model of the Y4_TR is performed including disturbances and assigning a trajectory identified considering the Jazero Crater, the selected MARS 2020 Mission landing site [11]. Finally, results of LQR simulations, conclusions and remarks are reported, highlighting the possible future steps.

1.3 Drone Applications Progressing in Space Exploration

In recent years innovative designs have also been added alongside the classic exploration approaches in order to increase the surface mobility and the autonomy level [2] [1]. Up to now, space exploration has been carried out through the use of telescopes and the launch of satellites, rovers and astronauts. However, recently many agencies are interested in robotic missions developing [1] [15] and, thanks to recent technological developments, drones represent a valid alternative to conventional exploration methods[1].

In particular, they focused on the design of drones capable of performing explorations in a planetary environment [13] [1] [5][6]. NASA has scheduled to launch in July 2020 the Mars 2020 Mission Perseverance Rover to demonstrate the viability and potential of heavier-than-air vehicles on the Red Planet [16].

The advantages deriving from the application of these systems concern a greater exploration range if compared to the classic surface exploration platforms, and a greater operational handling that could extends astronauts' capabilities. In addition, drones are designed to fly near the surface and therefore capable of providing data at a higher resolution than current orbiting systems [2].

Furthermore, these systems will operate in highly harsh environments, thus they must have a fair level of autonomy. Safer and faster aerobot navigation and precision landing are required to reduce dependence on human operators subjected to large communication delays [1].

They are classified as flying robots, also known as **UAVs** or **Aerobots** [2], and they are categorized basing on size, endurance or range [17]. Generally, they can be subdivided in :

- **Lighter than air vehicle (LTA)**: This concept is an airship with limits on payload capabilities set by the atmosphere conditions at the cruise altitude and by the gas lift capacity.
- **Heavier than air vehicle (HTA)**: This category is composed by drones which can work on two level of autonomy, that means with the assistance of a remote human operator or completely autonomously thanks to on-board computer. This second skill is the most interesting for a planetary exploration application.

The first mission concepts for planetary exploration involved LTA vehicles with balloon style design [18]. They can provide significant advantages for planetary exploration due to their potential for extended mission duration, long traverse, and extensive surface coverage capabilities [19].

However, the recent studies have been focused on the heavier than air vehicles application [6] [5] [2]. These exploration systems present many advantages; in particular, they can fly very close to the body surface, they also provide high resolution images and detailed information, and a great exploration range [2].

Until now many different designs have been proposed for a wide variety of tasks such as determining the potential landing sites for future human missions, to analyze the planet surface and to assist the future crewed expeditions as described in [2] [3] [20] [1].

1.4 Target Planets

The exploration of Solar System Planets and its related Satellites can provide information useful for the scientific progress [15], but not all bodies are easily accessible or explorable due to the highly hostile conditions found there.

Moreover, the drones application in planetary exploration require the presence of an atmosphere [2]. The parameters to be considered not only concern the composition of atmosphere, but also its dynamics.

Mars, Venus and Titan have been defined the most suitable candidates for the aerobot application basing on a comparative analysis of the planets characteristics ('Planets and Bodies Fact Sheet' [21]). Other planets such as Mercury and Pluto don't have a sufficient atmosphere, while others (Jupiter, Neptune, Saturn, Uranus) have violent storms and winds that would represent a huge problem for aerial platforms [2][6].

1.4.1 Titan

Titan, the largest moon in orbit around Saturn, represents a perfect laboratory for a planet-scale prebiotic chemistry analysis. It held great interest among researcher community since its exploration could lead to understanding more about life building blocks [22][23].

Moreover, it presents an attractive environment to test aerial platform due to its dense atmosphere and low gravity [24]. Figures 1.1 and 1.2 illustrates the categories that Pauken used in [24] to classify Titan aerobot proposals. Basically, they can be distinguished in HTA and LTA Vehicle Concepts.

The first Titan aerobots concepts date back to 1970 and they were LTA vehicle like mongolfiere style balloon. These system are ideal for a preliminary reconnaissance mission, they were designed for remote sensing and surface sampling [24]. The major advantages are the possibility of cruise altitude regulation (Altitude Control) and a long endurance thanks to the slower rate of gas diffusion on Titan [2][24].

Titan LTA Concepts		
Project	Design and Characteristics	Altitude Control
a) TSSM Montgolfiere Baloon - NASA/ESA 2018	A baloon style design for a TSSM that would fly 8 – 10km above the surface and carry a 144kg gondola including 25kg for the science payload	Provided by heating of ambient gas with a radioisotope power.
b)Titan Aerial Explorer	It's a Helium balloon style design designed to fly at 8 km altitude with a total floating mass of 170 kg including 19kg of scientific instruments and a 4.6 m diameter	By implementing a mechanical compression altitude control
c) Buoyant Winged Gliders	Filled wing concept that uses no power to fly. It could move through the air by making sequential ascents and descents.	Actuated by shifting compressed atmospheric gas between forward and afterword balloon sections.

Table 1.1: Titan LTA Concepts [24] - Figure 1.1

Rotary-wing and Fixed-Wing Body designs are the main mission concepts mostly proposed for exploration of Titan among HTA Vehicles. Fixed-Wing Body design presents a high level of controllability, payload capacity, and range. Moreover, the power requirement could be a disadvantage.

Among the most relevant Titan fixed wing designs there is the AVIATR (Aerial Vehicle for In situ and Airborne Titan Reconnaissance by Lemke (2011) [3], designed for reconnances missions but not able to perform sampling since AVIATR cannot descend to the surface for sampling [24].

The recent technology developments, most notably the development of sensor and control capabilities, allowed the multi-rotor concepts application for Titan's enviroment. Rotary-wing vehicles have the potential to enable Titan exploration at scales ranging from hundreds of kilometers to millimeters and they would benefit of the low gravity and high density requiring less power [22].

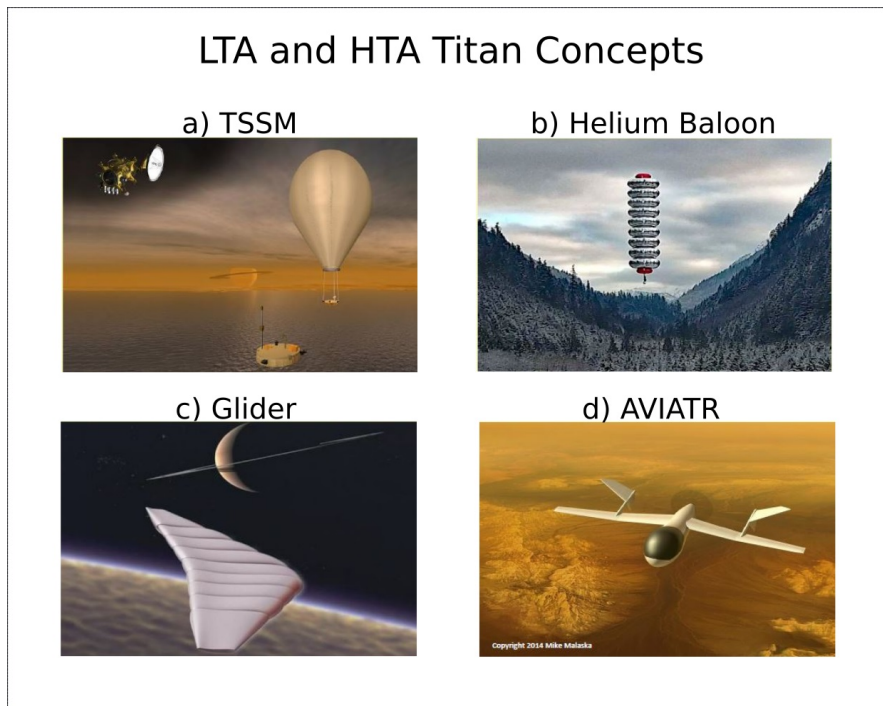


Figure 1.1: Overview of Aerial platform design to Explore Titan. Figure Credits to Malaska (2014)

Rotary-wing Design

Based on the great success in the rotorcrafts application in Martian exploration [24], an intensive study on rotary-wing propelled flight feasibility on Titan has been carried out [22]. In particular, aerial platforms with VTOL capability has been investigated since they could fill up the gap of sampling missions [25].

Dragonfly is the latest design proposed by JHU APL [22], inside the NASA New Frontiers Program. It's a dual-quadcopter concept which purpose is to explore moon's atmosphere and surface flying around organic dunes and impact crater floors to investigate the progression of prebiotic chemistry [26]. Moreover, Dragonfly would contribute to define a more accurate atmospheric profile to provide high resolution images of surface geology [22].

The mission concept proposed by Lorenz [22] is showed in Figure 1.2. The drone is delivered from space in an aeroshell and it descent with a parachute. The landing is controlled by rotors power regulation, that is provided by a radioisotope power supply. In addition, the vehicle implements a large battery that extents it life-limit. It is design to work as a conventional landing nearly indefinitely and it can also make periodic battery-powered rotor flight to reach new locations.

Dragonfly will accomplish reconnaissance and sampling mission, it would be

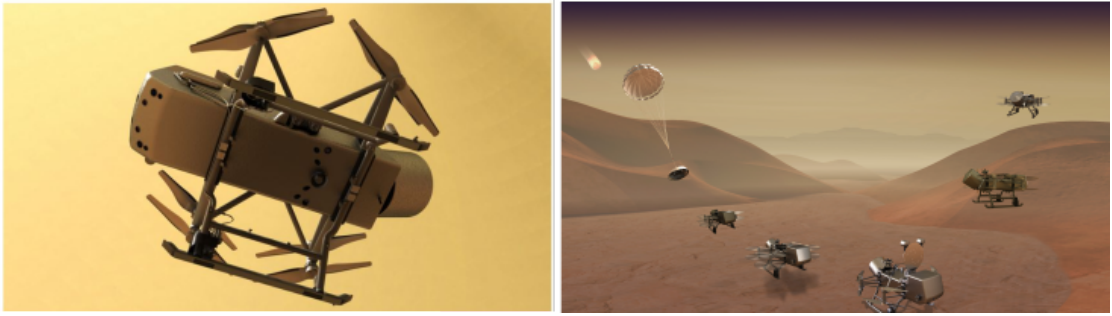


Figure 1.2: Dragonfly: A Dual-Quadrotor Lander Concept for Exploration at Titan. Image Credit: Johns Hopkins APL.

able to identify ideal landing sites and the areas to explore. Thus, great sensing and control capabilities for autonomous landing a site selection are required [22]. In order to improve these features, more detailed atmospheric models and analysis has to be conducted [27].

The Huygens Probe, the first human-made object to orbit Saturn, give scientists a detailed view of the moon's surface and complex atmosphere. Recently engineering-level atmospheric models have been developed for Titan and Neptune (Neptune-GRAM and Titan-GRAM) [27] applicable for engineering design analyses, mission planning, and operational decision making. However, some simplifications have been assumed to built Titan-GRAM and provided data are limited, thus many models need to be accounted to update the software and to obtain accurate Titan environment model.

1.4.2 Venus

Scientists are interested in understanding Venus evolutionary mechanisms, although it represents a planet unsuitable for human presence. Understanding Venus history could represent a key step in the discovery of exoplanets, sine one time it maybe was suitable for hosting life[2] [13].

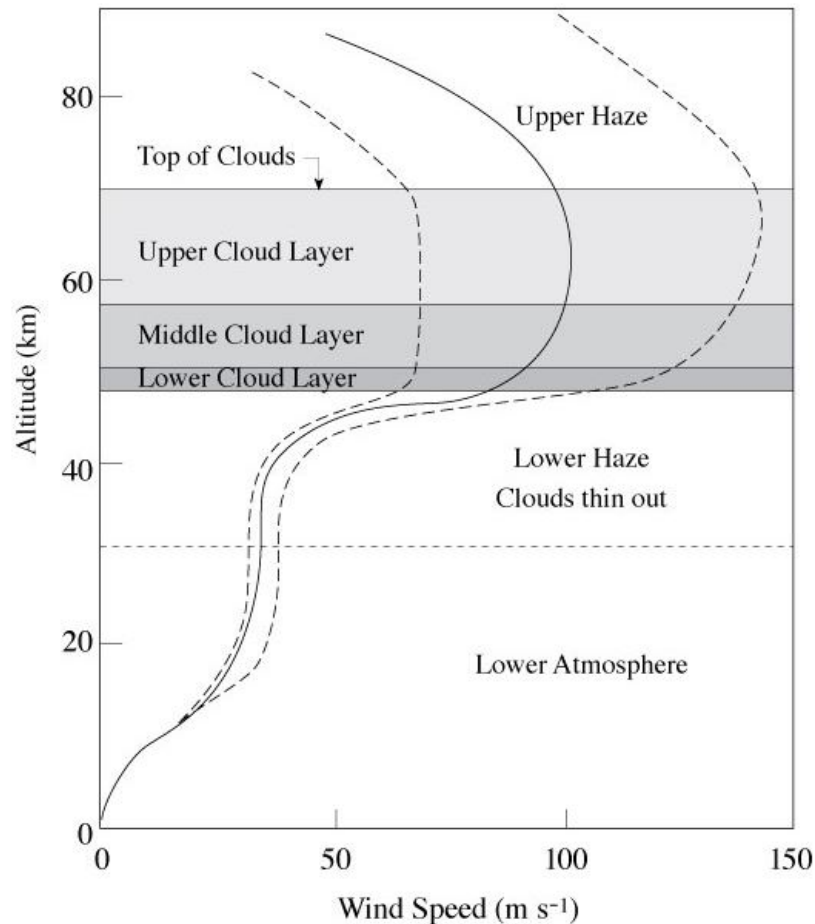


Figure 1.3: Wind speeds and cloud layers of Venus (Copyright 2010 Professor Kenneth R. Lang, Tufts University)

Up to now the planet exploration has been conducted only by spacecraft observations, but aerial platform concepts dates back to 2010 [2]. The first proposals for the study of the Venesian atmosphere were air balloons; later, in 2001, Landis prototyped a flying drone powered by solar energy, designed to be able to fly at an altitude between 40 and 50 *km*, where the pressure oscillates between 2 – 0.2 *bar* and the winds reach around 95*m/s* [2].

Most of Venus concepts are fixed-wing body and solar powered vehicle with an altitude range of $50 - 70 \text{ km}$, which is the most dynamic and interesting region in order to fly on planet [2]. This layer is an extremely hazardous and acidic environment for UAVs structural and electrical systems, since the ultraviolet radiation accelerates degradation through photochemistry at higher altitudes [2].

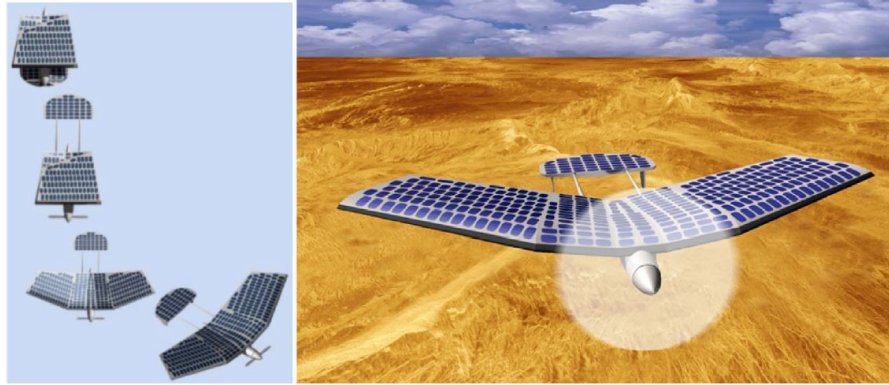


Figure 1.4: Venus Solar powered aircraft design by Landis (2006) [2]. The mission defined by Landis was composed of a solar powered drone designed to fly in the middle atmosphere powered by a nuclear isotope with a lifetime of 50 days to perform on the surface of Venus [2]

Drones which would fly in the Venus atmosphere should be able to overcome strong winds and caustic atmosphere, since the planet atmosphere is saturated with carbon dioxide and extremely acid, there is no a magnetosphere layer to protect the planet from solar winds. These features cause a greenhouse effects with extreme temperatures and pressure at the surface, therefore temperature control management is another relevant challenge to be faced, since on planet surface the mean temperature is about $698K$ [2].

1.4.3 Mars

Recently research studies have focused on martian drone development [5],[6], since its colonization represents a key step into the human exploration progress [28]. Much evidence shows that Mars was once supposed to be a hospitable, warm and watery place, and it is also the planet of the Solar System more similar to Earth. In addition, it has supposed to being an excellent test for future human explorations providing us with many answers on what could be the evolution of our planet [28].

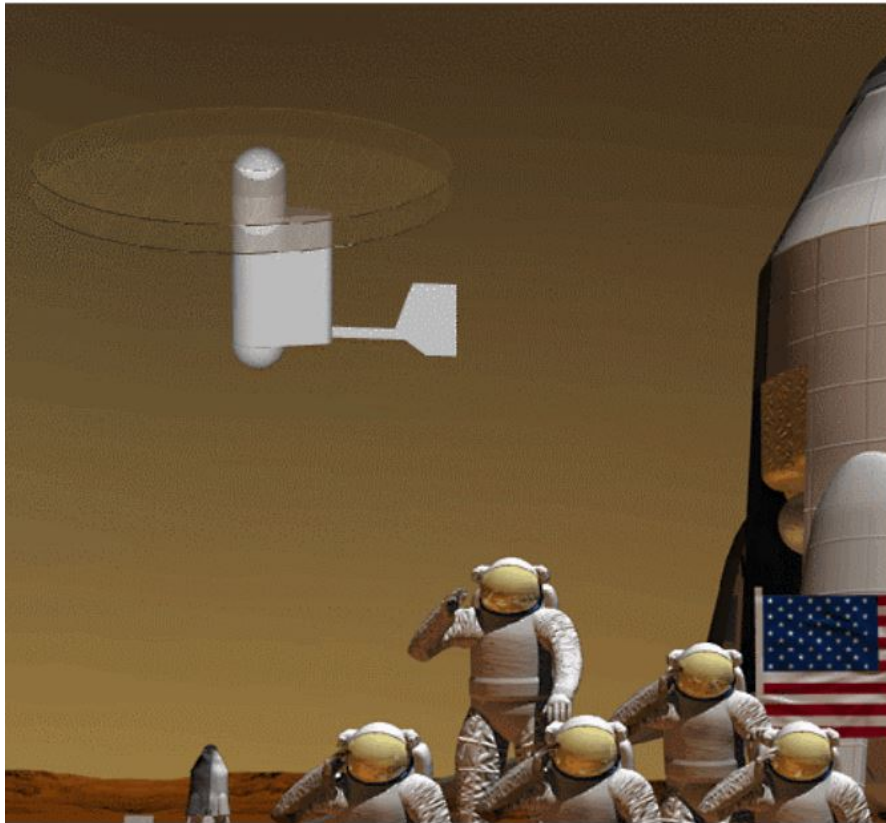


Figure 1.5: Future Mars Human Mission Concept

Table 1.2 reports the main 4 Science Goals for the Mars Exploration Program [28]. Goal 4 focuses concerns the robotic flight aerial assistants development and how they can help us to prepare for potential crewed missions identifying the optimal landing sites, assisting astronauts searching for resources and transporting equipment and exploring the territory [1]. Moreover, these precursors can reduce cost and risk of exploring the Red Planet by acquiring relevant information useful during missions design, implementation and future operations.

Mars Exploration Program, Science Goals	
N°	Goal
1	Determine if Life ever arose on Mars
2	Characterize the Climate of Mars
3	Characterize the Geology of Mars
4	Prepare for Human Exploration of Mars

Table 1.2: Mars Exploration Program, Science Goals

The necessity to perform multiple take off and landing led to consider helicopter like vehicles as the best candidates for the Mars exploration [5][6]. Considering the numerous advantages coming from Mars exploration, NASA has decided to include the small helicopter, Ingenuity, as part of future mission to Mars which will be able to operate independently in the Martian environment. It is a demonstration vehicle intended to verify the rotor-propelled flight on Mars and to test the navigation and control algorithm implemented.

The numerous existing data about Mars atmosphere model and drone concepts [3] [6], the high research interests in developing martian aerial platforms [1] and the technological improvements benefits also for other Bodies exploration as Titan [24] led to select Mars as target planet in the present work. The study is focused on rotor-crafts, since they have been indicated as a possible long term candidate [6] and many studies have been conducted on possible control and navigation strategies[3].

1.5 Mars Drones Background

The first Martian drone design proposals, as for Venus and Titan, were LTA concepts with a Montgolfiere balloon design or HTA vehicles, such as fixed wing body. However, these last concepts would be a single flight vehicles due to the lack of runway and difficulty of taking off and landing on the Mars surface[3].

This study focuses on the recent dominant design categories that are the rotary-wing like the Mars Helicopter[29] and hybrid aircraft with VTOL capabilities[3] [30] [31]. These concepts could accomplish multiple mission tasks and have greater surface mobility than classical exploration systems like rovers or lander [6]. Moreover, they can hover and fly at low-speeds and to take-off and land at unprepared and hazardous remote sites. Further, autonomous vertical lift planetary aerial

vehicles (PAVs) would have specific advantages and capabilities [6]. In particular, they would:

- Soft landing capability for vehicle reuse and remote-site monitoring.
- Provide greater resolution of surface details or of atmospheric phenomena, than an orbiter.
- Provide greater access to hazardous terrain than rovers and landers.

However, flying in the Martian atmosphere presents many challenges, since the atmosphere is very thick and the density extremely low [21], corresponding on Earth at an altitude of about 33.5 *Km* [2]. Moreover, one of main parameter to consider is the range of Reynolds number. For a drone flying on Mars it is one order less than on Earth, thus the drone should fly with very high speeds (Mach 0.6) to compensate for low density and Reynolds number effect [2]. The low Reynolds number that drones will achieve will impact also on sizing, indeed large lifting surfaces are required, as well as vehicle control.

1.5.1 Mars Helicopters

Aerial exploration of Mars with helicopters could provide mission capabilities beyond that of classical exploration systems (landers, rovers, or orbiters). They could help rover missions by scouting out safe traverse routes or providing reconnaissance on possible target destinations and as they could be used to explore areas that may not be reachable by rovers [29][5][6].

Recently, investigations and demonstrations related to rotary-wing technologies applicable to martian atmospheric flight are promoted by NASA Ames Research Center jointly JPL [29]. The concept of rotary-wing vehicles as aerial robots able to interface with the planetary surface dominates the design for vertical lift planetary aerial vehicles. Furthermore, Mars rotorcraft will not be independent agents, indeed they could be part of a greater collective of other robotic systems[29][4][6]. Ingenuity, Figure 1.6, is the Mars Helicopter developed by NASA as part of the Perseverance Mission. It is a technological demonstrator intended to verify rotor-propelled flight feasibility at Mars and to test the control and navigation strategies. Moreover, it will provide better mapping and guidance that would give future mission designer more information to help with travel routes planning and hazard avoidance [29].

Technological critical issues for Mars rotorcraft concern rotor aeromechanics as well as vehicle autonomy, flight control and navigation capabilities in a unknown environment. The key parameter affecting the aerodynamic properties of the Mars



Figure 1.6: Mars Helicopter Design Characteristic

Helicopter is the low density, since thin atmosphere reduces the achievable thrust for a given rotor size. Moreover, it also affects the flight dynamics (blade flapping) of the vehicle in ways that must be investigated and well-understood in order to design a control system. A secondary effect of the martian thin atmosphere is to significantly reduce the aerodynamics damping affecting up the blade flapping itself[4].

Flight Control Characteristics

Designing a robust control system for a helicopter is a challenging task in general, due to various unusual characteristics of helicopters as compared to other vehicles since they are typically unstable in open loop and are subject to high levels of vibration. The control design problem becomes more challenging when, as in the case of Ingenuity, the vehicle must take off and land on unprepared terrain and navigate without a GPS. Moreover, little prior information exists on how these differences affect the flight dynamics in the Martian environment that cannot be exactly replicated for testing on Earth [4].

The helicopter control system must work the first time it operates in its intended environment, so detailed modeling, analysis, and simulation, combined with testing in partially replicated environments are required. Simple analytical models are helpful in understanding the fundamental differences between Earth and Mars helicopter flight [29] [4]. The main GNC requirement is to safely perform several autonomous end-to-end flights and when designing controller two driving requirements has to be considered:

- Maintain adequate stability margins over the entire flight envelope;
- Limit horizontal excursions due to gust to avoid collisions.

1.5.2 Tilt-rotor Concepts

The tilt-rotor vehicles are classified as hybrid aircraft [3] and merges fixed-wing aircraft and helicopter advantages, indeed they are capable to perform vertical take off and landing. As remarked by Young [6] the tilt-rotors configuration represents a long-term candidate for Mars exploration, since it presents a good compromise between hover performance and cruise range/endurance, extremely important attributes for Mars exploration [5].

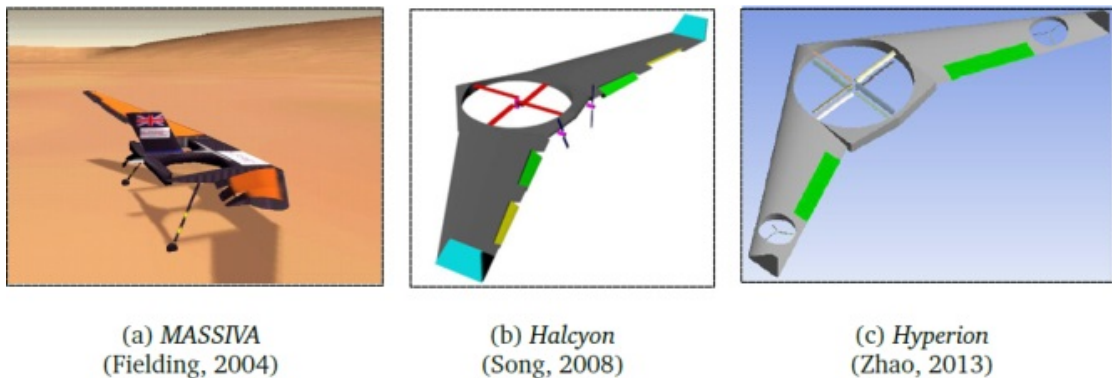


Figure 1.7: Previous SSC Tilt-Rotors

Surrey Space Center started to design tilt-rotors since 2004. The first concept was MASSIVA, followed by Halycon, inspired by its predecessor but with larger dimensions and powered by solar energy thanks to the installation of solar panels. Moreover, it provided for the use of two coaxial rotors with variable pitch and two propellers with fixed pitch. The third prototype, called Hyperion, aimed to reduce the mass of the drone and to use two wing-banded coaxial rotors. The latest concept dates back to 2016 and includes a Y4-TR configuration reported in Figure 2.1, which represents an evolution of its precursor with the addition of a cover for the banded-wing coaxial rotors [3].

However, one of the biggest issues for the Mars tilt-rotor configuration is their large dimension. Figure 1.6 by Young [6] shows how rotor sizing depends by rotor performances, in particular a rotor design point of $M_{tip} = 0.7$ and $C_L = 0.4$ is reported. The resulting rotors are quite large and will necessitate special consideration to be stored in the aeroshell entry vehicle and to be deployed.

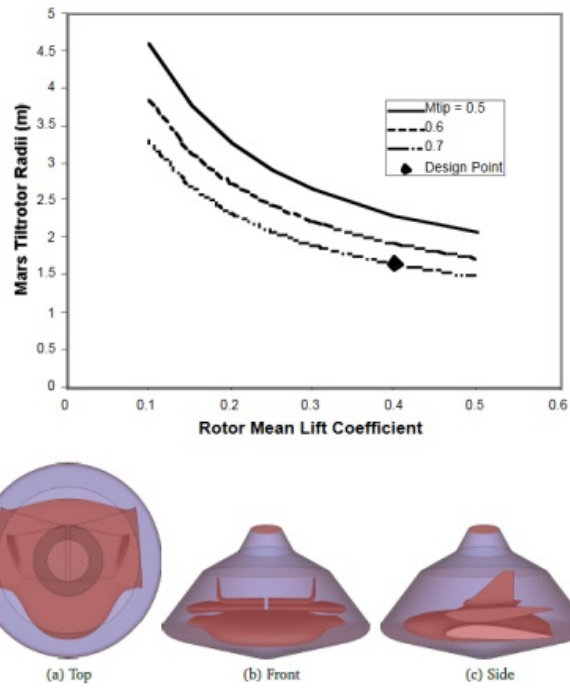


Figure 1.8: Mars Tilt-rotor Rotor Radii Size Estimates ($Mass = 10kg$) and Y4-TR stored into the aeroshell

Moreover, their deployment will be fairly complicated and will require astronaut-assisted assembly or an autonomous assembly process on the lander platform [5].

Chapter 2

Y4-TR Martian Aerobot Design

2.1 Introduction

The proposed Y4TR Martian aerobot has been conceived as a realistic aerial solution for exploring multiple locations on the Martian surface [3]. Its configuration combines two of the previous SSC Martian aerobot designs, with a total mass of $25Kg$ and, two large fixed coaxial counter rotating rotors embedded in the center of the flying wing body for vertical takeoff and two tilting-rotors for cruise and transition phases[3].

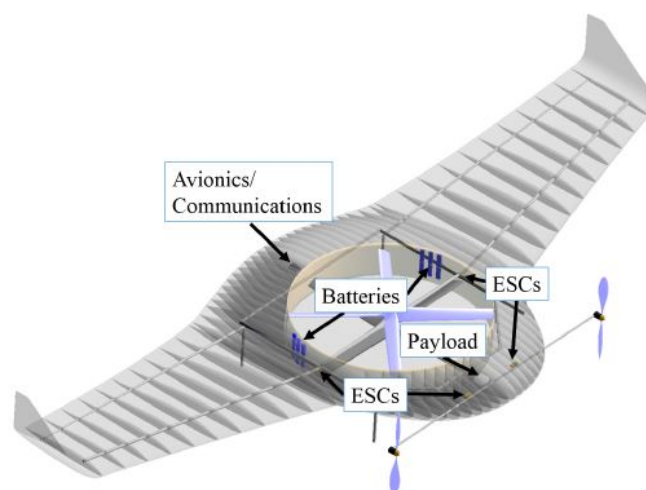


Figure 2.1: Overall Y4-TR Design and Assumed Location of Aerobot Subsystems

Mission Phase	Operations	Power (W)	Duration	Energy (kJ)
Morning	Contact Experiments	15	3.5 h	189
	Imaging	5		63
	Orbiter Communication	50		630
	On-Board Computer	10		126
	Phase Total	80		1008
Takeoff Transition	Tilt-Rotors	1550 (avg)	100 s	155
	Coaxial Rotors	6650 (avg)		665
	Flight Control	10		1
	Imaging	5		0.5
	Orbiter Communication	50		5
	On-Board Computer	10		1
	Phase Total	8275		827.5
Cruise Midsol 1130-1230	Tilt-Rotors	635 (avg)	1 h	2286
	Imaging	5		18
	Flight Control	10		36
	Orbiter Communication	50		180
	On-Board Computer	10		36
Phase Total	710	2556		
Landing Transition	Tilt-Rotors	300 (avg)	115 s	34.5
	Coaxial Rotors	6460 (avg)		742.9
	Flight Control	10		1.15
	Imaging	5		.575
	Orbiter Communication	50		5.75
	On-Board Computer	10		1.15
	Phase Total	6835		786.025
Afternoon	Contact Experiments	15	3.5 h	189
	Imaging	5		63
	Orbiter Communication	50		630
	On-Board Computer	10		126
	Phase Total	80		1008
Night	OBC Monitoring	10	16 h	576
	Thermal	10		576
	Phase Total	20		1152
Total				7337.525

Figure 2.2: Mars Aerobot Mission Profile

2.1.1 Mission Location and Objective

The primary Aerobot mission is to provide a platform for a 3kg science payload to conduct experiments and explore Mars surface and atmosphere [3]. As the final mission scientific objectives for the mission have not been determined, specific design of the payload was not accomplished. However, there are numerous payload options to choose from for the mission. Imaging equipment including narrow and wide angle cameras are necessary not only for scientific purposes, but also for flight navigation [3].

Analyzing Y4-TR Mission Profile reported in Figure 2.2, the cruise is the longest phase ($1h$) with an altitude $h = 1000m$ and involved the tilt-rotors to sustain flight. The coaxial rotors will operate during take-off and transition phases.

The Martian plain Isidis Planitia has been selected as the landing site and exploration region for the aerobot since it is an ideal operating region for the aerobot for both scientifically and engineering reasons [3].

Since it is situated so close to Mars' equator, centered about $12.9^\circ N$, the solar radiation will hit the aerobot's solar cells at a higher incident angle higher power generation. Moreover, the plain is large and fairly circular with a low latitude and low elevation, the latter aiding the aerobot while flying due to the higher atmospheric density. It is also relatively flat on the inner portions of the plain where the aerobot is planned to fly. This will aid with navigation and to find safe landing sites for the aerobot throughout its mission [3] [11].

2.2 General Layout

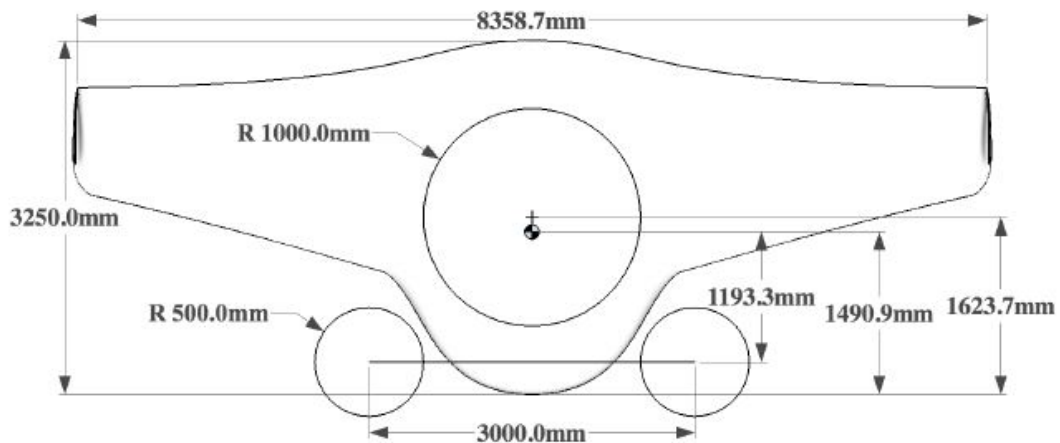


Figure 2.3: Basic Aerobot Dimensions

The Y4-Tilt Rotor Martian aerobot is composed by three main elements: a blended-wing body, two tilting rotors and two coaxial rotors. The main Aerobot geometrical features are reported in Figure 2.3, while the main body and rotors geometry (Figure 2.4 and 2.5) are reported in Appendix A and B.

Rotors	$mass$ (kg)	r_X (m)	r_Y (m)
Coaxial	4.65	0.1328	0
Tilting	1.72	1.1933	1.5

Table 2.1: Rotors Masses and absolute values of radial position components relative to the aerobot’s center of mass (CoM)

Since the Martian aerobot will mostly operate in horizontal flight (Cruise Phase - Figure 2.2), it is desirable for the aerobot to be most efficient while flying in this regime. Collins proposed that the Y4TR Martian aerobot have fixed pitch, variable speed coaxial rotors designed for hover and vertical flight, and fixed pitch, variable speed tilt-rotors designed for horizontal flight [3]. The tilt rotors have been designed using XROTOR and analyzed with the Blade Element Momentum Theory, they have to produce sufficient thrust for the aerobot’s horizontal flight and collaborate during transitions phases. The coaxial rotors, designed with CROTOR, have to overcome the aerobot’s weight during hover phases. Moreover, the coaxial rotors were designed to have a zero torque balance while hovering in the Martian atmospheric conditions.

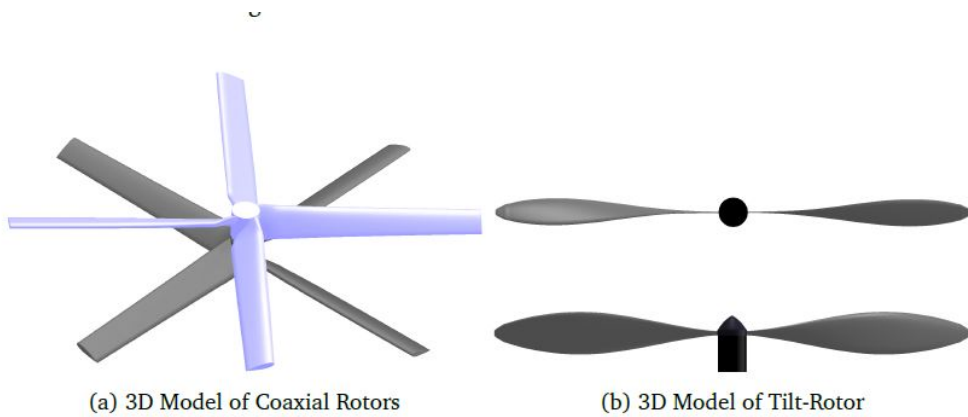


Figure 2.4: Tilt and Coaxial Rotors Design

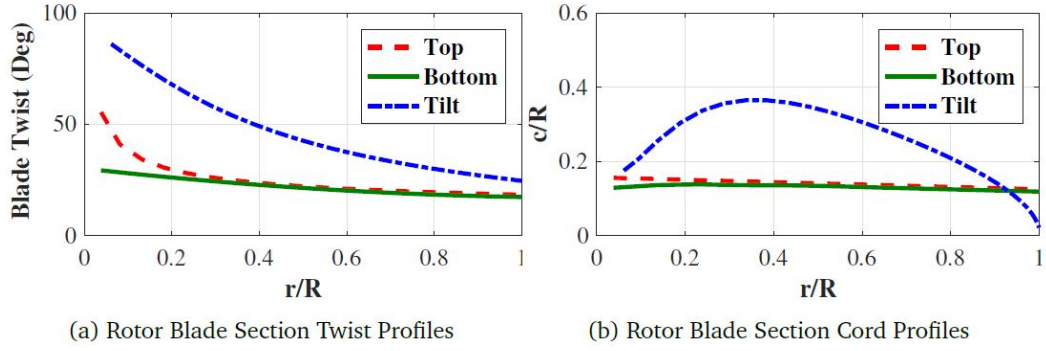


Figure 2.5: Martian Aerobot Rotor Geometries by Collins

2.2.1 Center of Mass location

The location of the aerobot's center of mass (CoM) is a critical design consideration as it will affect the stability and performance of the aerobot during all phases of flight. For a zero pitching moment in hover the moment generated by the tilt-rotors must balance the moment generated by the coaxial rotors.

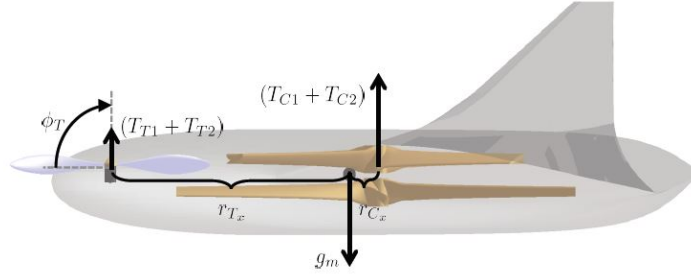


Figure 2.6: Forces acting on the Aerobot in Hover

$$(T_{T1} + T_{T2}) \sin \phi_T r_{Tx} = (T_{C1} + T_{C2}) r_{Cx} \quad (2.1)$$

- T_{T1} , T_{T2} are the thrust generated by the tilt-rotors.
- T_{C1} , T_{C2} are the thrust generated by the coaxial-rotors.
- r_{Tx} , r_{Cx} are the distances between tilt/coaxial rotors and Aerobot CM along longitudinal direction
- ϕ_T define the tilt-bar. orientation, equal to zero for horizontal flight and to 90° for hover condition.

2.2.2 Mass Model

The aerobot mass is assumed to be constant, neglecting the effects of dust accumulation that could affect its dynamics [3]. As reported in the Section 2.2.1 the CoM location has been estimated via *OpenVSP CAD* model [3] and it is located at 1.491 back from the nose, as shown in the Figure 2.3 in Section 2.2.

2.3 Reference Frames

2.3.1 Inertial Frame

The Mars Inertial frame, abbreviated MI, can be considered as an inertial frame reference since the operating altitude of the Martian Aerobot will be less than 1000m, so the curvature has no effects during flight. The MI is a North-east-down reference frame with

- The X and Y axes lying on the local Martian horizontal plane and they are used for describing the location of the Aerobot during its flight.
- The Z axis points downward.

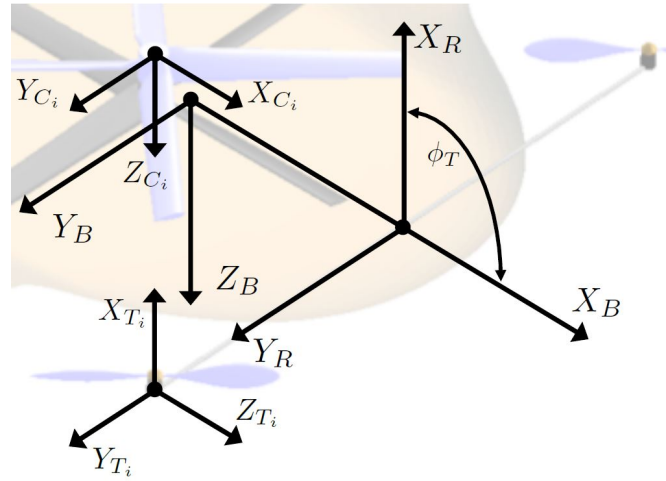


Figure 2.7: Y4-TR References Systems

2.3.2 Body Frame

The body frame is used to describe translation and rotational dynamics of the aerobot, it is fixed to the aerobot with its origin located at the center of mass. The axes are defined as follow:

- The X_B axis is aligned with the aerobot's nose;
- The Y_B axis is defined out the right wing of the aerobot orthogonal to X_B ;
- The Z_B axis points downward through the center of the aerobot orthogonal to $X_B - Z_B$ plane.

Rotation Matrices

The rotation matrices from the Inertial Reference System to the Body and vice versa are identified respectively as R_{I2B} and R_{B2I} , and defined by the following sequence of rotations:

$$R_{I2B} = R_1(\phi)R_2(\theta)R_3(\psi) \quad (2.2)$$

$$R_{B2I} = R_3^T(\psi)R_2^T(\theta)R_1^T(\phi) \quad (2.3)$$

Where:

$$R_1(\phi) = \begin{bmatrix} 1 & 0 & 0 \\ 0 & \cos(\phi) & \sin(\phi) \\ 0 & -\sin(\phi) & \cos(\phi) \end{bmatrix} \quad (2.4)$$

$$R_2(\theta) = \begin{bmatrix} \cos(\theta) & 0 & -\sin(\theta) \\ 0 & 1 & 0 \\ \sin(\theta) & 0 & \cos(\theta) \end{bmatrix} \quad (2.5)$$

$$R_3(\psi) = \begin{bmatrix} \cos(\psi) & \sin(\psi) & 0 \\ -\sin(\psi) & \cos(\psi) & 0 \\ 0 & 0 & 1 \end{bmatrix} \quad (2.6)$$

2.3.3 Tilt-Rotor Frame

The tilt rotor frame reference is used to define the rotor orientation respect to the body frame reference. It is located on the body $X - Z$ plane and centered on the tilt bar, with

- the Y_R axis aligned with body y axis
- the X_R axis is oriented depending on ϕ_T value

Rotation Matrices

The rotation matrices are defined through the tilt-rotor angle ϕ_T , represented in Figure 2.7. During horizontal flight $\phi_T = 0 \text{ rad}$ and the tilt rotor thrust is aligned with X_B axis, while during hover and vertical flight $\phi_T = \frac{\pi}{2}$ and the tilt rotor thrust component is directed perpendicular to the $X_B - Y_B$ plane. The transformations between tilt-rotor and body frames are determined through the following matrices:

$$R_{r2B} = R_2^T(\phi_T) = \begin{bmatrix} \cos(\phi_T) & 0 & \sin(\phi_T) \\ 0 & 1 & 0 \\ -\sin(\phi_T) & 0 & \cos(\phi_T) \end{bmatrix} \quad (2.7)$$

$$R_{B2r} = R_{r2B}^T = \begin{bmatrix} \cos(\phi_T) & 0 & -\sin(\phi_T) \\ 0 & 1 & 0 \\ \sin(\phi_T) & 0 & \cos(\phi_T) \end{bmatrix} \quad (2.8)$$

2.3.4 Local Rotor Frame

The Y4 Tilt-Rotor Martian Aerobot present four rotors overall, for each of them it is defined a local frame reference. For the tilt rotors the local frame reference is aligned with the tilt-rotor frame, while for the coaxial rotors is directed as the body frame. A representation of the different reference systems is shown in the Figure 2.7.

2.3.5 Stability Frame

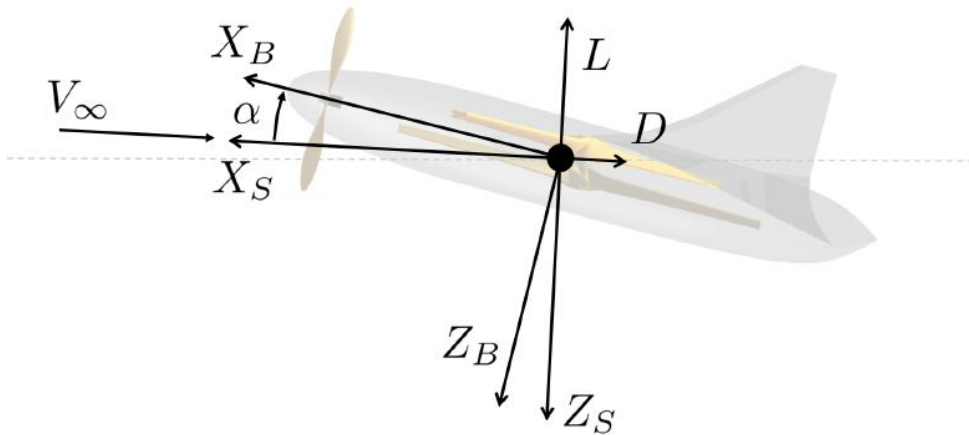


Figure 2.8: Stability Frame

The stability frame is adopted to determine the aerodynamic forces and moments acting on the Y-4 Tilt Rotor Aerobot during its flight. Considering the side-slip angle $\beta = 0$ and Figure:

- Y_S axis is oriented as the Y_B
- X_S is directed as relative wind
- The X_S and Z_S axes are rotated with respect to the body frame of α that represent the angle of attack.

The transformation between stability and body frame is calculated via the following matrices:

$$R_{S2B} = R_2(\alpha) = \begin{bmatrix} \cos(\alpha) & 0 & -\sin(\alpha) \\ 0 & 1 & 0 \\ \sin(\alpha) & 0 & \cos(\alpha) \end{bmatrix} \quad (2.9)$$

$$R_{B2S} = R_2^T(\alpha) = \begin{bmatrix} \cos(\alpha) & 0 & \sin(\alpha) \\ 0 & 1 & 0 \\ -\sin(\alpha) & 0 & \cos(\alpha) \end{bmatrix} \quad (2.10)$$

2.3.6 Inertia Model

For the Martian aerobot the hypothesis of rigid body for the overall vehicle cannot be considered valid since there are four spinning rotors and two of them are tilt-rotors. Therefore it can be seen as the combination of five rigid bodies each with its own inertia associated:

- Two Tilt Rotors.
- Two Coaxial Rotors.
- The main body.

The major inertia component derives from the main body, consisting of all the non-moving parts and whose inertia tensor is indicated with I_A and described in the Mars Inertial reference system allowing for obtain constant values.

Since the vehicle has a symmetry with respect to the $X - Z$ plane, the components I_{xy} and I_{yz} of the inertia products are zero and the tensor is presented in the form described below.

$$I_A = \begin{bmatrix} I_{xx_A} & 0 & I_{xz_A} \\ 0 & I_{yy_A} & 0 \\ I_{xz_A} & 0 & I_{zz_A} \end{bmatrix}_I \quad (2.11)$$

The two tilt rotors have been modeled in the respective local reference system, centered on the x-axis of rotation and parallel to the tilt-rotors reference system;

the products of inertia are negligible and therefore imposed equal to zero, while the value reported for I_{yy_T} and I_{zz_T} represents the average value on one rotation. Hence, the inertia tensor for tilt rotors can be expressed as illustrated in the Equation 2.12.

$$I_T = \begin{bmatrix} I_{xx_T} & 0 & 0 \\ 0 & I_{yy_T} & 0 \\ 0 & 0 & I_{zz_T} \end{bmatrix} = \begin{bmatrix} I_{xx_T} & 0 & 0 \\ 0 & I_{zz_T} & 0 \\ 0 & 0 & I_{zz_T} \end{bmatrix} \quad (2.12)$$

The two coaxial rotors, consisting of four spinning blades, represent the second largest inertia contribution and, as well as for the tilt rotors, the relative inertia tensor is modeled in the local reference system centered on the rotation axis z and parallel to the body reference system and reported below. Also in this case there is a plane of symmetry, the inertia products are negligible and therefore the inertia tensor is a diagonal matrix reported in the Equation 2.13.

$$I_C = \begin{bmatrix} I_{xx_C} & 0 & 0 \\ 0 & I_{yy_C} & 0 \\ 0 & 0 & I_{zz_C} \end{bmatrix} = \begin{bmatrix} I_{xx_C} & 0 & 0 \\ 0 & I_{xx_C} & 0 \\ 0 & 0 & I_{zz_C} \end{bmatrix} \quad (2.13)$$

Since in each pair of rotors they are counter-rotating and characterized by a similar rotation speed it is possible to neglect the gyroscopic effects, while those due to the tilting of the rotors are to be considered minimal because the inertia component due to the tilt rotors is very small if compared to that of the overall vehicle. The values of the components of the inertia tensors have been reported in the Table 2.2, while the values of the distances and masses necessary to determine the overall inertia of the Aerobot have been shown in Table 2.1.

$$I_B = I_A + 2(R_{r2B}I_T R_{r2B}^T) + \sum_{i=1}^2 m_{T_i}(r_{T_i}^{\vec{}} \cdot r_{T_i}^{\vec{}} I_{3x3} - r_{T_i}^{\vec{}} \times r_{T_i}^{\vec{}}) + 2I_C + \sum_{i=3}^4 m_{C_i}(r_{C_i}^{\vec{}} \cdot r_{C_i}^{\vec{}} I_{3x3} - r_{C_i}^{\vec{}} \times r_{C_i}^{\vec{}}) \quad (2.14)$$

The overall inertia of the aerobot is calculated by adding the five contributions previously illustrated, however some transformations are necessary to proceed. In detail, the coaxial inertia tensor must be transposed into the body reference system by applying the theorem of parallel axes, the same procedure is applied for the tilt rotors after alignment with the body system. The result of these transformations and the sum of the five components is reported in Equation 2.14 that represents the full Aerobot inertia tensor expressed in the body reference system, and where the radii vectors are expressed as:

	I_A	I_C	I_T
I_{xx}	29.355	0.312	0.055
I_{yy}	11.809	0.312	0.028
I_{zz}	40.556	0.622	0.028
I_{xy}	0	0	0
I_{xz}	-0.223	0	0
I_{yz}	0	0	0

Table 2.2: Inertia Tensor Values [$kg.m^2$]

$$r_{C_i}^{\vec{}} = \begin{bmatrix} r_{C_{X_i}} \\ 0 \\ 0 \end{bmatrix} \quad (2.15)$$

$$r_{T_i}^{\vec{}} = \begin{bmatrix} r_{T_{X_i}} \\ r_{T_{Y_i}} \\ 0 \end{bmatrix} \quad (2.16)$$

2.4 Y4-TR Control Strategy

The Martian aerobot is equipped with numerous effectors to control its rotational and translational motion. They are:

- δ_{EI} - Elevon deflection
- δ_{AI} - Aileron deflection
- Ω_{T_i} - Rotation Speed of the i-th tilt rotor
- Ω_{C_i} - Rotation Speed of the i-th coaxial rotor

A combination of these effectors will be used during the different flight phases. In particular:

- **Hover Flight**
 - Roll is controlled through differential thrust between the left and right tilt-rotors.
 - Pitch is controlled by varying the coaxial and tilt-rotor thrust.
 - Yaw is controlled by the aerodynamic torque of the four rotors.

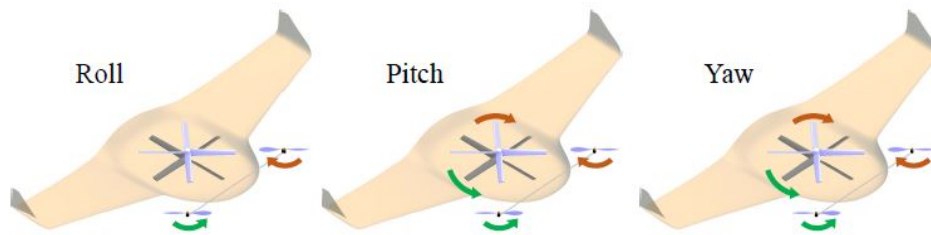


Figure 2.9: Controls for Hover

- The elevons are not used while in this configuration since there is insufficient airflow over them to generate any substantial moments.

- **Transition Phase**

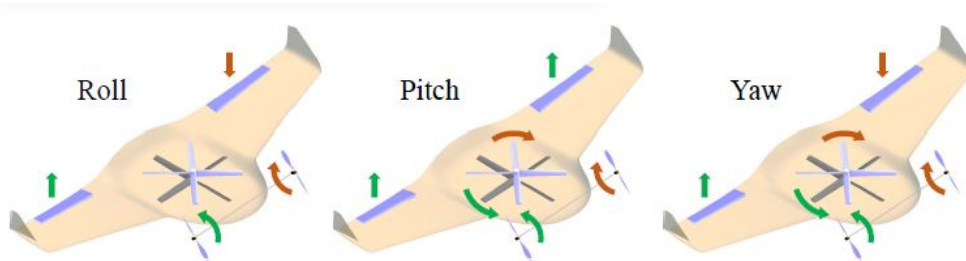


Figure 2.10: Controls for Hover

- Roll is controlled through differential thrust between the left and right tilt-rotors and differential deflection of the elevons.
- Pitch is controlled by varying the coaxial and tilt-rotor thrust, tilting the front tilt-rotors, and symmetric deflection of the elevons.
- Yaw is controlled by the aerodynamic torque of the four rotors, differential thrust between the left and right tilt-rotors, and differential deflection of the elevons.

- **Horizontal Flight**

- Roll is controlled through differential deflection of the elevons
- Pitch is controlled by symmetric deflection of the elevons
- Yaw is controlled through differential thrust between the left and right tilt-rotors, differential deflection of the elevons.
- The coaxial rotors are not used while in this configuration.

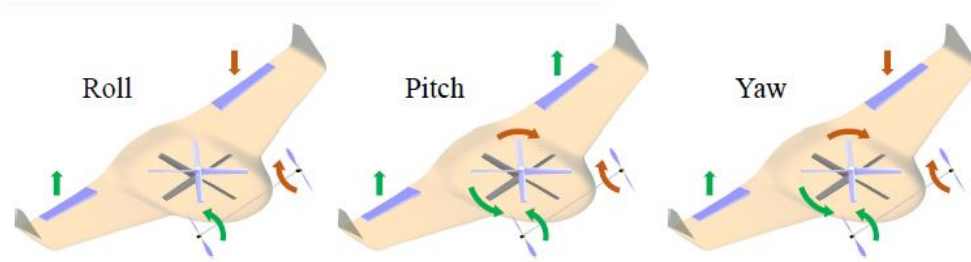


Figure 2.11: Controls for Hover

2.5 Tilt-Rotor Control Designs

The flight control design for martial tilt-rotor UAVs gets inspiration from terrestrial counterparts [3]. Flight control systems for Earth tilt-rotor UAVs can be separated into two main categories: linear and nonlinear. Generally, to implement a linear controller the nonlinear dynamic model of the system is linearized about an equilibrium condition simplifying the problem [3]. The classical PID controller and LQR are the two predominant forms of linear control applied to tilt-rotor UAVs, while the three most common nonlinear control systems implemented are backstepping, gain-scheduling, and nonlinear dynamic inversion [3].

Tilt-Rotors Control Design	
Prototype	Control
Halcyon	Multi-loop PID
Hyperion	H_∞ with μ synthesis
Y4_TR	SDRE

Table 2.3: Previous Tilt-Rotors Control Design

Table 2.3 reports a control design review for the SCC Tilt-rotor concepts. In particular, Song [31] proposed classical multi-loop proportional integral derivative (PID) control for the Halcyon aerobot with a focus on the horizontal flight phase. Transition control for the Hyperion aerobot was developed by Zhao and Underwood using a H_∞ controller with μ synthesis [3]. In order to fly both vertically and horizontally the tilt-rotor vehicle must transition smoothly between the two flight conditions. However, successfully transitioning a tilt-rotor aircraft between the vertical and horizontal phases of flight is a difficult control problem due to the inherent non-linearities and it is currently object of research [3]. Collins proposes an SDRE (State Dependent Riccati Equation Control) method since it is a well suited method for the transition flight phase because it can capture the non-linearities of the problem and offers great design flexibility [3].

Chapter 3

Modelling

3.1 Introduction

This Chapter is intended to illustrate Y4-TR Martian Aerobot mathematical modelling. The necessary Mars Environment and aerodynamics aerobot models are presented referring to Collins' work [3]. Moreover, a rotor performance analysis is conducted to define rotors thrust coefficients. Section 3.6 is dedicated to the complete dynamic model derivation description, while Section 3.7 illustrates how it's possible to obtain a simplified model for horizontal and hover flight conditions.

3.2 Mars Environment Models

Understanding Mars environments characteristics it's a key step to better design a Martian Aerobot [3]. This section highlights the significant environmental parameters that will impact the design and operation of the Martian aerobot. Moreover, the Atmosphere and Gravity Model are presented in Sections 3.3.1 and 3.3.2, respectively.

Mars is the planet in the Solar System closest to Earth, and represents an excellent candidate for human exploration [6]. However, there are substantial differences between the Red Planet and Earth, the main are certainly the atmospheric ones. The atmosphere of Mars is composed by 95% of carbon dioxide and the local atmospheric properties depend on several factors including: solar cycles, dust levels, seasons and geographical location [3] [32].

On Mars the temperature are lower than Earth and, also during summer, there are large variations between day and night. This changes in martian temperatures cause strong winds, which are quite mild on the surface during summer season but lightly stronger at mission operative altitude of 1000 *m*. They strongly increase

during winter seasons and with dust storms, also called dust devils [3].

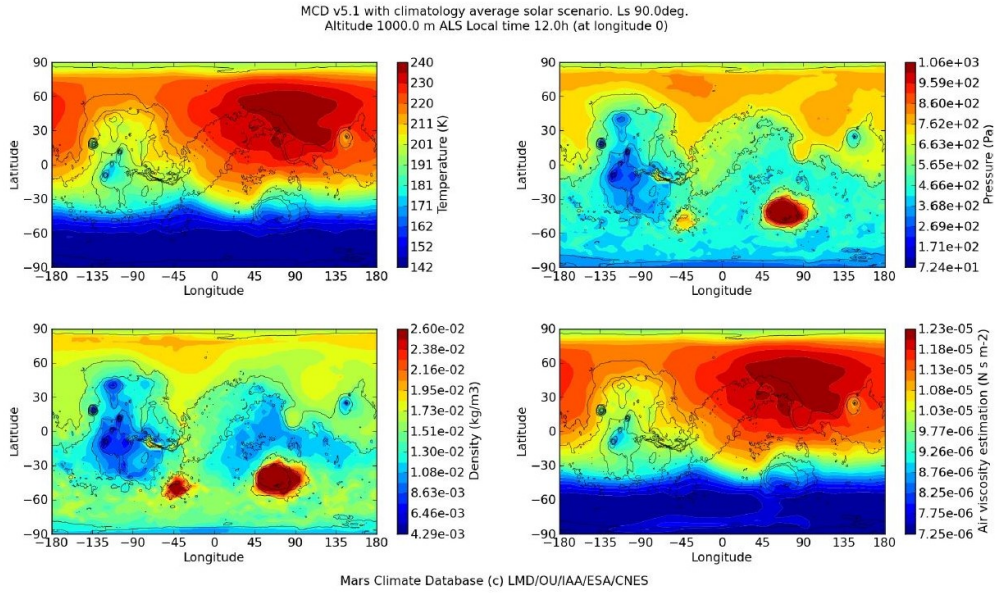


Figure 3.1: MCD Atmospheric Characteristics during a summer day at 1000 m of altitude

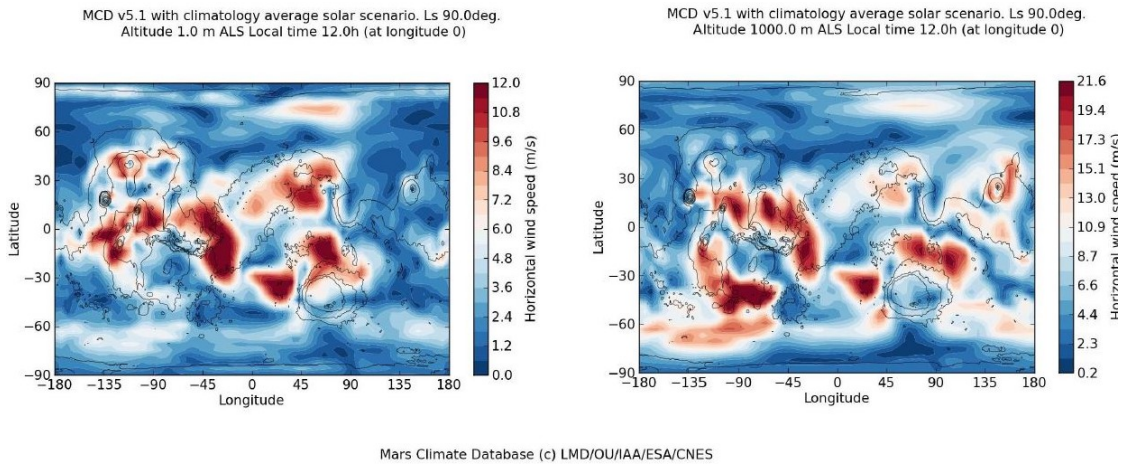


Figure 3.2: MCD Average Wind Characteristics in a martian summer day

Since high winds and dust storms are prevalent during the winter period, Song (2008) proposed conducting the aerobot’s mission during the late spring and early summer periods [3]. In the Figure 3.1 and Figure 3.2 are shown the results for a Martian summer day at ground level and for a mission altitude of 1000 m obtained with the *Mars Climate Database* (MCD) [12].

3.2.1 Atmosphere Model

The most accurate model to estimate average atmospheric parameters is the MCD [12], developed by several European universities.

However, a simpler model has been implemented in the simulator to compute the martian average atmospheric parameters since it is easier to implement in the simulator structure and returns accurate values for a preliminary study. It was realized by the Mars Global Surveyor (MGS) at NASA Glenn Research Center [14] [33] using measurements of the Martian atmosphere and capable to capture the effects of altitude on temperature, pressure and density through the following equations:

$$T[C^\circ] = \begin{cases} -31 - 0.000998h, & \text{if } h \leq 7000m \\ -23.4 - 0.00222h, & \text{if } h > 7000m \end{cases} \quad (3.1)$$

$$p = 0.699e^{-0.00009h} [kPa] \quad (3.2)$$

$$\rho = k \left(\frac{p}{0.1921(T + 273.1)} \right) \left[\frac{kg}{m^3} \right] \quad (3.3)$$

The parameter k is set equal to 1 [3] and accounts the effects of surface location, time of day and season.

However, in the future there will be necessary to implement more accurate model, for example using Mars-Gram that is an engineering-level atmospheric model widely used for diverse mission applications, including systems design, performance analysis, and operations planning for aerobraking, entry descent and landing, and aerocapture.

3.2.2 Gravity Model

Since the aerobot has been designed to fly relatively close to the surface, at a nominal altitude less than 1000 m , the Mars gravitational constant g_{σ° , indicated with the symbol σ° , can be considered constant and equal to a value of $g_{\sigma^\circ=3.72} m/s^2$ [3].

In the following equations the gravitational force agent on the aerobot CoM is expressed in the inertial and body reference systems considering no moments associated with it and the full aerobot mass ($m = 25 \text{ kg}$).

$$\vec{F}_{gI} = \begin{bmatrix} 0 \\ 0 \\ mg_{\sigma} \end{bmatrix} \quad (3.4)$$

$$\vec{F}_{gB} = \begin{bmatrix} -mg_{\sigma} \sin(\theta) \\ mg_{\sigma} \cos(\theta) \sin(\phi) \\ mg_{\sigma} \cos(\theta) \cos(\phi) \end{bmatrix} \quad (3.5)$$

3.3 Aerobot Aerodynamics Models

The aerodynamics models and data for the main body and for the estimation of the rotors performances are defined starting from Nathan Collins' work [3].

The interactions between each component are not considered, each part (main body, tilt rotors and coaxial rotors) is analyzed and modelled individually as first approach and the following simplifications are also considered:

- Parasite drag due to the landing gear and to the top and bottom coaxial rotors cover are not taken in account;
- The dust accumulation is neglected;
- The ground effect is not considered.

3.3.1 Main Body Aerodynamics Coefficients Estimation

The Y4-Tilt Rotor Martian Aerobot main body could be seen as a wing blended body, there is no a net distinction between fuselage and wing; its aerodynamics characteristics have been investigated by the SSC with the XFRL5 Software [3], that is able to conduct wing analysis using three different methods:

- Lifting Line Theory (LLT)
- Vortex Lattice Method (VLM)
- 3D Panel Method (3DP)

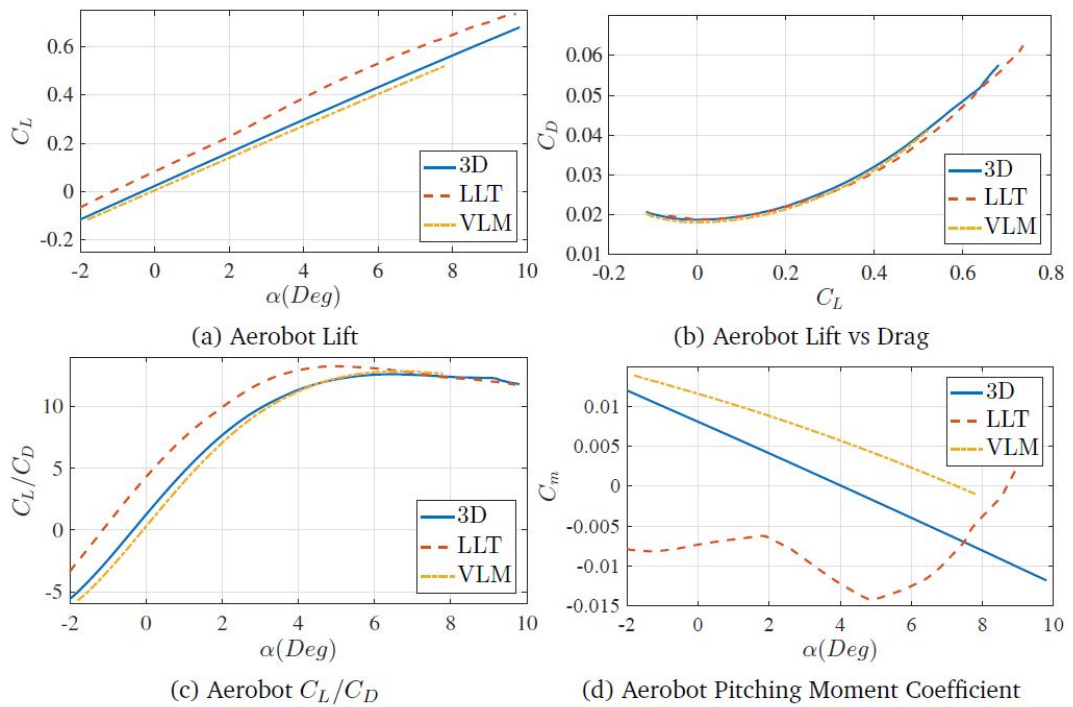


Figure 3.3: Martian Aerobot Polar in closed configuration [3].

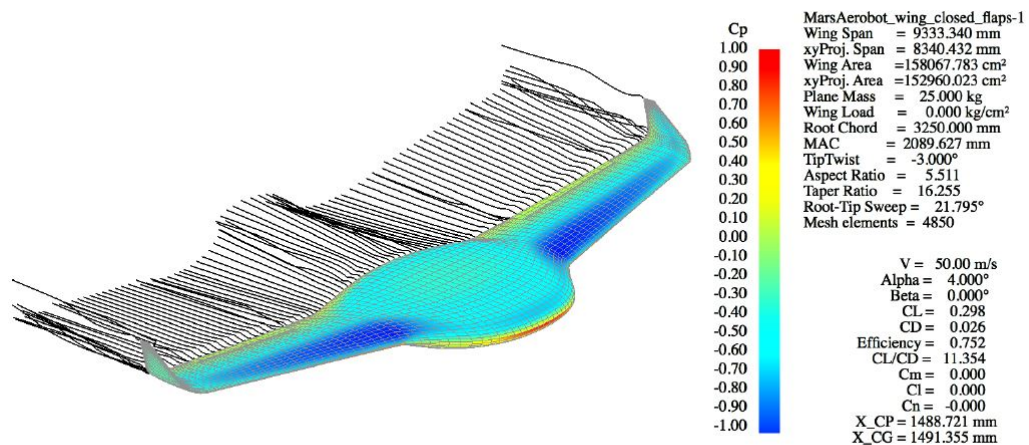


Figure 3.4: Martian Aerobot Pressure Distribution $\alpha = 4^\circ$ estimated with 3DP [3].

The Martian Aerobot polar for a nominal mission velocity of 50 m/s determined with the three different approaches is reported in the Figure 3.5, while the pressure distribution for an AoA of 4° is showed in Figure 3.4. In particular, these parameters have been directly extrapolated from the graphs reported in Figure 3.5.

- α_i - Induced angle of attack
- α_0 - Zero Lift angle of attack
- C_L - Aerobot Lift Coefficient
- C_{L0} - Aerobot Zero Lift Coefficient
- $C_{L\alpha}$ - Aerobot Lift Coefficient Slope
- C_{m0} - Zero Pitching Moment Coefficients
- α_e - Angle of attack in horizontal trim conditions, determined in Section 4.

Aerobot Zero Lift Coefficient

The Lift Coefficient curve is obtained extrapolating the data from the C_L presented Figure 3.3 and reported in Figure 3.5. The values of C_{L0} and α_0 for each method (LLT,3DP,VLM) are reported in Table 3.3 and used to calculate C_{L0MEAN} . In Table 3.2 are reported two values of mean. In particular:

- The mean of the first two values is used for zero lift coefficient $C_{L0MEAN} = 0.0553$
- The mean of all values is used as α_i , which is closer to the 3DP value. This parameter affects specially the drag and consequently the thrust needed for the equilibrium.

Aerobot Lift Coefficient Slope

The method used by Nathan Collins to calculate the aerodynamics coefficients e derivatives is the 3D Panel Method [3], so the blue line in the Figure 3.5 has been considered to determine the lift coefficient slope. The point data showed in Figure 3.5 have been collected from Figure 3.3, and the lift coefficient slope can be evaluated as:

$$C_{L\alpha} = \frac{C_{L(3DP)} - C_{L0(3DP)}}{\Delta\alpha_e} = \frac{0.298 - 0.025}{0.069} \frac{1}{rad} \cong 3.95 \frac{1}{rad} \quad (3.6)$$

Aerod. Coeff. Estimation					
	C_{L0}	$C_L(4^\circ)$	$\alpha_0[deg]$	$C_{L\alpha}$	$\alpha_i[deg]$
<i>LLT</i>	0.084	0.39	-1.1500	4.3835	1
<i>3DP</i>	0.025	0.298	-0.3487	3.9500	0.396
<i>VLM</i>	0.006	0.272	-0.1355	3.8105	0.09
Mean 1° - 2° Val.	0.055	0.344	-1.5	4.1	0.7
Mean All Val.	0.04	0.32	-0.55	4.04	0.5

Table 3.1: Martian Aerobot Coefficients Estimation

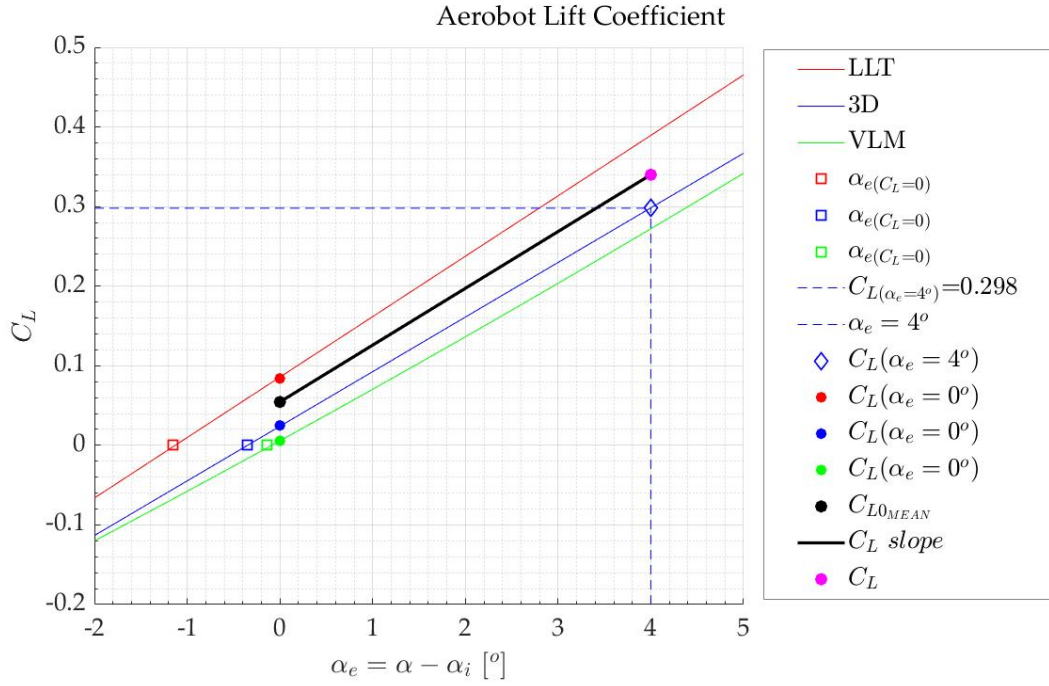


Figure 3.5: Martian Aerobot Polar

With this value it is possible to represent the $C_L = f(\alpha_e)$. Looking at Figure 3.5, the function starts at $\bar{C}_{L02} = 0.055$ and for $\alpha_e = 4^\circ$ gives $C_L = 0.34$, required for equilibrium in horizontal flight conditions, with a slope $C_{L\alpha} \cong 3.95 \frac{1}{rad}$.

From $C_L = f(\alpha_e)$ it's possible to estimate α_i reported in Table 3.3 as:

$$\alpha_{i_{3DP}} = \frac{C_L - C_{L\alpha}\alpha_e}{C_{L\alpha}} = \frac{0.298 - 3.95 * 4^\circ/57.3}{3.95} \cong 0.0174rad \cong 0.4^\circ \quad (3.7)$$

Zero Pitching Moment Estimation

In order to determine the C_{m0} value, the same method used to define C_{L0} is used. Figure 3.6 is obtained by linearly interpolating data from Figures 3.4. As well as for C_{L0} , in Table 3.2 there are reported three values, one for each method, and their mean is used to define C_{m0} .

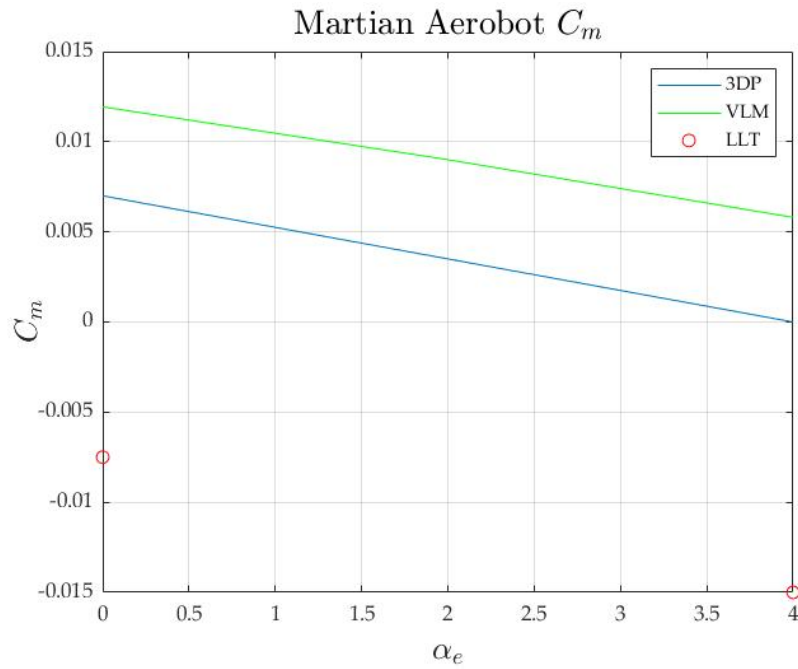


Figure 3.6: Pitching Moment Behaviour

C_{m0} Estimation	
	C_{m0}
<i>LLT</i>	-0.0075
<i>3DP</i>	0.007
<i>VLM</i>	0.012
Mean All Val.	0.0038

Table 3.2: Martian Aerobot zero pitching moment coefficient estimation

3.3.2 Aerodynamics Forces and Moments in the Body Frame

The aerodynamic derivatives, both dimensional and non-dimensional, provided by the XFRL5 software [3] and reported in Appendix A, are expressed in the stability reference system and therefore must be translated into the body reference system and then expressed in a suitable form to be implemented in the simulator.

Aerodynamics Forces

Expressing the aerodynamic forces as a Taylor expansion and performing a pre-multiplication of the equation terms by R_{S2B} , the equation obtained is the following:

$$\vec{F}_{aeroB}(\vec{x}_a) \simeq R_{S2B} \left(\vec{F}_{aeros}(\vec{x}_{a_{trim}}) + \left. \frac{\partial \vec{F}_{aeros}}{\partial \vec{x}_a} \right|_{\vec{x}_{a_{trim}}} (\vec{x}_a - \vec{x}_{a_{trim}}) \right) \quad (3.8)$$

where $\vec{x}_{a_{trim}}$ is the state vector in trim conditions.

This equation is rearranged to be implemented in the simulator by expressing the term \vec{S}_{F_a} as:

$$\vec{S}_{F_a} = R_{S2B} \left(\vec{F}_{aeros}(\vec{x}_{a_{trim}}) + \left. \frac{\partial \vec{F}_{aeros}}{\partial \vec{x}_a} \right|_{\vec{x}_{a_{trim}}} \vec{x}_{a_{trim}} \right) \quad (3.9)$$

and imposing:

$$B_{F_a} = R_{S2B} \left. \frac{\partial \vec{F}_{aeros}}{\partial \vec{x}_a} \right|_{\vec{x}_{a_{trim}}} \quad (3.10)$$

It follows that:

$$\vec{F}_{aeros} \simeq \vec{S}_{F_a} + B_{F_a} \vec{x}_a \quad (3.11)$$

The \vec{S}_{F_a} term can be expressed as:

$$\vec{S}_{F_a} = \begin{bmatrix} S_x \\ S_y \\ S_z \end{bmatrix} \quad (3.12)$$

While the matrix B_{F_a} contains the dimensional derivatives and has the following form:

$$B_{F_a} = \begin{bmatrix} X_U & X_V & X_W & X_P & X_Q & X_R & X_{\delta_{El}} & X_{\delta_{Al}} \\ Y_U & Y_V & Y_W & Y_P & Y_Q & Y_R & Y_{\delta_{El}} & Y_{\delta_{Al}} \\ Z_U & Z_V & Z_W & Z_P & Z_Q & Z_R & Z_{\delta_{El}} & Z_{\delta_{Al}} \end{bmatrix} \quad (3.13)$$

Considering a level straight uniform flight condition it's possible to impose that $S_y = 0$ and:

$$\begin{cases} X_V = X_P = X_R = X_{\delta_{Al}} = 0 \\ S_y = Y_U = Y_W = Y_Q = Y_{\delta_{El}} = 0 \\ Z_V = Z_P = Z_R = Z_{\delta_{Al}} = 0 \end{cases} \quad (3.14)$$

Definitely \vec{F}_{aero} can be expressed as:

$$\vec{F}_{aero} = \begin{bmatrix} S_x + UX_U + WX_W + QX_Q + X_{\delta_{El}}\delta_{El} \\ VY_V + PY_P + RY_R + Y_{\delta_{Al}}\delta_{Al} \\ S_z + UZ_U + WZ_W + QZ_Q + Z_{\delta_{El}}\delta_{El} \end{bmatrix} \quad (3.15)$$

Aerodynamics Moments

The method used to express aerodynamic forces is also applied for aerodynamic moments in order to obtain an expression similar to Equation 3.15. Firstly, the aerodynamic moments are expressed with Taylor's expansion and rotated in the body frame. Then, the equation is rearranged to obtain Equation 3.17, and, finally, Equation 3.23 is obtained introducing the dimensional derivatives matrix and considering horizontal leveled flight conditions (Equation 3.21-3.22).

$$\vec{M}_{aero_B}(\vec{x}_a) \simeq R_{S2B} \left(\vec{M}_{aero_s}(\vec{x}_{a_{trim}}) + \frac{\partial \vec{M}_{aero_s}}{\partial \vec{x}_a} \Big|_{\vec{x}_{a_{trim}}} (\vec{x}_a - \vec{x}_{a_{trim}}) \right) \quad (3.16)$$

$$\vec{S}_{M_a} = R_{S2B} \left(\vec{M}_{aero_s}(\vec{x}_{a_{trim}}) + \frac{\partial \vec{M}_{aero_s}}{\partial \vec{x}_a} \Big|_{\vec{x}_{a_{trim}}} \vec{x}_{a_{trim}} \right) \quad (3.17)$$

$$B_{M_a} = R_{S2B} \frac{\partial \vec{M}_{aero_s}}{\partial \vec{x}_a} \Big|_{\vec{x}_{a_{trim}}} \quad (3.18)$$

$$\vec{M}_{aero_s} \simeq \vec{S}_{M_a} + B_{F_a} \vec{x}_a \quad (3.19)$$

$$\vec{S}_{M_a} = \begin{bmatrix} S_l \\ S_m \\ S_n \end{bmatrix} \quad (3.20)$$

$$B_{M_a} = \begin{bmatrix} L_U & L_V & L_W & L_P & L_Q & L_R & L_{\delta_{El}} & L_{\delta_{Al}} \\ M_U & M_V & M_W & M_P & M_Q & M_R & M_{\delta_{El}} & M_{\delta_{Al}} \\ N_U & N_V & N_W & N_P & N_Q & N_R & N_{\delta_{El}} & N_{\delta_{Al}} \end{bmatrix} \quad (3.21)$$

$$\begin{cases} S_l = L_U = L_W = L_Q = L_{\delta_{El}} = 0 \\ M_V = M_P = M_R = M_{\delta_{Al}} = 0 \\ S_n = N_U = N_W = N_Q = N_{\delta_{El}} = 0 \end{cases} \quad (3.22)$$

$$\vec{M}_{aero} = \begin{bmatrix} VL_V + PL_P + RL_R + L_{\delta_{Al}}\delta_{Al} \\ S_m + UM_U + WM_W + QM_Q + M_{\delta_{El}}\delta_{El} \\ VN_V + PN_P + RN_R + N_{\delta_{Al}}\delta_{Al} \end{bmatrix} \quad (3.23)$$

3.4 Rotors Performances Estimation

In this section the performances of Tilt rotors are estimated with BET [9] and XROTOR [7] for horizontal flight conditions. For flight in hover only the XROTOR analysis is conducted, since BET doesn't allow to obtain consistent values. For the coaxial rotors the parameters reported by SCC have been compared with CROTOR analysis [8]. The tilt and coaxial rotor parameters and features are reported in Appendix A, as well as the rotor data used for CROTOR and XROTOR analysis [3].

3.4.1 Tilt-Rotor Analysis

In order to analyze tilt-rotors performance the following data are considered both for BET and XROTOR analysis:

- V - trim cruise speed
- ρ - density at trim altitude;
- $R = 0.5$ - rotor radius
- $N = 2$ - number of blades
- A - rotor area

Blade Element Theory

A relatively simple method of estimate the more detailed performance of a rotor is the Blade Element Theory. In this method the rotor is divided into a number of independent sections along the length (Figure 3.7). At each section a force

balance is applied involving 2D section lift and drag with the thrust and torque produced by the section. At the same time a balance of axial momentum is applied. This produces a set of non-linear equations that can be solved for each blade section with an iterative process, starting from an initial guess value of inflow. The resulting values of section thrust and torque can be summed to predict the overall performance of the rotor. The BET method is based on the lifting-line assumption, stall and compressibility effects are neglected to get an analytical solution.

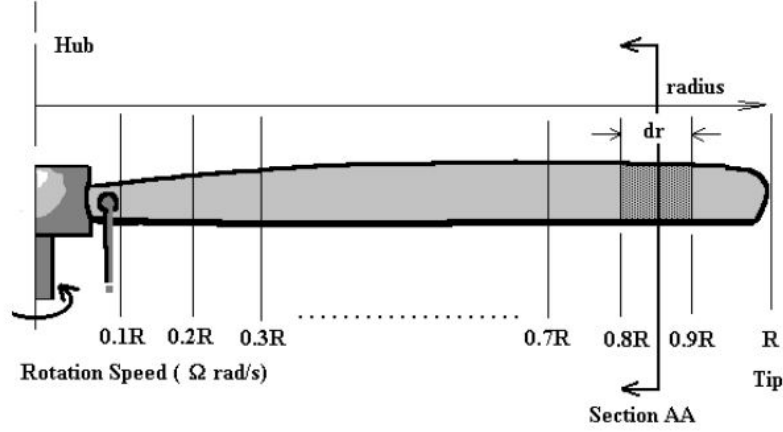


Figure 3.7: BET-Rotor blade subdivision

Looking at Figure 3.8 the blade section has a pitch angle β_0 measured from the plane of rotation to the zero-lift line. The air velocity seen by the blade has components:

- $U_T = \Omega r$ - tangent to the disk plane,
- $U_P = V + \nu$ - perpendicular to the disk plane

The resultant magnitude, the inflow angle and the local blade angle of attack can be estimated respectively as:

$$U = \sqrt{(U_T^2 + U_P^2)} \quad (3.24)$$

$$\phi = \text{atan}(U_P/U_T) \quad (3.25)$$

$$\alpha = \beta_0 - \phi \quad (3.26)$$

The section forces in terms of the lift and drag coefficient gives:

$$L = 1/2\rho U^2 cC_l \quad (3.27)$$

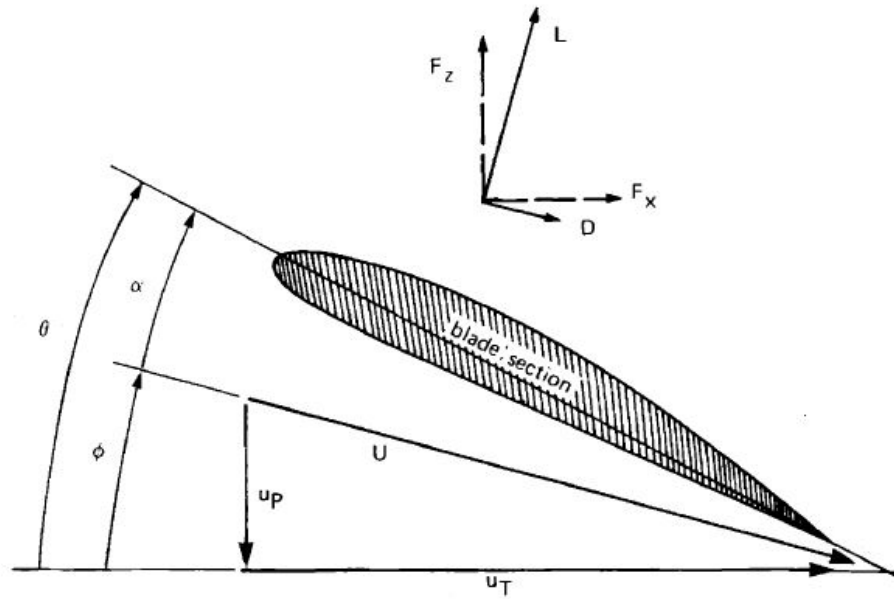


Figure 2-6 Blade section aerodynamics.

Figure 3.8: Blade parameters description

$$D = 1/2\rho U^2 c C_d \quad (3.28)$$

where C_l and C_d are function of the angle of attack.

Resolving the aerodynamic forces normal and parallel to the disk plane gives:

$$F_Z = L \cos(\phi) - D \sin(\phi) \quad (3.29)$$

$$F_X = L \sin(\phi) + D \cos(\phi) \quad (3.30)$$

In the end, the elemental thrust, torque and power are:

$$dT = N F_Z dr \quad (3.31)$$

$$dQ = N F_x r dr \quad (3.32)$$

$$dP = \Omega dQ \quad (3.33)$$

The total forces on the rotor are obtained by iterating over the blade span from root to tip.

In order to determine the magnitude of the induced velocity U_P and to calculate U_T accurately, an axial flow momentum balance must be applied to predict the induced effects on a given blade element. The following non linear equations are obtained:

$$\Delta T = 2\pi r \rho V_\infty^2 (1 + a) a dr \quad (3.34)$$

$$\Delta T = 4\pi r^3 V_\infty (1 + a) b \Omega dr \quad (3.35)$$

where:

- V_∞ is the free-stream velocity
- a and b are the induce coefficients
- r is the radius of the considered profile section

Because these final forms (Equations 3.34 3.35) of the momentum equation balance still contain the variables for element thrust and torque, they cannot be used directly to solve for inflow factors. However there now exists a nonlinear system of equations (3.24-3.25-3.26-3.31-3.32-3.34-3.35) that can be solved iteratively starting from an initial guess values of inflow factors a and b .

The BET is applied at Martian Aerobot tilt-rotors subdividing the blades in 29 sectors and considering the rotor profiles data reported in Appendix B, as well as blades discretization. In order to apply the BET algorithm, for each section the following parameters are defined:

- r_m/R - mean section radius divided by the R
- c_m/R - mean section chord divided by the R
- β_{0m}/R - mean section twist (respect to the zero lift line)

Moreover, to consider tip and hub losses, the first and final rotor blade section are not considered. It was decided to stop at about $0.9R$, where R is the rotor blade radius and start from $0.23R$.

XROTOR

XROTOR, written by Professor Mark Drela, was used to design the tilt-rotors and can be used for the design and analysis of ducted and free-tip propellers and windmills [7]. The software has many capabilities including the design of minimum

induced loss rotors, twist optimization, and modeling incoming slipstream effects from an upstream rotor. Using airfoil parameters and lifting-line theory it calculates the induced velocities by numerically solving the potential flow field about the propeller including the vortex sheet wake.

3.4.2 Coaxial Rotor Analysis

CROTOR is an extension of XROTOR that automates the process of converging counter-rotating rotors for design and analysis [8], was used to design and analyze the Martian aerobot’s large coaxial counter-rotating rotors [3]. Even if CROTOR does have the capability to model rotors inside a duct, it was decided to forgo this option and model the coaxial rotors as open rotors [3] for two reasons: first, the imbedded rotors are not conventional ducted rotors but rather fan-in-wing rotors which CROTOR does not have the capability to model, and second, it is unlikely such a thin duct will add any noticeable performance benefit. The specific parameters input into the software to analyze the tilt and coaxial rotors can be found in Appendix A.

3.4.3 Results

In this section the rotor performances analysis results are reported in Table 3.3-3.4-3.5 for Tilt in hover and horizontal flight and Coaxial rotors in hover. For the tilt-rotors in horizontal flight it is decided to use XROTOR results to determine the thrust coefficient C_T (Chapter 4) since these results are more consistent with Collins’ ones. The results in hover conditions are quite similar. However it is decided to use Collins’ data for tilt-rotor and Coaxial-rotors in hover.

Tilt-Rotor Horizontal			
Parameter	BET	XROTOR	Collins
Per rotor			
Thrust	6.29N	4.07N	4.05N
Total			
Thrust	12.59N	8.14N	8.1N

Table 3.3: Tilt-Rotor performances analysis in horizontal flight

Tilt-Rotor Hover		
Parameter	XROTOR	Collins
Per rotor		
Thrust	4.45 <i>N</i>	4.62 <i>N</i>
Total		
Thrust	8.9 <i>N</i>	9.28 <i>N</i>

Table 3.4: Tilt-Rotor performances analysis in hover flight condition

Coaxial-Rotor Hover Flight		
Parameter	XROTOR	Collins
Total Thrust	83 <i>N</i>	83.5 <i>N</i>

Table 3.5: Coaxial-Rotor Hover Flight performances analysis

3.5 Equations of Motion

The forces and moments generated by the motion of the rotors, aerodynamic forces and moments acting on the body and rotors, and any cross-coupling effects produced from the relative motion of the four rotors and body must be considered in order to fully describe the rotational and translational dynamics of the aerobot.

3.5.1 Newton’s Second Law

The translational dynamics is described through Newton’s Second Law, reported in Equation 3.36 in the inertial reference system.

$$\vec{F} = m \left[\frac{d\vec{V}}{dt} \right]_I = \begin{bmatrix} F_X \\ F_Y \\ F_Z \end{bmatrix} = m(\dot{\vec{V}}_B + \vec{\omega}_B \times \vec{V}_B) \quad (3.36)$$

where \vec{F} is given by the sum of the following terms:

- The Aerodynamics forces along X, Y, Z
- The Gravity force \vec{F}_g
- The Propulsive Thrust

Expliciting the Equation 3.34 for $\dot{\vec{V}}_B$ we have:

$$\dot{\vec{V}}_B = \begin{bmatrix} \dot{U} \\ \dot{V} \\ \dot{W} \end{bmatrix} = \frac{R_{I2B}\vec{F}_g + \vec{T}_{C_i} + R_{r2B}\vec{T}_{T_i} + \vec{F}_a}{m} - \vec{\omega}_B \times \vec{V}_B \quad (3.37)$$

Replacing each terms, the Equation 3.37 results as follow:

$$\dot{\vec{V}}_B = \frac{1}{m} \left(\begin{bmatrix} -mg_{\mathcal{G}} s\theta \\ mg_{\mathcal{G}} c\theta s\phi \\ mg_{\mathcal{G}} c\theta c\phi \end{bmatrix} - \begin{bmatrix} 0 \\ 0 \\ T_{C_i} \end{bmatrix} + \begin{bmatrix} c\phi_T & 0 & s\phi_T \\ 0 & 1 & 0 \\ -s\phi_T & 0 & c\phi_T \end{bmatrix} \begin{bmatrix} T_{T_i} \\ 0 \\ 0 \end{bmatrix} + \begin{bmatrix} X \\ Y \\ Z \end{bmatrix} \right) - \vec{\omega}_B \times \vec{V}_B \quad (3.38)$$

where:

$$\vec{\omega}_B \times \vec{V}_B = \begin{bmatrix} QW - VR \\ -(PW - RU) \\ PV - QU \end{bmatrix} \quad (3.39)$$

Explicating each component of the vector $\dot{\vec{V}}_B$ obtain the three equations that describe the translational dynamics are obtained:

$$\begin{cases} \dot{U} = (VR - QW) + \frac{X}{m} - g_{\mathcal{G}} s(\theta) + \frac{T_{T_i}}{m} c(\phi_T) \\ \dot{V} = (WP - UR) + \frac{Y}{m} - g_{\mathcal{G}} c(\theta) s(\phi) \\ \dot{W} = (UQ - VP) + \frac{Z}{m} + g_{\mathcal{G}} c(\theta) c(\phi) - \frac{T_{T_i}}{m} s(\phi_T) - \frac{T_{C_i}}{m} \end{cases} \quad (3.40)$$

Expressing aerodynamic forces as:

$$\begin{cases} X = S_X + X_U U + X_W W + X_Q Q + X_{\delta_{El}} \delta_{El} \\ Y = S_Y + Y_V V + Y_P P + Y_R R + Y_{\delta_{Al}} \delta_{Al} \\ Z = S_Z + Z_U U + Z_W W + Z_Q Q \end{cases} \quad (3.41)$$

the system of Equations 3.43 can be rewritten as:

$$\begin{aligned} \dot{U} = & \frac{S_x}{m} + \frac{UX_U}{m} + VR + W \left(\frac{X_W}{m} - Q \right) + \frac{QX_Q}{m} - g \sin \theta + \frac{\delta_{El} X_{\delta_{El}}}{m} + \\ & + \frac{\cos \phi_T (S_{T_{T1}} + B_{T_{T1}} \tilde{\Omega}_{T1})}{m} + \frac{\cos \phi_T (S_{T_{T1}} + B_{T_{T1}} \tilde{\Omega}_{T1})}{m} \end{aligned} \quad (3.42)$$

$$\dot{V} = -UR + \frac{VY_V}{m} + WP + \frac{PY_P}{m} + \frac{RY_R}{m} + g \cos \theta \sin \phi + \frac{\delta_{Al} Y_{\delta_{Al}}}{m} \quad (3.43)$$

$$\begin{aligned}
 \dot{W} = & \frac{S_z}{m} + U \left(\frac{Z_U}{m} + Q \right) - VP + \frac{WZ_W}{m} + \\
 & + \frac{QZ_Q}{m} + g \cos \theta \cos \phi + \frac{\delta_{El} Z_{\delta_{El}}}{m} + \\
 & - \frac{\sin \phi_T (S_{T_{T1}} + B_{T_{T1}} \tilde{\Omega}_{T1})}{m} + \\
 & - \frac{\sin \phi_T (S_{T_{T1}} + B_{T_{T1}} \tilde{\Omega}_{T2})}{m} + \\
 & - \frac{(S_{T_{C1}} + S_{T_{C2}})}{m} - \frac{\tilde{\Omega}_{C1} (C_{T_{C1}\tilde{\Omega}_{C1}} + C_{T_{C2}\tilde{\Omega}_{C1}})}{m} + \\
 & - \frac{\tilde{\Omega}_{C2} (C_{T_{C1}\tilde{\Omega}_{C2}} + C_{T_{C2}\tilde{\Omega}_{C2}})}{m}
 \end{aligned} \tag{3.44}$$

3.5.2 Euler's Rigid Body Equations

Euler's equations allow to describe the rotational dynamics of a body, the initial goal is to express the terms of the equation $\vec{\tau}_B = \vec{\tau}_{B_{est}}$. The $\vec{\tau}_B$ vector is composed of the torques generated by the following elements:

- The two counter-rotating tilt rotors;
- The two counter-rotating coaxial rotors;
- The Aerobot body.

$$\vec{\tau}_B = I_B \dot{\vec{\omega}}_B + \dot{I}_B \vec{\omega}_B + \vec{\omega}_B \times I_B \vec{\omega}_B + \sum_{i=1}^2 R_{r2B} \vec{\tau}_{T_i} + \sum_{i=3}^4 \vec{\tau}_{C_i} \tag{3.45}$$

where $\vec{\tau}_{T_i}$ and $\vec{\tau}_{C_i}$ are torques generated by the i -th tilt rotor and coaxial rotor respectively.

Tilt-Rotors Torque

The torque generated by the i -th tilt-rotor in its local frame is given by:

$$\vec{\tau}_{T_i} = I_T \dot{\vec{\omega}}_{T_i} + \vec{\omega}_{T_i} \times I_T \vec{\omega}_{T_i} \tag{3.46}$$

Expressing the Equation 3.46 and rearranging in terms of body acceleration leads to:

$$R_{r2B} \vec{\tau}_{T_i} = R_{r2B} I_T R_{r2B}^T \dot{\vec{\omega}}_B + R_{r2B} \left(I_T \left(\dot{R}_{r2B}^T \vec{\omega}_B + \dot{\tilde{\Omega}}_{T_i} \right) + (\vec{\omega}_{T_i} \times I_T \vec{\omega}_{T_i}) \right) \tag{3.47}$$

where:

$$\vec{K}_{T_i} = R_{r2B} \left(I_T \left(\dot{R}_{r2B}^T \vec{\omega}_B + \dot{\vec{\Omega}}_{T_i} \right) + (\vec{\omega}_{T_i} \times I_T \vec{\omega}_{T_i}) \right) \quad (3.48)$$

Thus, the Equation 3.48 can be expressed as:

$$R_{r2B} \vec{\tau}_{T_i} = R_{r2B} I_T R_{r2B}^T \dot{\vec{\omega}}_B + \vec{K}_{T_i} \quad (3.49)$$

The total torque generated by both tilt-rotors is then:

$$\sum_{i=1}^2 R_{r2B} \vec{\tau}_{T_i} = 2 R_{r2B} I_T R_{r2B}^T \dot{\vec{\omega}}_B + \vec{K}_{T_1} + \vec{K}_{T_2} \quad (3.50)$$

Coaxial-Rotors Torque

The torque generated by the i – th coaxial rotor in its local frame considering its rotational speed $\vec{\omega}_{C_i}$ is given by:

$$\vec{\tau}_{C_i} = I_C \dot{\vec{\omega}}_{C_i} + \vec{\omega}_{C_i} \times I_C \vec{\omega}_{C_i} \quad (3.51)$$

Rearranging in terms of body acceleration lead to:

$$\vec{\tau}_{C_i} = I_C \dot{\vec{\omega}}_B + I_C \dot{\vec{\Omega}}_{C_i} + \vec{\omega}_{C_i} \times I_C \vec{\omega}_{C_i} \quad (3.52)$$

where:

$$\vec{K}_{C_i} = I_C \dot{\vec{\Omega}}_{C_i} + \vec{\omega}_{C_i} \times I_C \vec{\omega}_{C_i} \quad (3.53)$$

Finally, the total torque generated by the coaxial rotors is:

$$\sum_{i=3}^4 \vec{\tau}_{C_i} \quad (3.54)$$

Total Torque

The terms $\vec{\tau}_{C_i}$ and $\vec{\tau}_{T_i}$, which appear in the total torque expression, have been explained in the previous sections. To complete the description it's necessary to express the \dot{I}_B , that is the rate of change of the aerobot's body inertia tensor, and to rearrange the Equation 3.52, which represents the total torque, in terms of body acceleration.

$$\vec{\tau}_B = I_B \dot{\vec{\omega}}_B + \dot{I}_B \vec{\omega}_B + \vec{\omega}_B \times I_B \vec{\omega}_B + \sum_{i=1}^2 R_{r2B} \vec{\tau}_{T_i} + \sum_{i=3}^4 \vec{\tau}_{C_i} \quad (3.55)$$

$$\dot{I}_B = \begin{bmatrix} -s(2\phi_T)(I_{xx_T} - I_{zz_T})\dot{\phi}_T & 0 & -c(2\phi_T)(I_{xx_T} - I_{zz_T})\dot{\phi}_T \\ 0 & 0 & 0 \\ c(2\phi_T)(I_{xx_T} - I_{zz_T})\dot{\phi}_T & 0 & s(2\phi_T)(I_{xx_T} - I_{zz_T})\dot{\phi}_T \end{bmatrix} \quad (3.56)$$

$$\vec{\tau}_B = (I_B + 2(R_{r2B} I_T R_{r2B}^T + I_C)) \dot{\vec{\omega}}_B + \dot{I}_B \vec{\omega}_B + \vec{\omega}_B \times I_B \vec{\omega}_B + \vec{K}_{T_1} + \vec{K}_{T_2} + \vec{K}_{C_3} + \vec{K}_{C_4} \quad (3.57)$$

Torques acting on Aerobot Center of Mass

To solve the equation $\tau_{B_{est}} = \tau_B$, the term $\tau_{B_{est}}$ which represents the total external torques, acting on the aerobot, needs to be expressed.

$$\vec{\tau}_{B_{est}} = \sum_{i=1}^2 \left(\vec{r}_{T_i} \times R_{r2B} \vec{T}_{T_i} + R_{r2B} \vec{\tau}_{T_{ext_i}} \right) + \sum_{i=3}^4 \left(\vec{r}_{C_i} \times R_{r2B} \vec{T}_{C_i} + R_{r2B} \vec{\tau}_{C_{ext_i}} \right) + \vec{M}_{aeroB} \quad (3.58)$$

where:

- Tilt and Coaxial Rotor thrust vectors can be expressed as:

$$\vec{T}_{T_i} = \begin{bmatrix} T_{T_i} \\ 0 \\ 0 \end{bmatrix} \quad (3.59)$$

$$\vec{T}_{C_i} = \begin{bmatrix} 0 \\ 0 \\ T_{C_i} \end{bmatrix} \quad (3.60)$$

- Position vectors relative to the Aerobot CoM are given by:

$$\vec{r}_{T_i} = \begin{bmatrix} r_{T_{X_i}} \\ r_{T_{Y_i}} \\ 0 \end{bmatrix} \quad (3.61)$$

$$\vec{r}_{C_i} = \begin{bmatrix} r_{C_{X_i}} \\ 0 \\ 0 \end{bmatrix} \quad (3.62)$$

- External Torque vectors ancting on the Aerobot can be expressed as:

$$\vec{\tau}_{T_{ext_i}} = \begin{bmatrix} Q_{T_i} \\ 0 \\ 0 \end{bmatrix} \quad (3.63)$$

$$\vec{\tau}_{C_{ext_i}} = \begin{bmatrix} 0 \\ 0 \\ Q_{C_i} \end{bmatrix} \quad (3.64)$$

Rotational Equation of Motion

Setting $\vec{\tau}_B = \vec{\tau}_{B_{ext}}$ and substituting Equation 3.54 and 3.55 and solving for $\dot{\vec{\omega}}_B$ leads to:

$$\begin{aligned} \dot{\vec{\omega}}_B = & (I_B + 2(R_{r2B}I_T R_{r2B}^T + I_C))^{-1} \left(\sum_{i=1}^2 (\vec{r}_{T_i} \times R_{r2B} \vec{T}_{T_i} + R_{r2B} \vec{\tau}_{T_{ext_i}}) + \right. \\ & + \sum_{i=3}^4 (\vec{r}_{C_i} + \vec{\tau}_{C_{ext_i}}) + \vec{M}_{aeroB} - \dot{I}_B \vec{\omega}_B - \vec{\omega}_B \times I_B \vec{\omega}_B + \\ & \left. - \vec{K}_{T_1} - \vec{K}_{T_2} - \vec{K}_{C_3} - \vec{K}_{C_4} \right) \end{aligned} \quad (3.65)$$

Equation 3.65 represents the system of three coupled nonlinear rotational equations of motion expressed in the aerobot's body frame. Explaining each term of the vector it's possible to obtain the following equations:

$$\begin{aligned} \dot{P} = & \frac{1}{k_{dpr}} (V(k_{p2}N_V - k_{r1}LV) + \\ & + P(-k_{r1}L_P + k_{p2}N_P + \dot{\phi}_T(k_{p5}k_{r1} - k_{p2}k_{r4}) + Qk_{p2}(k_{r1} - k_{r2})) + \\ & + Q(-k_{r1}(I_{xx_C} - I_{zz_C})(\Omega_{C1} + \Omega_{C2}) + \\ & + R(k_{p2}^2 + k_{p3}k_{r1}) + (\Omega_{T1} + \Omega_{T2})(I_{xx_T} - I_{zz_T})(k_{p2} \cos \phi_T - k_{r1} \sin \phi_T)) + \\ & + R(-k_{r1}L_R + k_{p2}N_R + \dot{\phi}_T(k_{p4}k_{r1} - k_{p2}k_{r3})) + \\ & + \dot{\phi}_T((\Omega_{T1} + \Omega_{T2})(I_{xx_T} - I_{zz_T})(k_{p2} \cos \phi_T - k_{r1} \sin \phi_T)) + \\ & + \tilde{\Omega}_{T1}(B_{T_{T1}}r_{T_{y1}}(k_{p2} \cos \phi_T - k_{r1} \sin \phi_T) - B_{Q_{T1}}(k_{p2} \sin \phi_T + k_{r1} \cos \phi_T)) + \\ & + S_{T_{T1}}r_{T_{y1}}(k_{p2} \cos \phi_T - k_{r1} \sin \phi_T) - S_{Q_{T1}}(k_{p2} \sin \phi_T + k_{r1} \cos \phi_T) + \\ & + \tilde{\Omega}_{T2}(B_{Q_{T2}}(k_{p2} \sin \phi_T + k_{r1} \cos \phi_T) + B_{T_{T2}}r_{T_{y1}}(k_{r1} \sin \phi_T - k_{p2} \cos \phi_T)) + \\ & + S_{Q_{T2}}(k_{p2} \sin \phi_T + k_{r1} \cos \phi_T) + S_{T_{T2}}r_{T_{y1}}(k_{r1} \sin \phi_T - k_{p2} \cos \phi_T) + \\ & + k_{p2}(S_{Q_{C1}} - S_{Q_{C2}} + \tilde{\Omega}_{C1}(C_{Q_{C1}\tilde{\Omega}_{C1}} - C_{Q_{C2}\tilde{\Omega}_{C1}})) + \\ & + \tilde{\Omega}_{C2}(C_{Q_{C1}\tilde{\Omega}_{C2}} - C_{Q_{C2}\tilde{\Omega}_{C2}})) + \\ & + \delta_{Al}(k_{p2}N_{\delta_{Al}} - k_{r1}L_{\delta_{Al}}) + (\dot{\Omega}_{T1} + \dot{\Omega}_{T2})I_{xx_T}(\sin \phi_T k_{p2} + \cos \phi_T k_{r1}) + \\ & - (\dot{\Omega}_{C1} + \dot{\Omega}_{C2})k_{p2}I_{zz_C} \end{aligned} \quad (3.66)$$

$$\begin{aligned}
 \dot{Q} = & \frac{1}{k_{q1}}(UM_U + WM_W + QM_Q + P^2k_{p2} - R^2k_{p2} - 2I_{zz}\ddot{\phi}_T + \\
 & + P(\sin \phi_T(I_{zzT} - I_{xxT})(\Omega_{T1} + \Omega_{T2}) + (I_{zzC} - I_{xxC})(\Omega_{C1} + \Omega_{C2}) - Rk_{q2}) + \\
 & - R \cos \phi_T(I_{xxT} - I_{zzT})(\Omega_{T1} + \Omega_{T2}) + \sin \phi_T(\tilde{\Omega}_{T1}B_{T_{T1}}r_{t_{x1}} + \tilde{\Omega}_{T2}B_{T_{T2}}r_{t_{x2}}) + \\
 & + r_{C_{x1}}(S_{T_{C1}} + S_{T_{C2}} + \tilde{\Omega}_{C1}(C_{T_{C1}\tilde{\Omega}_{C1}} + C_{T_{C2}\tilde{\Omega}_{C1}}) + \tilde{\Omega}_{C2}(C_{T_{C1}\tilde{\Omega}_{C2}} + C_{T_{C2}\tilde{\Omega}_{C2}})) + \\
 & + \delta_{El}M_{\delta_{El}} + S_m)
 \end{aligned} \tag{3.67}$$

$$\begin{aligned}
 \dot{R} = & \frac{1}{k_{dpr}}(V(k_{p2}L_V - k_{p1}N_V) + \\
 & + P(k_{p2}L_P - k_{p1}N_P + \dot{\phi}_T(k_{p1}k_{r4} - k_{p2}k_{p5}) - Q(k_{p2}^2 - k_{p1}k_{r2})) + \\
 & + Q((\Omega_{C1} + \Omega_{C2})k_{p2}(I_{xxC} - I_{zzC}) - Rk_{p2}(k_{p1} + k_{p3}) + \\
 & + (\Omega_{T1} + \Omega_{T2})(I_{xxT} - I_{zzT})(k_{p2} \sin \phi_T - k_{p1} \cos \phi_T)) + \\
 & + R(k_{p2}L_R - k_{p1}N_R + \dot{\phi}_T(k_{p1}k_{r3} - k_{p2}k_{p4})) + \\
 & + p\dot{h}i_T((\Omega_{T1} + \Omega_{T2})(I_{xxT} - I_{zzT})(k_{p2} \sin \phi_T - k_{p1} \cos \phi_T)) + \\
 & + \tilde{\Omega}_{T1}(B_{Q_{T1}}(k_{p1} \sin \phi_T + k_{p2} \cos \phi_T) + B_{T_{T1}}r_{T_{y1}}(k_{p2} \sin \phi_T - k_{p1} \cos \phi_T)) + \\
 & + S_{Q_{T1}}(k_{p1} \sin \phi_T + k_{p2} \cos \phi_T) + S_{T_{T1}}r_{T_{y1}}(k_{p2} \sin \phi_T - k_{p1} \cos \phi_T) + \\
 & + \tilde{\Omega}_{T2}(B_{T_{T2}}r_{T_{y1}}(k_{p1} \cos \phi_T - k_{p2} \sin \phi_T) - B_{Q_{T2}}(k_{p1} \sin \phi_T + k_{p2} \cos \phi_T)) + \\
 & + S_{T_{T2}}r_{T_{y1}}(k_{p1} \cos \phi_T - k_{p2} \sin \phi_T) - S_{Q_{T2}}(k_{p1} \sin \phi_T + k_{p2} \cos \phi_T) + \\
 & + k_{p2}(S_{Q_{C2}} - S_{Q_{C1}} + \tilde{\Omega}_{C1}(C_{Q_{C2}\tilde{\Omega}_{C1}} - C_{Q_{C1}\tilde{\Omega}_{C1}}) + \tilde{\Omega}_{C2}(C_{Q_{C2}\tilde{\Omega}_{C2}} - C_{Q_{C1}\tilde{\Omega}_{C2}})) + \\
 & + \delta_{Al}(k_{p2}L_{\delta_{Al}} - k_{p1}N_{\delta_{Al}}) - (\dot{\Omega}_{T1} + \dot{\Omega}_{T2})I_{xxT}(\sin \phi_T k_{p1} + \cos \phi_T k_{p2}) + \\
 & + (\dot{\Omega}_{C1} + \dot{\Omega}_{C2})k_{p1}I_{zzC})
 \end{aligned} \tag{3.68}$$

The Constants k_i

The k_i parameters contain the terms present in the Equations 3.66-3.67-3.68 which only depend on ϕ_T angle and on design parameters. They are expressed in the following form:

$$k_{p1} = I_{xx_A} + 4I_{xx_C} + 2m_T r_{T_y}^2 + 4I_X X_T \cos^2 \phi_T + 4I_{zz_T} \sin^2 \phi_T \tag{3.69}$$

$$k_{p2} = I_{xz_A} + \sin \phi_T \cos \phi_T (4I_{zz_T} - 4I_{xx_T}) \tag{3.70}$$

$$k_{p3} = -I_{yy_A} + I_{zz_A} - 4I_{xx_C} + 4I_{zz_C} + 2m_T r_{T_y}^2 + \sin^2 \phi_T (4I_{xx_T} - 2I_{zz_T}) + 2I_{zz_T} \cos^2 \phi_T - 2I_{zz_T} \quad (3.71)$$

$$k_{p4} = -2I_{xx_T} \cos^2 \phi_T - I_{xx_T} \cos 2\phi_T + \sin^2 \phi_T (2I_{xx_T} - 4I_{zz_T}) + I_{zz_T} \cos 2\phi_T \quad (3.72)$$

$$k_{p5} = I_{xx_T} (-\sin 2\phi_T) + \sin \phi_T \cos \phi_T (4I_{zz_T} - 4I_{xx_T}) + I_{zz_T} \sin 2\phi_T \quad (3.73)$$

$$k_{q1} = I_{yy_A} + 2m_C r_{C_X}^2 + 4I_{xx_C} + 2m_T r_{T_x}^2 + 4I_{zz_T} \quad (3.74)$$

$$k_{q2} = I_{xx_A} - I_{zz_A} - 2m_C r_{C_X}^2 + 4I_{xx_C} - 4I_{zz_C} - 2m_T r_{T_x}^2 + \sin^2 \phi_T (4I_{zz_T} - 4I_{xx_T}) + \cos^2 \phi_T (4I_{xx_T} - 4I_{zz_T}) \quad (3.75)$$

$$k_{r1} = I_{zz_A} + 2m_C r_{C_X}^2 + 4I_{zz_C} + m_T (2r_{T_x}^2 + 2r_{T_y}^2) + 4I_{xx_T} \sin^2 \phi_T + 4I_{zz_T} \cos^2 \phi_T \quad (3.76)$$

$$k_{r2} = -I_{xx_A} + I_{yy_A} + 2m_C r_{C_X}^2 + m_T (2r_{T_x}^2 - 2r_{T_y}^2) + \cos^2 \phi_T (2I_{zz_T} - 4I_{xx_T}) - 2I_{zz_T} \sin^2 \phi_T + 2I_{zz_T} \quad (3.77)$$

$$k_{r3} = I_{xx_T} \sin 2\phi_T + \sin \phi_T \cos \phi_T (4I_{xx_T} - 4I_{zz_T}) - I_{zz_T} \sin 2\phi_T \quad (3.78)$$

$$k_{r4} = 2I_{xx_T} \sin^2 \phi_T - I_{xx_T} \cos 2\phi_T + \cos^2 \phi_T (4I_{zz_T} - 2I_{xx_T}) + I_{zz_T} \cos 2\phi_T \quad (3.79)$$

$$k_{dpr} = k_{p2}^2 - k_{p1} k_{r1} \quad (3.80)$$

3.5.3 Kinematics Equations

The kinematic equations have been used to relate the body angular velocity $\vec{\omega}_B$ with the Euler rates vector designated with $\dot{\vec{E}}$.

$$\vec{\omega}_B = R_1(\phi)R_2(\theta) \begin{bmatrix} 0 \\ 0 \\ \dot{\psi} \end{bmatrix} + R_1(\phi) \begin{bmatrix} 0 \\ \dot{\theta} \\ 0 \end{bmatrix} + \begin{bmatrix} \dot{\phi} \\ 0 \\ 0 \end{bmatrix} = J^{-1}\dot{\vec{E}} \quad (3.81)$$

Solving for $\dot{\vec{E}}$ leads to:

$$\dot{\vec{E}} = J\vec{\omega}_B \quad (3.82)$$

The last equation represents the three coupled nonlinear kinematic equations, explained below.

$$\begin{cases} \dot{\phi} = p + q \sin \phi \tan \theta + r \cos \phi \tan \theta \\ \dot{\theta} = q \cos \phi - r \sin \phi \tan \theta \\ \dot{\psi} = q \frac{\sin \phi}{\cos \theta} + r \frac{\cos \phi}{\cos \theta} \end{cases} \quad (3.83)$$

3.5.4 Flight Path Equations

The flight path equations are needed to track the desired flight path or hover condition of the aerobot. It's possible to obtain the velocity expressed in the inertial reference system starting from the velocity in the body frame and through the rotational matrix R_{B2I} as explained below.

$$\vec{V}_I = R_{B2I}\vec{V}_B \quad (3.84)$$

$$\begin{cases} \dot{X} = U \cos \theta \cos \psi + V(\sin \phi \sin \theta \cos \phi - \cos \phi \sin \psi) \\ \dot{Y} = U \cos \theta \sin \psi + V(\sin \phi \sin \theta \sin \phi + \cos \phi \sin \psi) \\ \dot{Z} = -U \sin \theta + V \sin \phi \cos \theta + W \cos \phi \cos \theta \end{cases} \quad (3.85)$$

3.6 Simplified Equations

It is quite common in martian aerobot preliminary studies to simplified the dynamic model, as for Mars Helicopter [4] and this section is intended to illustrate how it is possible to simplify the dynamics equations [34].

Only horizontal straight and hover flight are considered for a preliminary analysis of Y4_TR Aerobot dynamics behaviour in Mars enviroment. As example, analyzing the first Translation Equation (Equation 3.42), considering horizontal straight flight:

- $\phi_T = 0^\circ \rightarrow \cos \phi_T = 1$;
- Expressing aerodynamics forces in X_B direction as X ;
- representing rotor thrust along X_B with T_X .

The equation can be simplified as:

$$\dot{U} = (RV - QW) - g \sin \theta + X/m + T_x/m \quad (3.86)$$

Applying the same procedure to the other equations, it's possible to simplified Translation and Rotational Dynamics Equation as follow:

- Translation Dynamics

$$\begin{cases} \dot{U} = (RV - QW) - g \sin \theta + X/m + T_x/m \\ \dot{V} = (PW - RU) + g \sin \phi \cos \theta + Y/m \\ \dot{W} = (QU - PV) + g \cos \phi \cos \theta + Z/m + T_z/m \end{cases} \quad (3.87)$$

- Rotational Dynamics

$$\begin{cases} \dot{P} = -(I_z - I_y)QR/I_x + (PQ + \dot{R})I_{xz}/I_x + L/I_x \\ \dot{Q} = -(I_x - I_z)PR/I_y - (P^2 - R^2)I_{xz}/I_y + M/I_y \\ \dot{R} = -(I_y - I_x)PQ/I_z - (QR + \dot{P})I_{xz}/I_z + N/I_z \end{cases} \quad (3.88)$$

Chapter 4

Development of the Y4-TR Martian Aerobot Dynamics Simulator

4.1 Introduction

The purpose of this chapter is to illustrate the overall simulator structure and the implementation of the complete dynamics model of the Y4-TR MATLAB/Simulink environment.

Moreover, as illustrated in the Chapter 3, the equations that describe the dynamics of the aerobot can be simplified in straight horizontal flight condition and hovering too; in this way is possible to obtain the classical equations of the flight dynamics. Also these last equations will be implemented in a new Simulink model (CFME Model), and compared with the complete dynamic model to verify two equation system equivalence in horizontal and hover flight condition.

The second describes the overall structure of the simulator, subdividing the operations that it performs in steps. Then, the algorithms and strategies used to determine the trim conditions and the relative results are presented. The Section 4.4.1 conceptually describes the implementation in Simulink of the complete and simplified dynamic model.

Both the dynamics models have been tested in the two flight conditions (horizontal and hover) and the obtained results are compared with each other in the last section of the chapter. As the results show, it is possible to use a simplified system of equations in the case of the analysis of the drone dynamics in horizontal flight and in hover. However, the same assumption cannot be used when the transition phase is analyzed, for which the non linear model should be exploited.

4.2 General Simulator Structure

The simulator has been designed to include both the nonlinear model of the drone dynamics and the CFME Model. The main structure consists of:

- A pre-processing block composed by composed by the list of Matlab subroutines, reported in the Table 4.1, that allow to import constants and models and to determine the trim conditions.
- Two Simulink models: the Y4_TR.slx that describes the complete dynamic model and the CFME.slx that implements the simplified dynamics.

Matlab Script and Models	
Subroutines	Used to
ImportConstants.m	Import the constants which not depend on flight condition
InputVariables.m	Specify the flight conditions and import the relative variables
massmodel.f	Implement the aerobot mass model described in the chapter 2(TBC)
Atm.f	Implement the Martian atmosphere model described in the chapter 2(TBC)
InertiaModel.f	Implement the aerobot inertia model described in the chapter 2(TBC)
TrimCondition.m	Implement the algorithm to determine the trim variables based on flight conditions

Table 4.1: Matlab Subroutines implemented in the Aerobot Simulator

The overall scheme of the simulator and how it works can be described through the flow chart reported in the Figure n.nn that illustrates the following steps:

- 1) First, all the constant variables related to the aerobot body and the rotors features that are independent of flight condition are imported with the ImportConstants file. The massmodel, for example, is recalled by ImportConstants subroutine since the aerobot mass is assumed constant.
- 2) Through InputVariables it's possible to define the flight conditions to analyze: horizontal straight flight or hovering condition; the transitions phase from take-off to horizontal flight has been neglected in this preliminary study.
- 3) Based on the choice made at the previous point all the variables which depends on flight condition are set, such as:

- V - cruise speed ;
 - ϕ_T - tilt-rotors angle.
 - h - nominal cruise altitude.
 - Ω - rotors rotational speed.
 - The aerobot configuration (Open/Closed).
 - $C_\alpha, C_{M\alpha}, C_{M\delta_{El}}$ - aerodynamic derivatives
 - C_{L0}, C_{D0} - aerodynamic coefficients.
 - The Atmospheric Parameters with the Atm Model basing on
- 4) Once all the variables have been set, the trim conditions are determined by recalling TrimCondition that implements a classical approach of flight mechanics (Section 4.3). Then, all the aerodynamic forces are expressed in a form suitable for the Y4_TR complete dynamics and the CFME Simulink models; i.e. in the form expressed by the equations n.n (tbi).
- 5) Finally, it's possible to choose which Simulink model to execute and get the results that show the trend of the variables describing the aerobot dynamic model and its motion over the simulation set time.

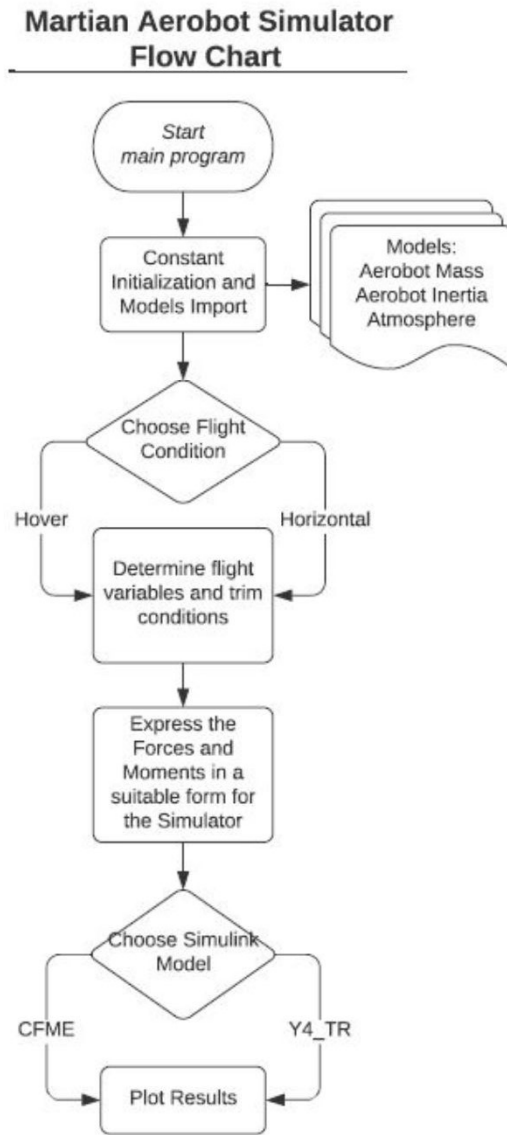


Figure 4.1: Martian Aerobot Simulator Flow Chart

4.3 Trim Conditions Determination

The trim conditions are determined based on flight condition and the algorithm used for the horizontal flight trim and strategy adopted for the flight in hover will be illustrated in this section.

4.3.1 Horizontal flight conditions

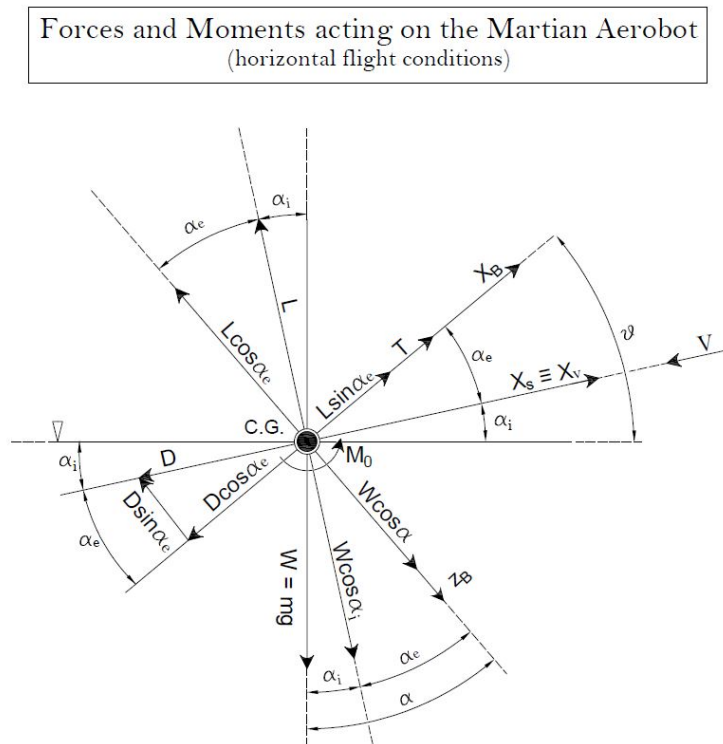


Figure 4.2: Forces acting on the Aerobot in the Horizontal Flight conditions

The scheme of forces and moments reported in the Figure 4.1 presents the forces and moments and their projections acting on the Aerobot CoM and considered to find the horizontal flight trim conditions. In particular:

- L is the total lift
- D is the aerobot resistance
- T is the total torque
- α_e is the equilibrium angle of attack

- α_i is the induced angle
- θ is the pitch angle
- W is the aerobot weight applied at CoM

Moreover, also their projections along body and inertial axes are reported. They are considered in order to define the thrust and moments acting in X_B and Z_B directions.

The algorithm used to determine trim conditions is a iterative process synthesized in the Figure 4.3 and it can be described through the following steps:

- All the constant variables have been declared through the first step described in the overall structure. The variables used in this algorithm include:
 - C_{L0}, C_{D0}
 - The V in horizontal flight condition
 - α_i
- The process starts by setting:
 - A maximum and minimum values for the equilibrium angle of attack, respectively $\alpha_{e_{max}} = 10^\circ$ and $\alpha_{e_{min}} = -10^\circ$.
 - The starting values of $\alpha_e = \alpha_{e_{min}}$.
 - The step variation of α_e for each iteration equal to 0.001 rad .
 - The tolerance $toll$ set at 0.001.
- The first step of the algorithm is to determine the lift and drag coefficient, and the force component along the z_B axis through the equations reported below.

$$C_L = C_{L0} + C_{L\alpha}\alpha_e \quad (4.1)$$

$$C_D = C_{D0} + \frac{C_L^2}{\pi AR} \quad (4.2)$$

$$C_Z = -(C_L \cos(\alpha_e) + C_D \sin(\alpha_e)) \quad (4.3)$$

$$Z_B = \frac{1}{2}C_Z\rho SV^2 \quad (4.4)$$

$$W_B = mg \cos(\alpha_e + \alpha_i) \quad (4.5)$$

- The component of the force determined with the Equation 4.4 is compared with the weight component W_B along the z_B axis as reported in the Equation 4.5 . If their difference is greater than the set tolerance, the process restarts and the α_e is incremented of the imposed step variation. Otherwise the found value of α_e is set as $\alpha_{e_{TRIM}}$ and, finally, it's possible to determine the other trim conditions trough the equations illustrated below.

- The elevon deflection:

$$\delta_{El} = -\frac{C_{m0} + C_{m\alpha}\alpha_e}{C_{m\delta_{El}}} \quad (4.6)$$

- The pitch angle:

$$\theta = \alpha_{e_{TRIM}} + \alpha_i \quad (4.7)$$

- The Drag and Lift components:

$$L = qSC_L; \quad D = qSC_D \quad (4.8)$$

where S is the aerobot lifting surface in the Closed Configuration and $q = \frac{1}{2}\rho V^2$ is the dynamic pressure.

- The Trim Thrust generated by both tilt-rotors:

$$T_{TRIM} = 2 C_{T_{tilt}} \rho A_t R_t^2 \Omega_T^2 \quad (4.9)$$

where:

- * $C_{T_{tilt}}$ is the single tilt rotor thrust coefficients derived as described in the Section n.n.
- * Ω_T is the tilt rotors rotational speed, that is determined as reported in the Section n.n.n. The two tilting-rotors are counter-rotating, but their rotation speed in equal in module for the nominal horizontal flight condition.
- * A_t is the tilt rotor surface and R_t represents its radius.

The results have been showed in the Table 4.2 and can be used to run both Y4_TR and CFME models.

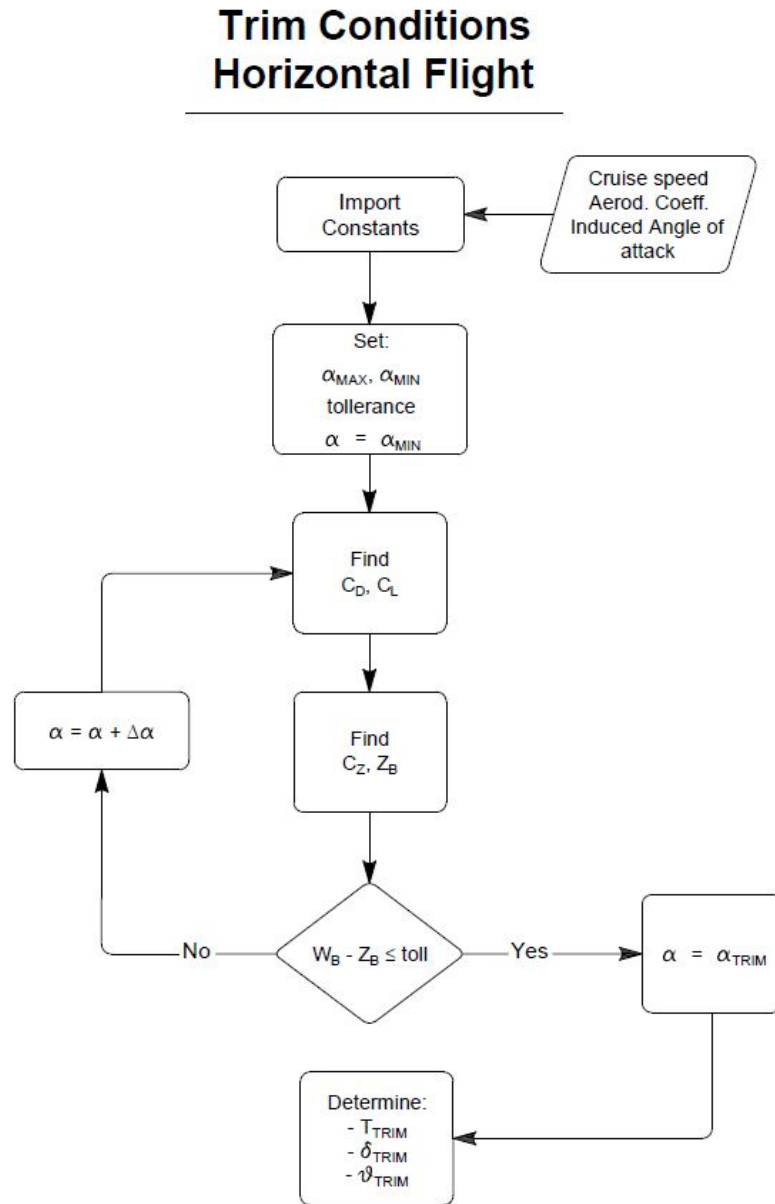


Figure 4.3: Trim Conditions in Horizontal Flight - Flow Chart

4.3.2 Hover Flight Conditions

Looking at the scheme of the forces shown in the Figure 2.6 where the X_B axis is considered aligned with the horizon line, the desired trim thrust necessary to

sustain the flight in the hovering conditions has been determined knowing the aerobot weight W as

$$T_{TRIM} = T_{tilt_{TOT}} + T_{coax_{TOT}} = W \quad (4.10)$$

The tilt-rotor thrust is set at the 10% of the total thrust necessary to sustain flight in hover condition [3]. Considering this assumption the thrust generated by the rotors (tilting and coaxial rotors system) can be determined as

$$T_{tilt_{TOT}} = 0.1 W , T_{coax_{TOT}} = 0.9 W \quad (4.11)$$

$$C_T = \frac{T_{TRIM}}{\rho A \Omega^2 R^2} \quad (4.12)$$

The trim rotation speed Ω of the tilt and coaxial- rotors can be calculated starting from the relative C_T determined in the Section n.n.n and by inverting the Equation 4.12, where:

- A is the rotor section area.
- R is the rotor radius.
- Ω is the rotation rotor speed.

4.4 Simulink Models

The intent of this Section is to describe the Simulink models developed for the simulation of the complete and simplified dynamics of the Y4-Tilt Rotor Aerobot. As reported in the introduction paragraph, the Y4_TR Model implements the complete non-linear dynamics of the aerobot, while the CFME Model describes the simplified drone dynamics and, as remarked in Chapter 3(tbi).

For both models the variables, which have been defined through the passages illustrated in paragraph 4.2 and that remain constant, are recalled. In particular, these data relate to:

- The geometric design data of the aerobot.
- The ϕ_T angle.
- The aerobot mass and inertia.

Moreover, for the Y4_TR complete model the constant k_i are determined by implementing the Equations n-n in Simulink and they are assumed to be constant considering that ϕ_T does not change during all the simulation time.

4.4.1 Y4_TR Model

The Figure 4.3 illustrates a general overview of the feedback closed loop system build in Simulink to describe and control the complete dynamics and the motion of the aerobot. The model is composed by:

- The blocks that describe the translation and rotation dynamics described by the Second Newton's Law and by the Euler's equations, that implements the set of the six non-linear equations given by n.n.n-n.n.n(tbi). The translation dynamics subsystem receives as input the components of the translation and rotation velocity expressed into the body frame(U, V, W, P, Q, R), the kinematics angles ϕ and θ and the control input; while the block related to the rotation dynamics takes in input only the control inputs and U, V, W, P, Q, R .
- The Kinematics Equations subsystem, that allows to determine the aerobot orientation referring to the MI Reference through the angles ϕ, θ, ψ . It takes as input the body rotation velocity components and the angles ϕ and θ that come out from the same block at the next simulation step.
- The Flight Path Equation subsystem, that represents the Inertial Navigation Equations used to establish the aerobot position respect to the MI Reference system (Equations n.n.n-n.n.n)

- The disturbances block that is added to the feedback variables. As will be discussed in the Chapter 5, the main source of disturbance for the aerobot flying in the Mars environment will be the presence of the wind and the oscillation from its mean value. These disturbs can be translated in terms of perturbations of U and W velocity components.

In the same figure the controller and its allocation are represented too. The control block takes as input the tracking error determined as the difference between the desired reference value and the variables values coming from the feedback line at the i -th instant of simulation. However, the controller design will be discussed more in detail in the Chapter 6.

The references, as well as the initialization values of the variables, have been set at the trim condition for the chosen flight condition and determined as described in the Paragraph 4.3.

4.4.2 CFME Model

The general structure of the CFME Simulink model is similar to the Y4_TR one described in the previous paragraph. However, as remarked in the introduction, the dynamics equations in the case of horizontal flight and hover flight can be simplified. The obtained system of equations represents the classical set of the the flight mechanics equations; therefore the blocks related to rotational and translational dynamics will be modified by implementing the Equations n.nn and n.nn in Simulink as illustrated by the conceptual scheme reported in the Figure 4.6.

4.5 Test and Results

Both Simulink models have been tested in horizontal and hover flight conditions in absence of the disturbances and with the control inputs set to the trim value. In this section the results deriving from these simulation will be presented and commented.

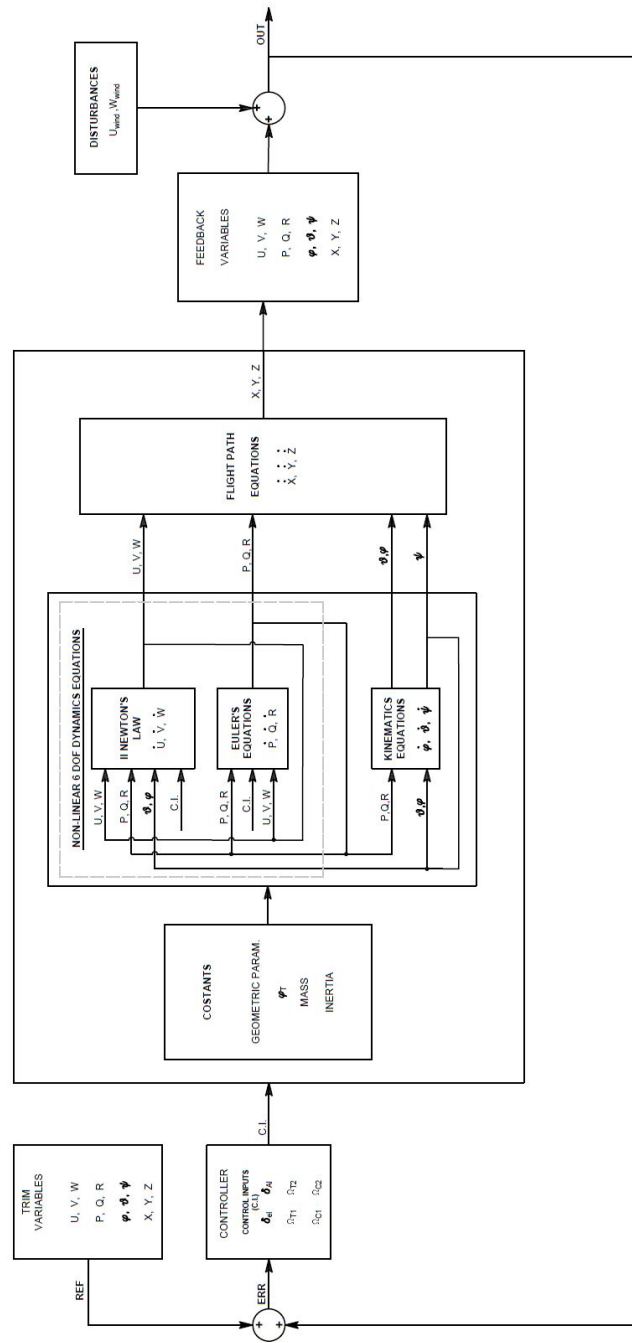


Figure 4.4: Y4_TR Simulink Model

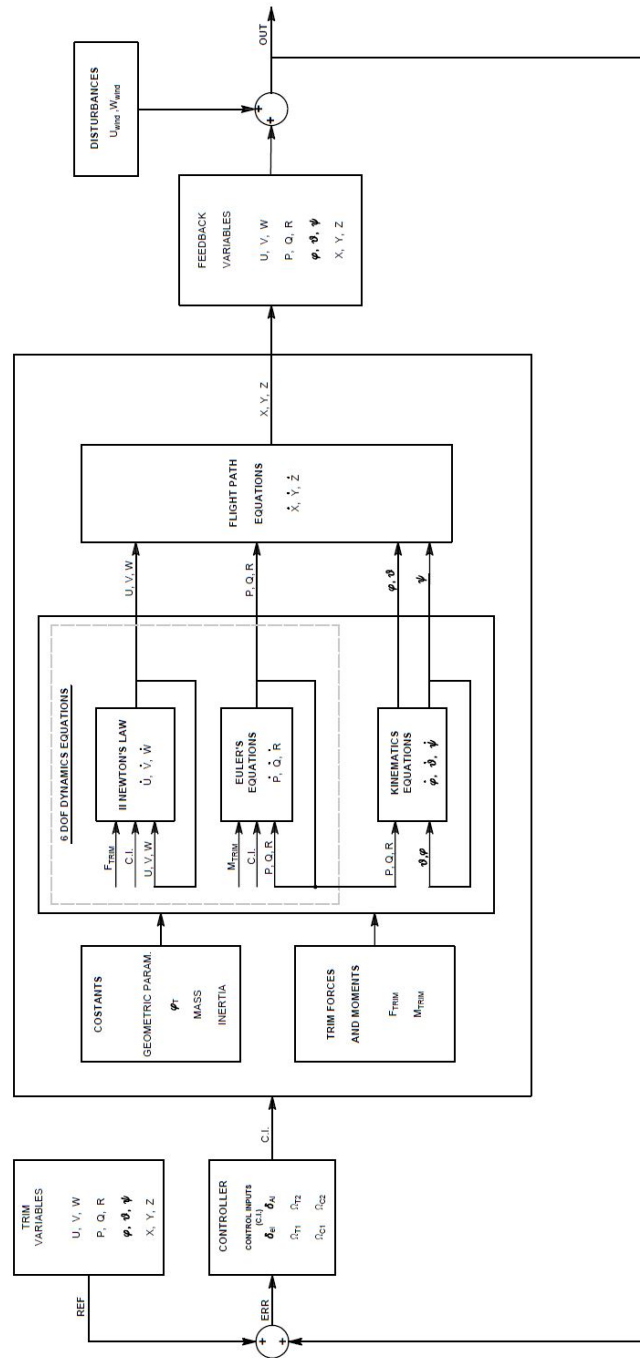


Figure 4.5: CFME Simulink Model

4.5.1 Test in Horizontal Straight Flight

In the horizontal flight conditions the variables were initialized as presented in the second column of Table 4.2 and the simulation time is set to the total duration of the mission that the aerobot will perform. In the third column of the same table have been presented the expected results at the end of simulation.

In the Table 4.3 the control inputs settings for the longitudinal horizontal flight are reported. The elevon angle has been determined with the trim condition analysis, while the rotation speeds have been assumed equal to the values given by Collins [3]. For the horizontal flight only the tilting rotors are involved, indeed the aerobot is in the Closed Configuration during the straight flight and the coaxial rotors are covered and their rotation speed is equal to zero.

Vectors Initialization		
Parameter	Set to	$t_f = 3600s$
X	$0\ m$	$1000\ m$
Y	$0\ m$	$0\ m$
Z	$h_{TRIM} = -1000\ m$	$-1000\ m$
V	$0\ m/s$	$0\ m/s$
U	$V \cos \alpha_{e(TRIM)} = 49.8782\ m/s$	$49.8782\ m/s$
W	$V \sin \alpha_{e(TRIM)} = 3.48\ m/s$	$3.48\ m/s$
θ	4.4°	4.4°
ϕ, ψ	0°	0°
p, q, r	$0\ rad/sec$	$0\ rad/sec$

Table 4.2: Variables Initialization for Horizontal Straight Flight

Control Input Settings	
Parameter	Set to
δ_{AI}	0°
δ_{EI}	-1°
$\Omega_{T_{1,2}}$	$290\ rad/sec$
$\Omega_{C_1}, \Omega_{C_2}$	$0\ rad/sec$

Table 4.3: Control Input Settings - Trim in Horizontal Conditions

The variables behaviour in function of the time have been tabled in the figures reported in the Section 4.5.3. As expected, their values for both the Y4_TR and CFME Model are time invariant in the absence of the disturbances excepting for the X variable that increases linearly over time since a trajectory to follow has not yet been assigned in this section; later, in Chapter 6, the drone’s behavior will be analyzed in presence of disturbances and for an assigned trajectory.

4.5.2 Test in Hover Flight

Table 4.4 reports the initialization values of the variables used to test both the Simulink models in hover flight conditions. The nominal altitude is assumed to be the same than the previous case, while the X is expected to remains constant at the initial set position. In hover flight condition the aerobot is in the Open Configuration, so the rotation speed of the coaxial rotors it’s not zero, but they have been imposed at the trim values suggested by Collins [3].

The results for both Simulink models in horizontal and hover conditions have been reported in the Section 4.5.3, in both cases the behavior of the functions respects the expected values.

Vectors Initialization		
Parameter	Set to	$t_f = 3600s$
X, Y	$0 m$	$0 m$
Z	h_{TRIM}	$-1000 m$
U, V, W	$0 m/s$	$0 m/s$
θ, θ, ψ	0°	0°
p, q, r	$0 rad/sec$	$0 rad/sec$

Table 4.4: Variables Initialization for Flight in Hover

Control Input Settings	
Parameter	Set to
δ_{Al}, δ_{El}	0°
$\Omega_{T_{1,2}}$	$297rad/sec$
Ω_{C_1}	$183rad/sec$
Ω_{C_2}	$181rad/sec$

Table 4.5: Control Input Settings - Trim in Hover Conditions

Chapter 5

System Linearization and Disturbances Modelling

5.1 LTI System

In compliance with the approach proposed in [4] for the preliminary analysis of UAVs behavior on Mars, the Y4-TR dynamics linearized considering horizontal straight flight as equilibrium conditions. In order to linearize the equations of motion it is supposed that the fundamental variables can be expressed as the sum of their equilibrium value and an unknown perturbation, that means:

$$\begin{cases} U = U_0 + u, V = V_0 + v, W = W_0 + w \\ P = P_0 + p, Q = Q_0 + q, R = R_0 + r \\ X_{E,G} = X_{E,G0} + x_{E,G}, Y_{E,G} = Y_{E,G0} + y_{E,G}, Z_{E,G} = Z_{E,G0} + z_{E,G} \\ \Phi = \Phi_0 + \phi, \Theta = \Theta_0 + \theta, \Psi = \Psi_0 + \psi; \end{cases} \quad (5.1)$$

where the perturbations are indicated with lowercase letters, while the subscript 0 indicates the reference equilibrium condition.

The same will also be done for control efforts and throttle.

$$\mathbf{u}(t) = \mathbf{u}_0 + \Delta\mathbf{u}(t) = [\delta_{a0} + \delta_a(t), \delta_{e0} + \delta_e(t), \delta_{T0} + \delta_T(t)]^T \quad (5.2)$$

5.1.1 Linearized Dynamics Equations

By replacing the Equations 5.1 in the simplified translation Equations 3.87 and remembering that by definition of stationary initial conditions:

$$\frac{dU_0}{dt} = \frac{dV_0}{dt} = \frac{dW_0}{dt} = 0 \quad (5.3)$$

It follows that:

$$\begin{cases} m(\dot{u} + W_0q + Q_0w - R_0v - V_0r) = \Delta X_G + \Delta X_A + \Delta X_T \\ m(\dot{v} + U_0r + R_0u - P_0w - W_0p) = \Delta Y_G + \Delta Y_A + \Delta Y_T \\ m(\dot{w} + V_0p + P_0v - Q_0u - U_0q) = \Delta Z_G + \Delta Z_A + \Delta Z_T \end{cases} \quad (5.4)$$

As an example, the last of the Equations 5.4 relative to the translation along the axis Z_B) is analyzed considering Equation 5.3:

$$\begin{aligned} m[(0 + \dot{w}) + (P_0 + p)(V_0 + v) - (Q_0 + q)(U_0 + u)] = \\ (Z_{G0} + \Delta Z_G) + (Z_{A0} + \Delta Z_A) + (Z_{T0} + \Delta Z_T) \end{aligned} \quad (5.5)$$

Simplifying the equal terms and neglecting small terms (pv equ), it follows that:

$$m(P_0V_0 - Q_0U_0) = \Delta Z_{G0} + Z_{A0} + Z_{T0} \quad (5.6)$$

So you get:

$$m[\dot{w} + P_0v + pV_0 + pv - Q_0u - qU_0 - qu] = \Delta Z_G + \Delta + \Delta Z_T \quad (5.7)$$

The same procedure is applied to Equations, obtaining the linearized rotational equations.

$$\begin{cases} I_{xx}\dot{p} - I_{xz}\dot{r} - I_{xz}(P_0q - Q_0p) - (I_{yy} - I_{zz})(Q_0r + R_0q) = \Delta L_A + \Delta L_T \\ I_{yy}\dot{q} - 2I_{xz}(R_0r - P_0p) - (I_{zz} - I_{xx})(R_0p + P_0r) = \Delta M_A + \Delta M_T \\ I_{zz}\dot{r} - I_{xz}\dot{p} - I_{xz}(Q_0r + R_0q) - (I_{xx} - I_{yy})(P_0q + Q_0p) = \Delta N_A + \Delta N_T \end{cases} \quad (5.8)$$

5.1.2 Perturbations of the Weight Components

In this section the perturbed gravitational actions are linearized starting with the following set of equation:

$$\begin{cases} \Delta X_G = -mg_{\mathcal{G}} \sin(\theta) \\ \Delta Y_G = -mg_{\mathcal{G}} (\cos \theta \sin \phi) \\ \Delta Z_G = mg_{\mathcal{G}} (\cos \theta \cos \phi) \end{cases} \quad (5.9)$$

The Euler's angles are expressed as a combination of initial values and perturbations:

$$\Theta = \Theta_0 + \theta, \quad \Phi = \Phi_0 + \phi, \quad \Psi = \Psi_0 + \psi \quad (5.10)$$

Substituting the following trigonometric relationship in Equation 5.9:

$$\begin{aligned}
 \cos(\Phi_0 + \phi) &\simeq \cos(\Phi_0) - \phi \sin(\Phi_0) \\
 \cos(\Theta_0 + \theta) &\simeq \cos(\Theta_0) - \theta \sin(\Theta_0) \\
 \sin(\Theta_0 + \theta) &\simeq \sin(\Theta_0) + \theta \cos(\Theta_0) \\
 \sin(\Phi_0 + \phi) &\simeq \sin(\Phi_0) + \phi \cos(\Phi_0)
 \end{aligned} \tag{5.11}$$

And with the hypothesis of small perturbations, that allows to impose:

$$\cos(\phi) \simeq 1, \sin(\phi) \simeq \phi, \cos(\theta) \simeq 1, \sin(\theta) \simeq \theta \tag{5.12}$$

The perturbations of weight components in body axes are obtained:

$$\begin{cases}
 \Delta X_G = -mg_{\mathcal{G}} \cos(\Theta_0)\theta \\
 \Delta Y_G = -mg_{\mathcal{G}} (\sin(\Theta_0) \sin(\Phi_0)\theta + \phi \cos(\Theta_0) \cos(\Phi_0)) \\
 \Delta Z_G = -mg_{\mathcal{G}} (\sin(\Theta_0) \cos(\Phi_0)\theta + \phi \cos(\Theta_0) \sin(\Phi_0))
 \end{cases} \tag{5.13}$$

Moreover, in Horizontal trim conditions they become:

$$\begin{cases}
 \Delta X_G = -mg_{\mathcal{G}} \cos(\Theta_0)\theta \\
 \Delta Y_G = mg_{\mathcal{G}} \cos(\Theta_0)\phi \\
 \Delta Z_G = -mg_{\mathcal{G}} \sin(\Theta_0)\theta
 \end{cases} \tag{5.14}$$

5.1.3 Linearized Kinematics Equations

The kinematics equations, in the case of horizontal straight flight, can be simplified:

$$\dot{\phi} = p, \dot{\theta} = q, \dot{\psi} = r \tag{5.15}$$

This equation is valid only for the analysis of linearized equations and for the analyzed flight condition (horizontal flight).

5.1.4 State Space Representation

Linearizing dynamics equations and considering straight horizontal flight conditions it's possible to separate longitudinal and lateral dynamics and rewrite the complete system as:

$$\dot{x}_{Lon} = A_{Lon}x_{Lon} + B_{Lon}u_{Lon} \tag{5.16}$$

$$\dot{x}_{Lat} = A_{Lat}x_{Lat} + B_{Lat}u_{Lat} \tag{5.17}$$

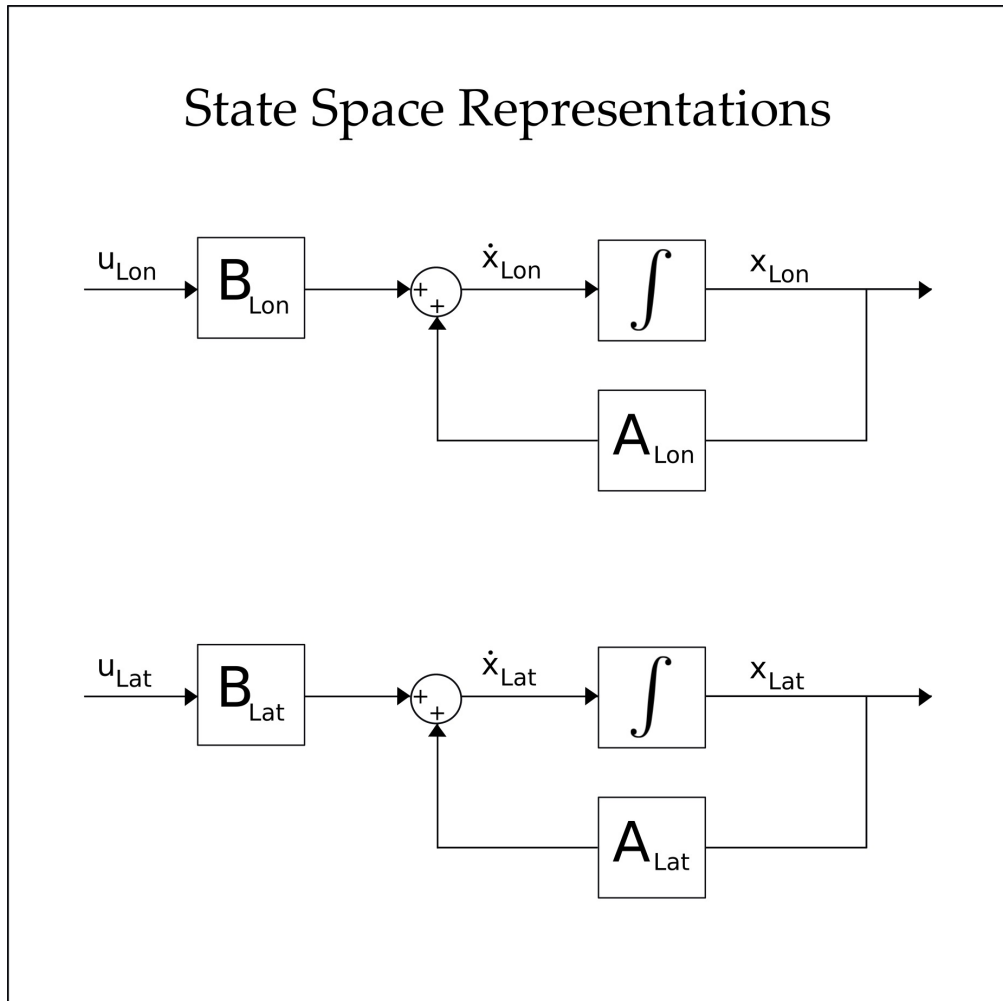


Figure 5.1: State Space Representation

Equation 5.17 is given by:

- x_{Lon} is the longitudinal state vector in terms of perturbations from equilibrium point

$$x_{Lon} = [u, q, w, \theta, h] \quad (5.18)$$

With h the altitude by the third of Equations 3.82.

- u is the longitudinal controls vector

$$u_{Lon} = [\delta_{El}, \Omega_{T1}, \Omega_{T2}] \quad (5.19)$$

- A_{Lon} is the state matrix, reported in Appendix C

- B_{Lon} is the input-to-state matrix, reported in Appendix C

The terms in the Equation 5.18 represent:

- x_{Lat} is the lateral state vector in terms of perturbations from equilibrium point

$$x_{Lat} = [v, p, r, \phi, \psi] \quad (5.20)$$

With h that represents the altitude and is given by the third of Equations 3.82.

- u_{Lat} is the lateral controls vector

$$u_{Lat} = [\delta_{Al}, \Omega_{T1}, \Omega_{T2}] \quad (5.21)$$

- A_{Lat} is the state matrix, reported in Appendix C
- B_{Lat} is the input-to-state matrix, reported in Appendix C

5.2 Martian Disturbances Analysis

The purpose of this section is to analyze the possible sources of disturbance acting on the aerobot to design an appropriate control law.

The analysis started from the study of the parameters whose variations mostly affect the drone flight [3] [32]; among the main ones it is possible to list:

- Atmospheric tides
- Gravity field variation
- Topography
- Wind

The one that most influences the dynamics of the Martian drone is the wind [3], whose model implemented in Simulink is detailed in the Section 5.2.2

5.2.1 Atmospheric tides

The local Mars atmospheric properties depend on several factors including: solar cycles, dust levels, geographical location and season [3] [32]. While Mars does have defined months, it is often easier to measure time in Solar Longitude (LS) as described in Figure 5.2. The varying incident insolation over the course of a Martian day causes large differences in surface temperature between day and night.

Month Number	Ls Range (Degrees)		Sol Range		Duration (in sols)	Notes
1	0	30	0.0	61.2	61.2	Northern Hemisphere Spring Equinox at Ls=0
2	30	60	61.2	126.6	65.4	
3	60	90	126.6	193.3	66.7	Aphelion (largest Sun-Mars distance) at Ls=71
4	90	120	193.3	257.8	64.5	Northern Hemisphere Summer Solstice at Ls=90
5	120	150	257.8	317.5	59.7	
6	150	180	317.5	371.9	54.4	
7	180	210	371.9	421.6	49.7	Northern Hemisphere Autumn Equinox at Ls=180 Dust Storm Season begins
8	210	240	421.6	468.5	46.9	Dust Storm Season
9	240	270	468.5	514.6	46.1	Perihelion (smallest sun-Mars distance) at Ls=251 Dust Storm Season
10	270	300	514.6	562.0	47.4	Northern hemisphere Winter Solstice at Ls=270 Dust Storm Season
11	300	330	562.0	612.9	50.9	Dust Storm Season
12	330	360	612.9	668.6	55.7	Dust Storm Season ends

Figure 5.2: Martian Seasons and Solar Longitude

For example the diurnal variation of surface temperature can be as large as 100 K in regions characterized by low thermal inertia. These variation also gives rise to global oscillations in atmospheric pressure, temperature, and winds [32].

The most important information concerning thermal tides were taken with the MGS mission [33] [32]: the diurnal thermal tide was found to have an amplitude of about 4 K, defined as the deviation from the mean temperature state, with larger amplitudes (exceeding 8 K) during the dustiest conditions.

The observation of semidiurnal tides (with a period of half a solar day) also goes back to the Viking Orbiter observations [32]. While in a clear atmosphere the diurnal tide is dominant in the Martian tropics, the amplitude of the semidiurnal tide increased with increasing dust loading as solar heating became distributed over a larger part of the atmosphere [32]. With the MGS mission a maximum amplitude of about 16 K is found at southern high latitudes at altitudes of 5–7 scale heights during the southern winter season. During the northern winter season, comparable semidiurnal amplitudes are observed in the northern high latitudes, and also at low latitudes the semidiurnal amplitude can reach 6–8 K.

Since Y4-TR is designed to fly during spring or summer Mars seasons, with a

Operation Time of $1h$, the effects of diurnal and semi-diurnal tides can be neglected.

5.2.2 Gravity field variation

The gravitational force on Mars is less than the terrestrial one, and is not uniform across the planet's surface. Due to Red Planet's ellipsoid shape, its surface gravity varies both with altitude and latitude, with higher gravitational forces at low altitudes and high latitudes over the poles [3] [32].

The aerobot will fly relatively close to the Martian surface, $h < 1000m$, so the gravitational constant is assumed to be constant equal to $3.72 m/s^2$ over the Isidis Planitia region as shown in Figure 5.3 [3].

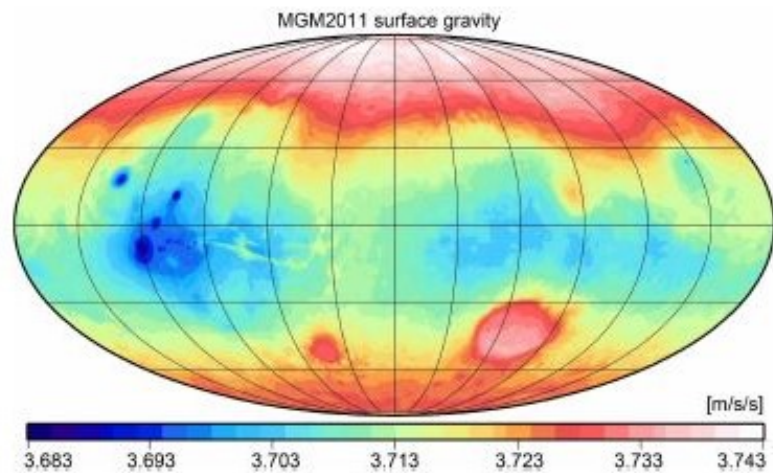


Figure 5.3: Global Gravity Map of Mars [35]

5.2.3 Topography

Mars has some of the most extreme topography in the solar system and it has also the tallest mountain and largest canyon system. In this work Isidis Planitia has been selected as Mission Location [3]. It represents an ideal region for the aerobot for several reasons, both scientifically and engineering ones.

Isidis Planitia is a large and circular plain with a low latitude and low elevation. Since it is situated so close to Mars' equator the solar radiation will hit the aerobot's solar cells at a higher incident angle allowing higher power generation than at higher latitudes. The lower elevation will aid the aerobot while flying due to the higher atmospheric density. It is also relatively flat on the inner portions of the plain where the aerobot is planned to fly. This will aid with navigation tasks and finding safe landing sites for the aerobot throughout its mission [3].

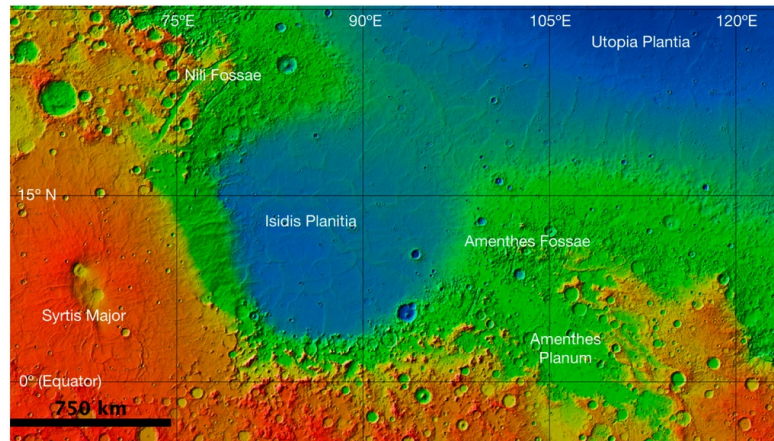


Figure 5.4: Isidis Planitia

5.2.4 Wind

As shown in Figure 3.2, during the summer period the Martian winds are fairly mild on the surface, and are slightly stronger at the mission altitude of 1000m. The wind speeds increase during the the dust storm seasons and winter. The force of the Martian winds is an order of magnitude smaller than on Earth due to the lower atmospheric density.

Considering the mission location Isidis Planitia it's possible to analyze the winds average during different seasons. During the dust Devils Storm Seasons ($L_s = 270^\circ$) the winds reach up about 15 m/s, and they would be a problem for the aerobot flight, for this reasons it has been designed to operate during $L_s = 0^\circ$ and $L_s = 90^\circ$.

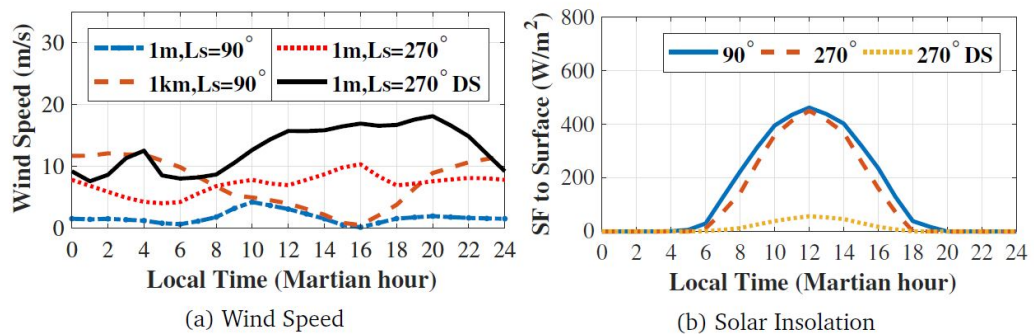


Figure 5.5: Daily Wind Speeds and Solar Insolation for Isidis Planitia During Summer, Winter, and Dust Storm Conditions

5.2.5 Wind Disturbances Model

A simplified disturbances model is obtained recovering mean wind intensity values in horizontal and vertical direction through MCD [12] for a time window between 12AM and 13PM with a 1 minute sample time, that is Y4-TR Operation Time [3] (Figure 2.2). Then, a Matlab function has been created to interpolate the obtained values, deriving the trend of the mean disturbances due to the average wind for each instant of simulation.

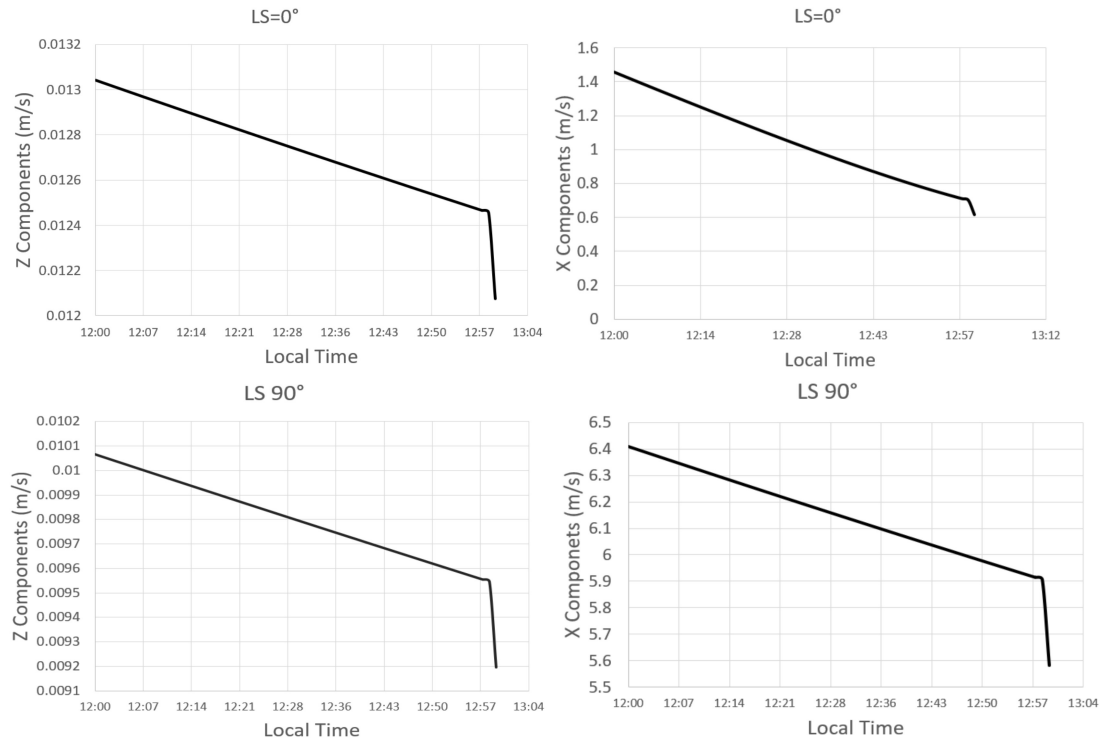


Figure 5.6: Wind Components in Spring and Summer

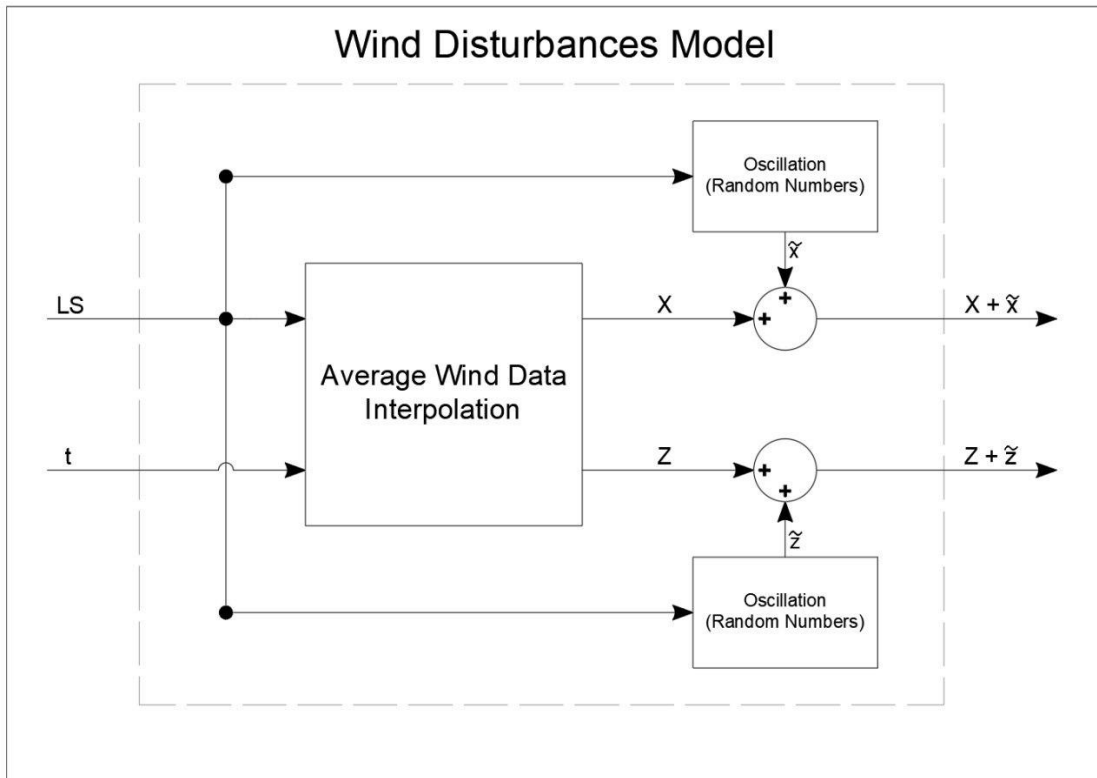


Figure 5.7: Wind Disturbance Model

Figure 5.7 represents the final wind model implemented in the simulator. In order to include possible oscillations from the mean value, blocks of random numbers has been added to the model considering the variances of the value reported in Figure 5.6. The outputs of the Disturbances Model Block are the wind components along the longitudinal and vertical direction for the selected LS , reported in Figure 5.8. Results for both $LS = 0^\circ$ and $LS = 90^\circ$ are used to test aerobot model in horizontal flight conditions.

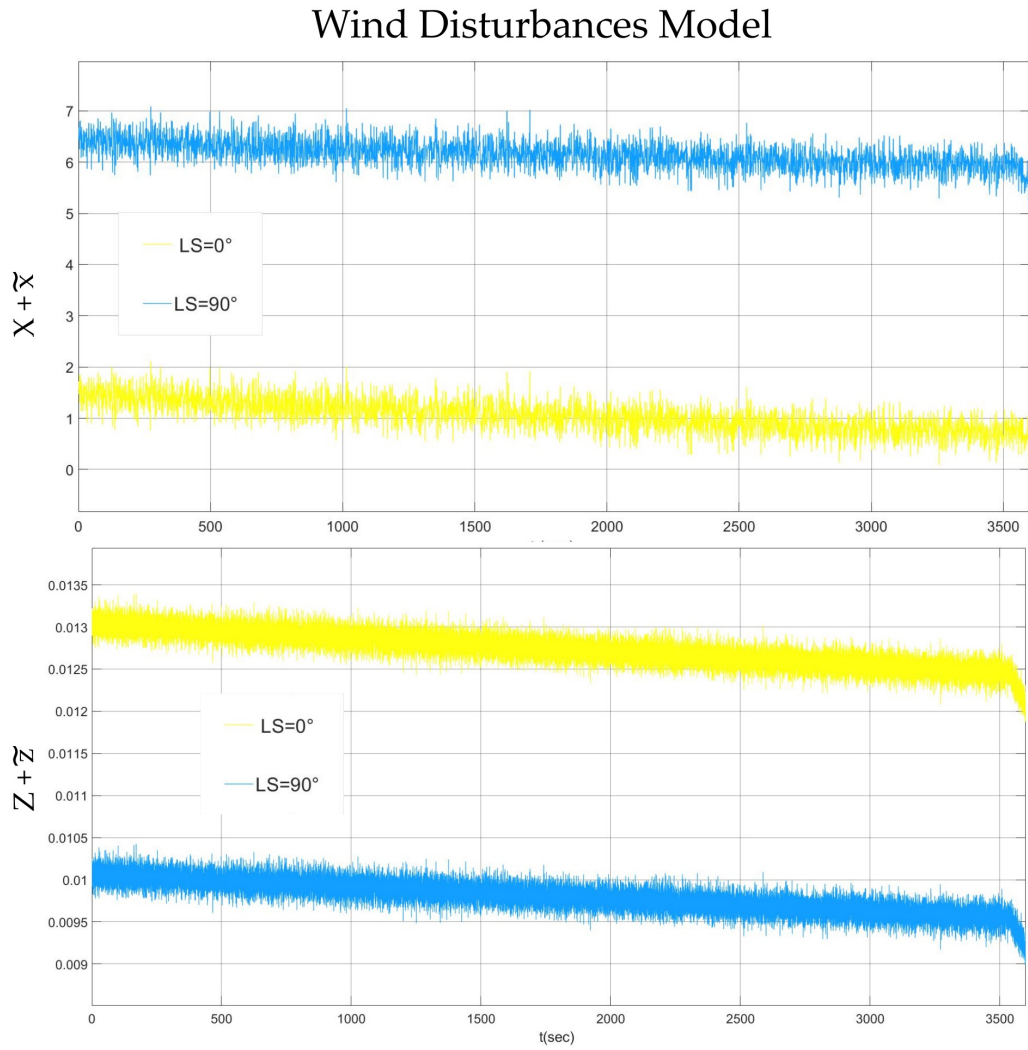


Figure 5.8: Wind Disturbance Model (Longitudinal and Vertical Components)

Chapter 6

Controller Design

6.1 Hybrid UAVs Control Laws Classification

Flight control systems are required to regulate the UAVs' motion to perform their missions tasks successfully. The goal of the control system is to stabilize the UAV as well as to minimize the tracking error between the desired reference command and the measured response of the UAV [10].

There are two strategies for Hybrid UAVs to accomplish these tasks, namely, the classical control theory and the modern control theory. The second approach, known as modern control, is to design a control system that handles the full UAV dynamics. Therefore, a better performance for MIMO systems is achieved compared to the classical approach in which the control gains are selected individually. This quick and direct modern control approach can be utilized for time varying and time invariant systems, while the classical approach is mainly for time invariant systems [36].

Flight control systems can be classified into linear and nonlinear based on the dynamics of the Hybrid UAV model. Generally, Hybrid UAVs' models are nonlinear. However, those models are commonly linearized using relative equilibrium points. Although linear controllers are easy to implement, reduce the computational effort and minimize the design time, but their performance degrade when operating away from the local equilibrium point [36].

However, current Hybrid UAVs implement non-linear controllers (backstepping, gain-scheduling and dynamic inversion are the most common) since the transition flight results in operation far away from the relative equilibrium condition. Moreover, nonlinear controllers operate in a much wider profile than linear ones which

are restricted within a specific operating region. Also, they consider the full and real dynamics of the UAV and take into account for the nonlinear aerodynamic and kinematic effects, actuator saturations and rate limitations [36][37].

This work, in which only the horizontal flight condition is considered, is focuses on linear control strategy applications as their are easier to implement in a preliminary study phase. Among most diffused linear modern control techniques for Hybrid UAVs there are:

- The PID controllers, which can be implemented in Hybrid UAVs for altitude control, attitude angles control and velocity control by just changing the control gains. It is very common among UAVs control strategy since it represents a concrete starting design point as it does not require extensive knowledge of the model. However, PID controller does not account for the cross coupling effects present in UAVs.
- The LQR, which easily handles complex dynamic systems and multiple actuators. It is robust with respect to process uncertainty, asymptotically stable if the system is controllable. On the other hand, LQR requires access to the full state which is not always possible. Due to their robustness, LQR controllers are extremely suitable for Hybrid UAV flight control systems and for this reason LQR controllers have been selected to control the aerobot during horizontal flight.

6.2 Linear Quadratic Regulator

The LQR control law can be applied to linearized systems, considering the plant in state-space form [38] [39]:

$$\dot{x} = Ax + Bu \quad (6.1)$$

and assuming that all of the n states x are available for the controller. The control is designed in the form of a static state feedback:

$$u = Kx(t) \quad (6.2)$$

which for MIMO system can be translated as:

$$\begin{bmatrix} u_1 \\ \cdot \\ \cdot \\ \cdot \\ u_n \end{bmatrix} = \begin{bmatrix} K_{11} & K_{12} & K_{1n} \\ \cdot & \cdot & \cdot \\ \cdot & \cdot & \cdot \\ \cdot & \cdot & \cdot \\ K_{n1} & K_{n2} & K_{nn} \end{bmatrix} \begin{bmatrix} x_1 \\ \cdot \\ \cdot \\ \cdot \\ x_n \end{bmatrix} \quad (6.3)$$

Combining the Equations 6.1 and 6.2 and dropping the dependence on t :

$$\dot{x} = Ax + BKx \quad (6.4)$$

$$\dot{x} = (A + BK)x \quad (6.5)$$

And so the system can be represented as:

$$\dot{x} = A_{CL}x \quad (6.6)$$

where:

$$A_{CL} = (A + BK) \quad (6.7)$$

The goal is to determine K . Since we are envisioning a continuous time LTI system, the closed-loop stability is defined by the eigenvalues of matrix A_{CL} , which shall be located in the left-half plane.

In addition, B has to be defined in such way that all states can be controlled by the input vector u . This characteristic is called controllability, and we can guarantee that our system is fully controllable if and only if the rank of the controllability matrix C is equal to the dimension of the design space, i.e. $\text{rank}(C(A, B)) = n$.

The LQR, in the context of optimal control, and more generally of automatic controls and linear time-invariant dynamic systems, is a dynamic compensator

obtained following the minimization of a cost index $J(x, u)$, function of states x and input u .

The performance index (cost function) which governs the closed loop system is set as:

$$J_{\infty} = \int_0^{\infty} x^T(\tau)Qx(\tau) + u^T(\tau)Ru(\tau)d\tau \quad (6.8)$$

where the quadratic terms involve two weighting matrices, Q and R , positive semidefinite. The objective is to find a control input that minimizes the cost function:

$$J_{\infty} = \int_0^{\infty} x^T(\tau)Qx(\tau) + u^T(\tau)Ru(\tau)d\tau \quad (6.9)$$

It's possible to demonstrate that such optimal feedback law is given by

$$K_{LQR} = -R^{-1}B^T P \quad (6.10)$$

where $P > 0$ is the solution of so-called Algebraic Riccati Equation (ARE):

$$A^T P + PA - PBR^{-1}B^T P = -Q \quad (6.11)$$

6.3 Overall Control Architecture

The overall control architecture is here presented and shown in Figure 6.1. For the nonlinear 6DOF UAVs model two types of LQR control sub-systems are designed following the procedure reported in Section 6.2 and considering the linearized system reported in Section 5.2.4. They are:

- Longitudinal Sub-System - K_{Lon} , to control speed along X_B and Z_B , as well as altitude and pitch angle. Moreover, the wind disturbances are accounted for the Longitudinal Control Subsystem.
- Lateral Sub-System - K_{Lat} , to control speed along Y_B , as well as bank ϕ and yaw ψ angles and rotational speed p and q .
- Cruise altitude h is controlled through the Longitudinal Control Sub-system
- Position on $X - Y$ plane is controlled through the yaw angle.

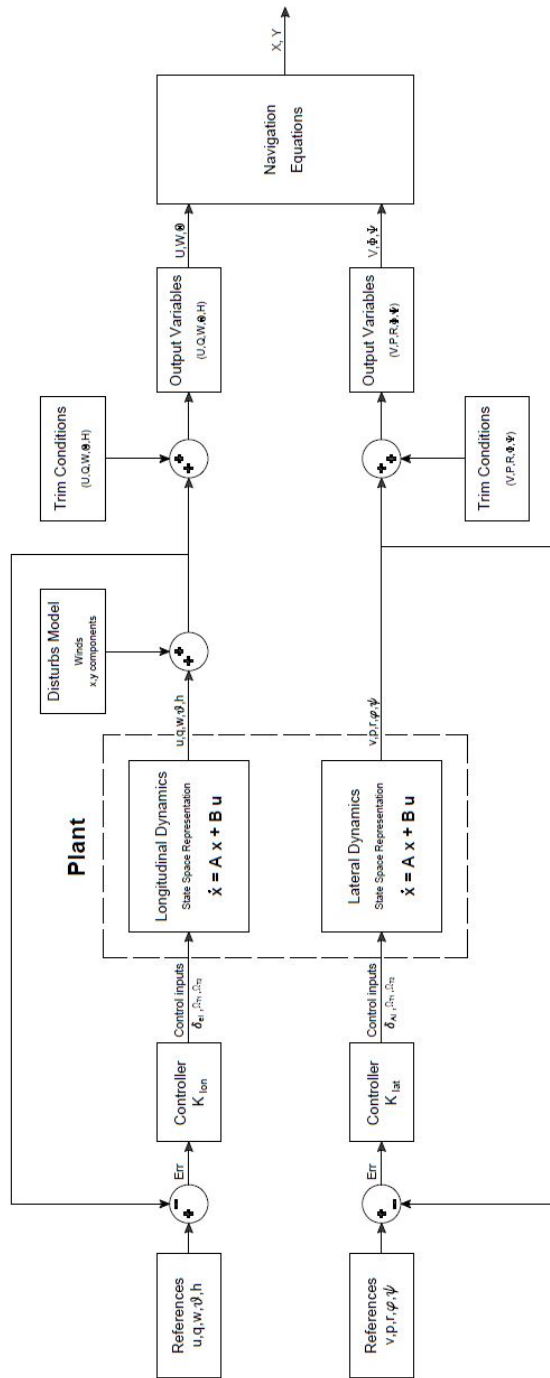


Figure 6.1: Overall Control Architecture

6.3.1 References Settings

For both the longitudinal and latero-directional dynamics, the references are set equal to zero, as they refer to the perturbations with respect to the equilibrium conditions. Only with regard to the yaw angle variable, a different strategy is adopted, since through the variation of this parameter it is possible to assign the trajectory that the drone must follow.

6.3.2 LQR Tuning

Generally, the matrices Q and R are chosen as [38]:

$$Q = \begin{bmatrix} q1 & & & \\ & q2 & & \\ & & \cdot & \\ & & & \cdot \\ & & & & qn \end{bmatrix} \quad (6.12)$$

$$R = \rho \begin{bmatrix} r1 & & & \\ & r2 & & \\ & & \cdot & \\ & & & \cdot \\ & & & & rn \end{bmatrix} \quad (6.13)$$

$$q_i = \frac{1}{t_{si} x_{imax}^2}, r_i = \frac{1}{u_{imax}^2}$$

where:

- t_{si} is the desired settling time set to few seconds.
- x_{imax} is a constraint on $|x_i|$, estimated by N.Collins' thesis [3]
- u_{imax} is a constraint on $|u_i|$ estimated by tables and plots in [3]
- ρ is chosen to trade-off regulation versus control effort.

The procedure to tuning the LQR can be listed as:

- Choose the weighting matrices Q and R.
- Solve the Riccati equation through the Matlab command $K = -lqr(A, B, Q, R)$.
- Compute the feedback gain $u(t) = Kx(t)$
- If the transient response specification or the magnitude constraints are not met, you have to restart from the first step.

K_{Lon} and K_{Lat} are defined using this iterative procedure and the results are presented below and estimating the constraints from [3].

K_{Lon}

The state and input-to state matrix for the longitudinal linearized system, reported in Appendix C, are considered. Following the previous illustrated steps and assigning $\rho = 1$, the weightings matrices are defined iteratively and they are set as follow:

$$Q_{Lon} = \begin{bmatrix} 1000 & 0 & 0 & 0 & 0 \\ 0 & 100 & 0 & 0 & 0 \\ 0 & 0 & 1 & 0 & 0 \\ 0 & 0 & 0 & 1 & 0 \\ 0 & 0 & 0 & 0 & 1 \end{bmatrix} \quad (6.14)$$

$$R_{Lon} = \begin{bmatrix} 0.1 & 0 & 0 \\ 0 & 0.1 & 0 \\ 0 & 0 & 0.1 \end{bmatrix} \quad (6.15)$$

 K_{Lat}

The state and input-to state matrix for lateral linearized system, reported in Appendix C, are considered. Following the previous illustrated steps, the weightings matrices are defined iteratively as follow:

$$Q_{Lat} = \begin{bmatrix} 0.01 & 0 & 0 & 0 & 0 \\ 0 & 0.001 & 0 & 0 & 0 \\ 0 & 0 & 1 & 0 & 0 \\ 0 & 0 & 0 & 1 & 0 \\ 0 & 0 & 0 & 0 & 1000 \end{bmatrix} \quad (6.16)$$

$$R_{Lat} = \rho \begin{bmatrix} 10 & 0 & 0 \\ 0 & 10 & 0 \\ 0 & 0 & 10 \end{bmatrix} \quad (6.17)$$

with $\rho = 10$.

6.4 Test and Results

6.4.1 Gust Step

The controller is tested in different conditions. Firstly, for the longitudinal velocity U a gust step of $5m/s$ is considered, that could be a typical value of gust wind during martian summer. Moreover, the effects on the other longitudinal dynamics variables are presented. Figure 6.3 represents the effect on U and aerobot position on $X - Y$ plane, while Figure 6.4 present the results for the altitude H , vertical velocity W , Eulers' angle θ and rotational speed Q . The lateral dynamics parameters are not affected by this disturb, they keep their reference values constants.

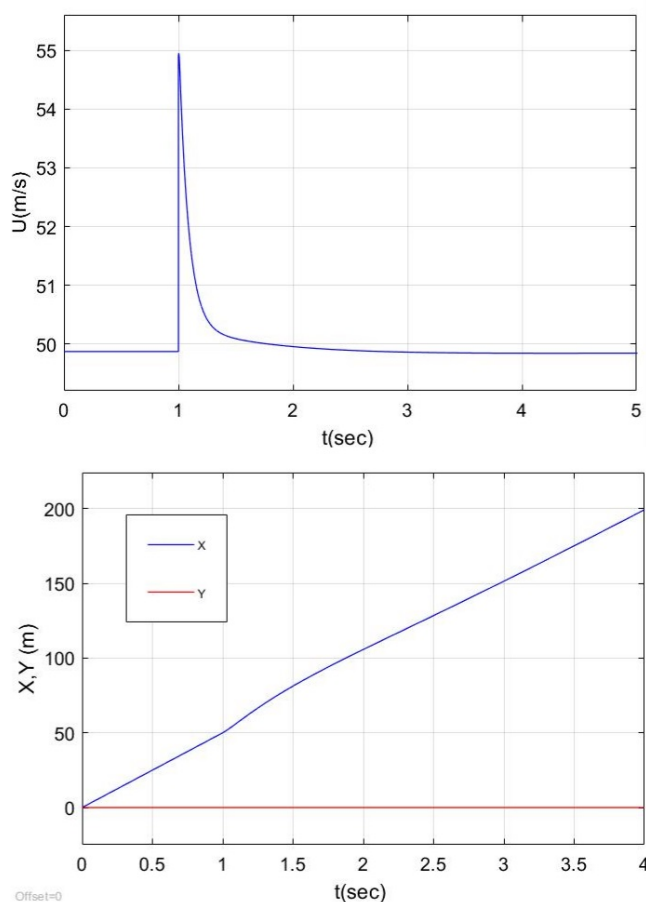


Figure 6.2: U response at gust step of $5m/s$

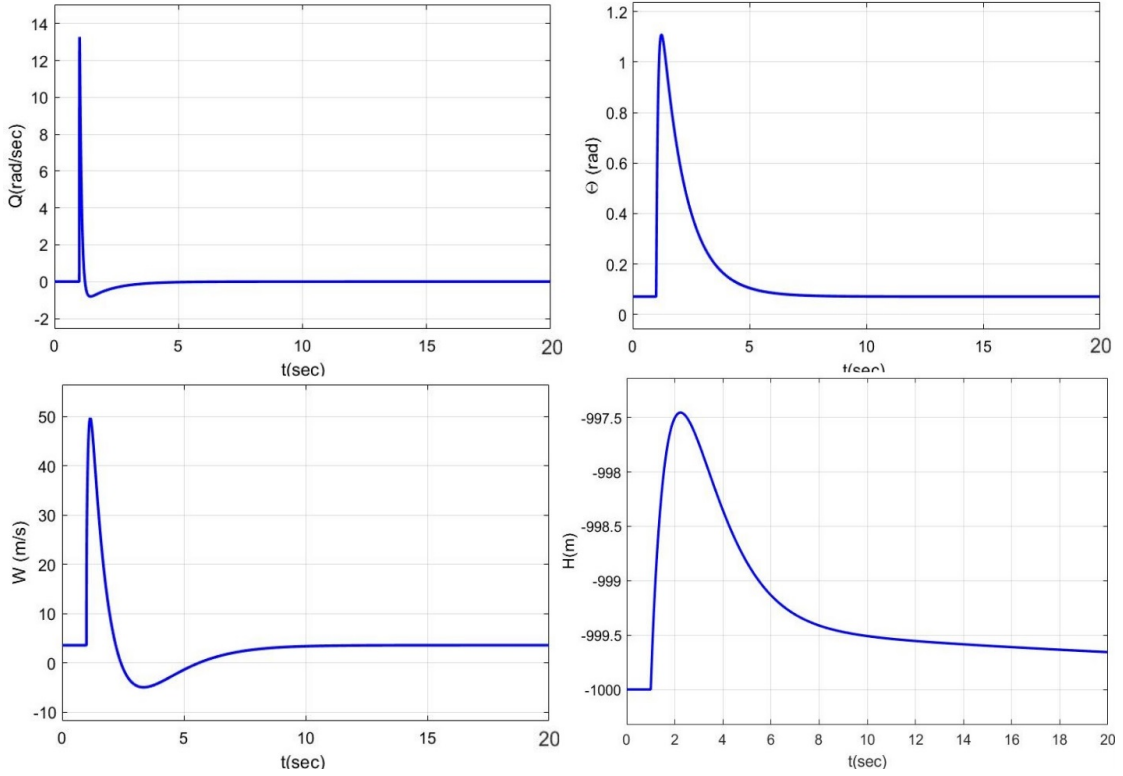


Figure 6.3: H response for a gust step of $5m/s$ of U

The controller is able to bring back the parameters at set reference values keeping the weighting matrices assigned in the previous section. It is designed to avoid great variation of U, H and position, in order to prevent collisions. As shown in Figure 6.3, the aerobot starts from an initial point which coordinates are indicate as $(0,0)$ and deviates slightly from its when the disturb occurs, but it is capable to return on its trajectory (linear in this case). Figure 6.4 presents the effects on longitudinal variables. The altitude get an overshoot of about $2.5m$, that is definitely acceptable. The Q and R matrix are tuned in order to have a great trajectory tracking performances and a reasonable settling time. Since that W and Q present quite high overshoot values, but in about 2 and 1.5 seconds respectively they are significantly reduced.

6.4.2 Trajectory

A second test is performed by assigning a square trajectory. It is defined identifying Jazero Crater, inside the Isidis Basin (Figure 6.4), as a possible exploration site. The aerobot motion in the X-Y plane is controlled through a series of yaw angle steps respect to the Martian Inertial Frame and assuming as starting point the center of Jazero Crater at the coordinates $18^{\circ}24'36''$ N - $77^{\circ}41'24''$ E.

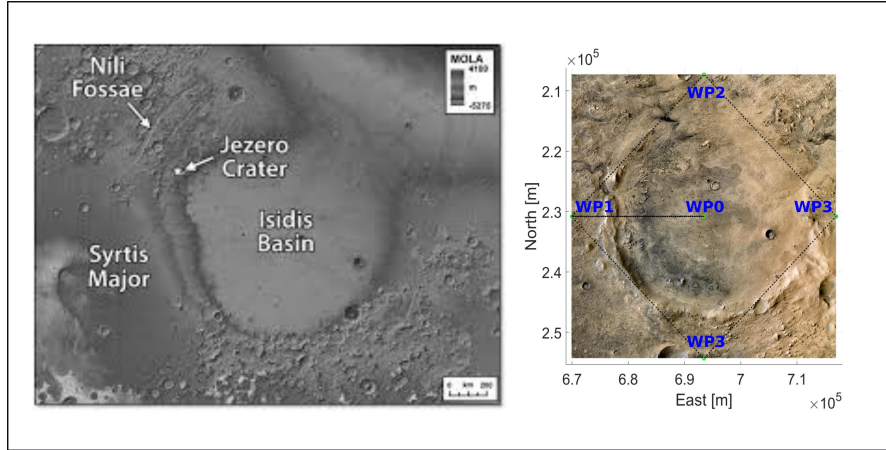


Figure 6.4: Left: Selected Mission Site - Jazero Crater, inside the Isidis Basin. Right: Assigned Trajectory

In order to define the sequence of yaw angle step the operational mission parameters of the Aerobot during the horizontal flight are considered:

- Cruise Speed: 50 m/s
- Endurance: $1h = 3600s$
- Range $180Km$ per flight
- Cruise Altitude $h = 1Km$

The yaw angle step values are determined considering Figure 6.5, and reported in Table 6.1. The steps sequence can be described as follow:

- The drone starts from the Wait-Point 1 (WP1) at $t = 0$.
- After 470 seconds it arrives in WP2 and a step of $\Psi = -135^{\circ}$ is assigned and the areobot results aligned with x'_B direction.
- Three step of $\Psi = -90^{\circ}$ every $665s$ are assigned to reach again WP2.
- A final step of $\Psi = -135^{\circ}$ is assigned to return at the starting point WP1.

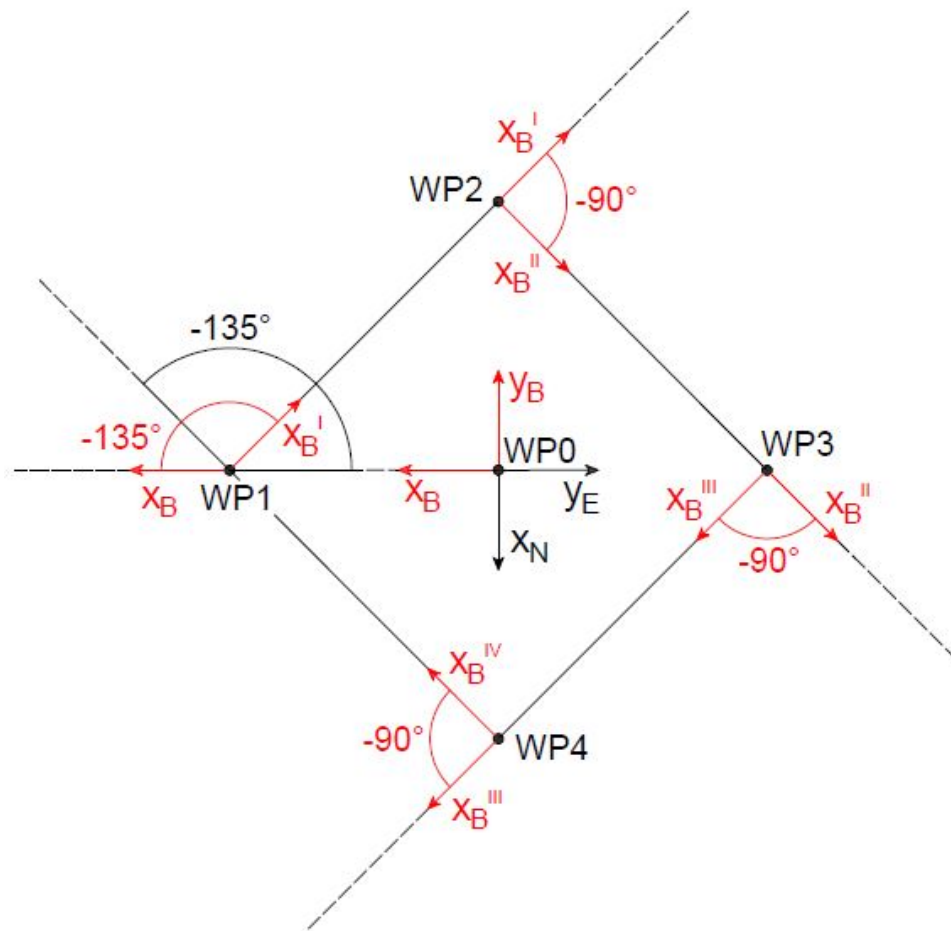


Figure 6.5: Trajectory definition

Yaw Step Sequence		
N°	Step value	at t(sec)
1	-135°	470
2	-90°	1135
3	-90°	1800
4	-90°	2465
5	-135°	3130

Table 6.1: Yaw Step Sequence

The trajectory is firstly tested without the presence of disturbs. It follows that the aerobot correctly tracks the assigned path, as presented in Figure 6.7. Moreover, the effects of yaw step on lateral dynamics variables are presented in Figure 6.6. The variables P, Q, R, Φ presents great oscillations from their reference values when the yaw step occurs, but after few seconds they reach their references values. Only bank angle Φ presents a greater settling time. The turning manoeuvres would be more difficult on Mars, since its lower gravitational force reduce the turning rate and increase the turning radius for a given flight speed and bank angle [3]. Therefore, an aircraft flying on Mars cannot easily make small, high turn rate maneuvers like their terrestrial counterparts [3].

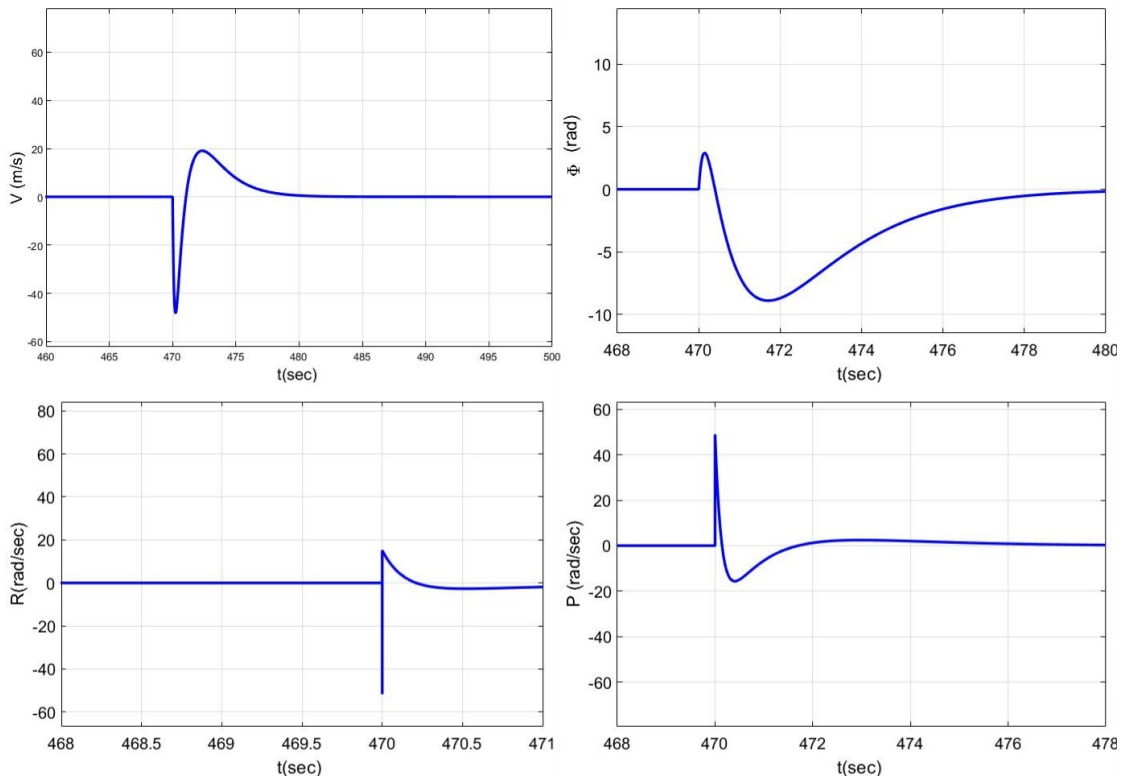


Figure 6.6: P, Q, R, Φ

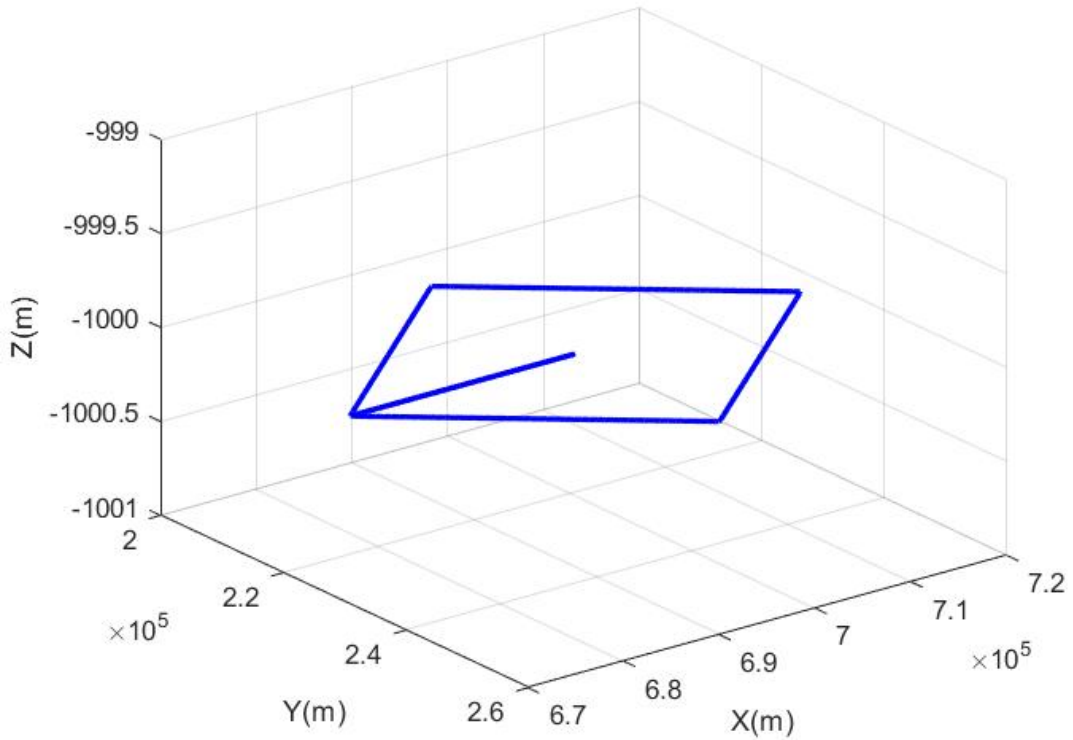


Figure 6.7: Trajectory without disturbances

6.4.3 Trajectory and Wind Disturbances

The Y4-TR behaviour is tested considering only the horizontal straight flight phase, in presence of wind disturbances and for an assigned trajectory. Both minimum and maximum disturbances are considered, $LS = 90^\circ$ and $LS = 0^\circ$ respectively. In both cases, the drone follows the assigned trajectory, as shown in Figures 6.8 and 6.9.

However, it get slightly higher oscillations respect to reference values in the case of $LS = 0^\circ$, since the disturbances reach higher values along vertical direction as reported in Figure 5.8. Furthermore, for $LS = 90^\circ$ the initial overshoot is wider ($3.3m$) than in the case $LS = 0$ ($0.5m$) due to the presence of more intense disturbances along vertical and horizontal directions at the beginning of the operating phase; its modulation could take place through the choice of different weights for the matrices Q and R for both lateral and longitudinal control, but preliminarily it is decided to keep the previously reported weights as they allowed to obtain a more accurate trajectory tracking and this initial peak is therefore considered acceptable.

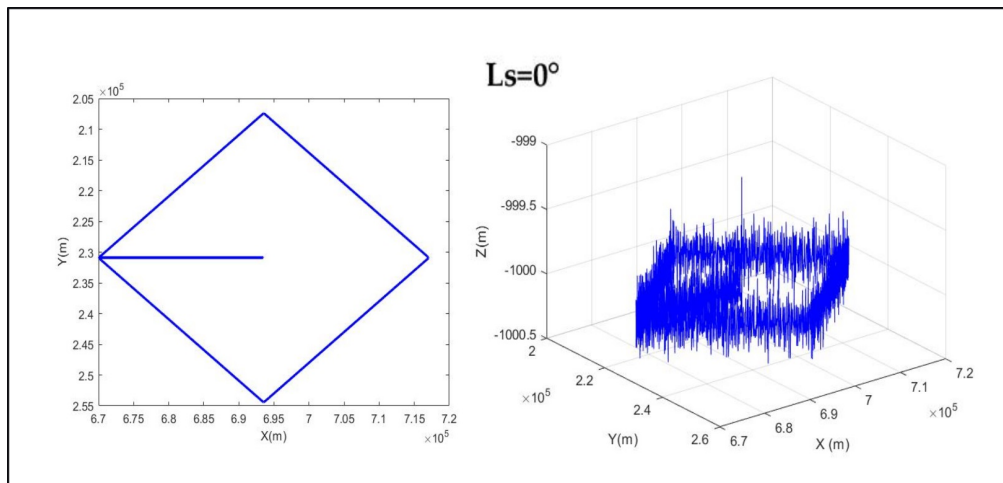


Figure 6.8: Results for $LS = 0^\circ$

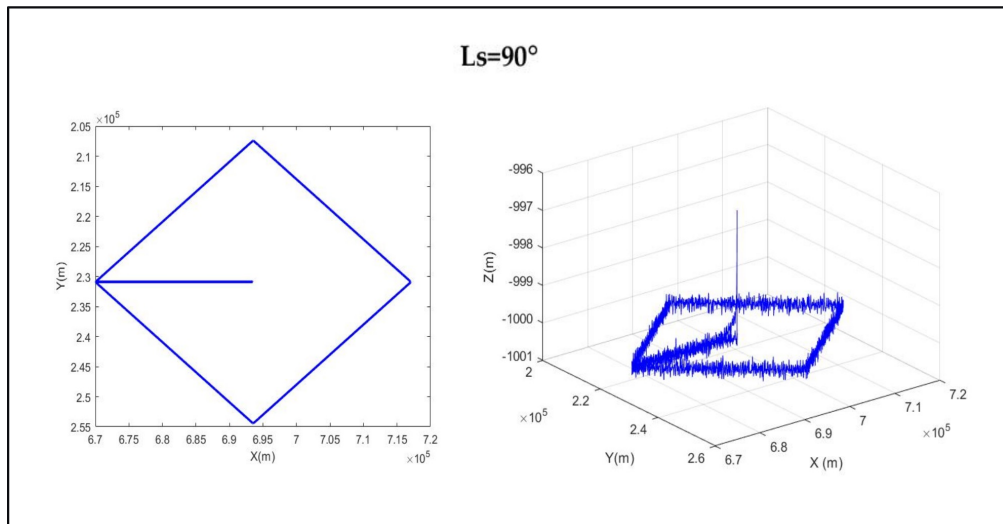


Figure 6.9: Results for $LS = 90^\circ$

Chapter 7

Conclusion and Future Work

7.1 Conclusion

The main objective of this thesis is to develop a simulator for a 6DOF non-linear dynamic model for a martian UAVs and to design a control law able to manage the drone in presence of disturbances and for an assigned trajectory.

Starting from drone applications in planetary exploration, Mars is identified as the target planet for this study. Moreover, analyzing martian aerobot background applications, the dynamic model of Y4-TR by N.Collins [3] is chosen to be implemented in the simulator and its mathematical model is presented.

Since its relevant operation phase is the cruise, only the horizontal straight flight condition is considered for a preliminary study. In this flight conditions the tilt-rotor equation can be simplified, as well as for hover conditions. The trim conditions and rotors performance are estimated for both phases after the aerodynamics features are estimated extrapolating data from N. Collins' work and the obtained results are consistent with ones provided by Collins. Two dynamics model are presented: a complete one, which takes in account the non-linearity of the problem, and a simplified model, which can be used to test both horizontal and hover conditions. The two models are tested for the defined trim conditions and the results show that both are stable in both considered conditions. The simplified model can be adopted to analyze this two phases.

In order to implement a control law to manage the drone in presence of disturbances and for an assigned trajectory, the dynamic model is linearized considering horizontal flight as equilibrium point. Moreover, an analysis on main martian disturbances sources is conducted and it led to identifying the presence of the wind

and the oscillations from its mean value as the main disturb to consider. Among different control strategy for terrestrial and martian UAVs the LQR is chosen since it is extremely suitable for Hybrid UAV flight control systems. It is tuned for an assigned trajectory and in presence of disturbances.

The LQR is tested firstly for a gust step of $5m/s$ along U longitudinal speed, and the controller is able to bring back values at their references values, even if they present quite high overshoot. Moreover, the altitude and the $X - Y$ positions are satisfactorily controlled, this is a relevant feature since the controller should avoid collisions. However, the other state variables present great oscillations that should to be reduced by redefining the LQR weighting matrices. At preliminary study phase they could be considered acceptable.

A second test is conducted considering the assigned trajectory, and it follows that the LQR controller is able to manage UAVs position that correctly follows the trajectory. Finally, both disturbance and assigned path are considered and the results shows that the designed controller is capable of control drone motion.

7.2 Future Work

Some recommendations for future works are proposed here. Firstly, the LQR controller should be re-modulate to reduce variables overshoot and should be tested also for the non-linear model to verify if it could control correctly the drone motion.

Moreover, a more extensive aerodynamic performances estimation should to be conducted using powerful software like Mars-Gram, as well as a rotor performances estimation in order to obtain aerodynamics coefficients for the entire flight envelope and to analyze also the transition phases, which are the most delicate stage of tilt-rotor flight.

A more accurate Mars environmental parameters analysis should be conducted, implementing a more precise atmosphere model to take into account also small atmospheric perturbations that could affects drone dynamics, such as temperature, pressure and density tides.

The study on drone control in the Martian environment is still in a preliminary stage and many analyzes must be conducted to provide the aerial platforms with adequate control. Linear control systems can help in the first design steps thanks to their simplicity, but since the unpredictability of the planetary environments it will be necessary to study of more refined control laws.

Non-linear control laws should be investigated and applied especially for tilt-rotor configurations, since presumably the linear control laws wouldn't be able to stabilize the drone during transitions phases.

Appendix A

Rotor Blades Features

A.1 Rotors Geometries

TILT - ROTOR GEOMETRY		
Zero Lift angle $\alpha_0 = -2$ deg - SD8000		
Radius - $R = 0.5$ m		
r/R	c/R	β_0 (deg)
0.61167E-01	0.18261E-01	97.908
0.94044E-01	0.22982E-01	94.842
0.13990	0.34215E-01	90.485
0.18882	0.49410E-01	86.626
0.23844	0.67324E-01	83.061
0.28797	0.87063E-01	79.751
0.33702	0.10771	76.679
0.38534	0.12827	73.829
0.43273	0.14778	71.191
0.47902	0.16531	68.754
0.52406	0.18009	66.508
0.56771	0.19156	64.444
0.60985	0.19939	62.551
0.65034	0.20351	60.820
0.68908	0.20402	59.242
0.72594	0.20123	57.808
0.76084	0.19553	56.510
0.79367	0.18733	55.338
0.82433	0.17710	54.286
0.85275	0.16524	53.346
0.87884	0.15213	52.512
0.90253	0.13809	51.778
0.92376	0.123309	51.139
0.94247	0.10828	50.589
0.95860	0.92851E-01	50.130
0.97211	0.77424E-01	49.753
0.98296	0.62071E-01	49.471
0.99113	0.47488E-01	49.292
0.99658	0.34933E-01	49.263
0.99932	0.27174E-01	49.366

Top Coax ROTOR GEOMETRY		
Zero Lift angle $\alpha_0 = -3.831$ deg - Eppler387		
Radius - $R = 1$ m		
r/R	c/R	β_0 (deg)
0.38009E-01	0.15619	54.524
0.81211E-01	0.15479	44.606
0.13204	0.15317	30.612
0.18325	0.15152	29.071
0.23418	0.14990	27.435
0.28457	0.14827	25.958
0.33423	0.14669	24.831
0.38300	0.14512	23.913
0.43074	0.14359	23.349
0.47732	0.14210	22.914
0.52260	0.14065	22.271
0.56645	0.13924	21.723
0.60876	0.13788	21.252
0.64940	0.13659	20.844
0.68827	0.13533	20.488
0.72526	0.13415	20.176
0.76026	0.13303	19.902
0.79318	0.13197	19.661
0.82392	0.13099	19.447
0.85241	0.13008	19.260
0.87857	0.12923	19.097
0.90232	0.12847	18.955
0.92359	0.12779	18.831
0.94234	0.12719	18.726
0.95851	0.12668	18.638
0.97205	0.12624	18.565
0.98292	0.12589	18.508
0.99111	0.12562	18.465
0.99658	0.12545	18.437
0.99932	0.12536	18.422

Bottom Coax ROTOR GEOMETRY		
Zero Lift angle $\alpha_0 = -3.831$ deg		
Radius - $R = 1$ m		
r/R	c/R	β_0 (deg)
0.38009E-01	0.12941	29.296
0.81211E-01	0.13254	28.494
0.13204	0.13629	27.549
0.18325	0.13781	26.597
0.23418	0.13858	25.650
0.28457	0.13734	24.714
0.33423	0.13635	23.791
0.38300	0.13629	22.885
0.43074	0.13586	22.289
0.47732	0.13508	21.854
0.52260	0.13399	21.211
0.56645	0.13260	20.663
0.60876	0.13096	20.192
0.64940	0.12976	19.784
0.68827	0.12856	19.428
0.72526	0.12744	19.116
0.76026	0.12638	18.842
0.79318	0.12537	18.601
0.82392	0.12444	18.387
0.85241	0.12358	18.200
0.87857	0.12277	18.037
0.90232	0.12205	17.895
0.92359	0.12140	17.771
0.94234	0.12083	17.666
0.95851	0.12035	17.578
0.97205	0.11993	17.505
0.98292	0.11960	17.448
0.99111	0.11934	17.405
0.99658	0.11918	17.377
0.99932	0.11909	17.362

A.2 Rotor Blades discretization

TILT - ROTOR				
Sector	r_m/R	dr_m/R	c_m/R	β_{0_m} (deg)
1	7.76E-2	3.29E-2	2.06E-2	9.64E+1
2	1.17E-1	4.59E-2	2.86E-2	9.27E+1
3	1.64E-1	4.89E-2	4.18E-2	8.86E+1
4	2.14E-1	4.96E-2	5.84E-2	8.48E+1
5	2.63E-1	4.95E-2	7.72E-2	8.14E+1
6	3.12E-1	4.91E-2	9.74E-2	7.82E+1
7	3.61E-1	4.83E-2	1.18E-1	7.53E+1
8	4.09E-1	4.74E-2	1.38E-1	7.25E+1
9	4.56E-1	4.63E-2	1.57E-1	7.00E+1
10	5.02E-1	4.50E-2	1.73E-1	6.76E+1
11	5.46E-1	4.37E-2	1.86E-1	6.55E+1
12	5.89E-1	4.21E-2	1.95E-1	6.35E+1
13	6.30E-1	4.05E-2	2.01E-1	6.17E+1
14	6.70E-1	3.87E-2	2.04E-1	6.00E+1
15	7.08E-1	3.69E-2	2.03E-1	5.85E+1
16	7.43E-1	3.49E-2	1.98E-1	5.72E+1
17	7.77E-1	3.28E-2	1.91E-1	5.59E+1
18	8.09E-1	3.07E-2	1.82E-1	5.48E+1
19	8.39E-1	2.84E-2	1.71E-1	5.38E+1
20	8.66E-1	2.61E-2	1.59E-1	5.29E+1
21	8.91E-1	2.37E-2	1.45E-1	5.21E+1
22	9.13E-1	2.12E-2	1.31E-1	5.15E+1
23	9.33E-1	1.87E-2	1.16E-1	5.09E+1
24	9.51E-1	1.61E-2	1.01E-1	5.04E+1
25	9.65E-1	1.35E-2	8.51E-2	4.99E+1
26	9.78E-1	1.08E-2	6.97E-2	4.96E+1
27	9.87E-1	8.17E-2	5.48E-2	4.94E+1
28	9.94E-1	5.45E-2	4.12E-2	4.93E+1
29	9.98E-1	2.74E-2	3.11E-2	2.47E+1

Top-Coaxial				
Sector	r_m/R	dr_m/R	c_m/R	$\frac{\beta_{0_m}}{1}$
5.96E-2	4.32E-2	15.549E-2	76.827	
2	1.07E-1	5.08E-2	15.399E-2	59.912
3	1.58E-1	5.12E-2	15.235E-2	45.1475
4	2.09E-1	5.09E-2	15.071E-2	42.7885
5	2.59E-1	5.04E-2	14.909E-2	40.414
6	3.09E-1	4.97E-2	14.748E-2	38.3735
7	3.59E-1	4.88E-2	14.591E-2	36.7875
8	4.07E-1	4.77E-2	14.436E-2	35.5875
9	4.54E-1	4.66E-2	14.285E-2	34.806
10	5.00E-1	4.53E-2	14.138E-2	34.0495
11	5.45E-1	4.39E-2	13.995E-2	33.1325
12	5.88E-1	4.23E-2	13.856E-2	32.349
13	6.29E-1	4.06E-2	13.724E-2	31.674
14	6.69E-1	3.89E-2	13.596E-2	31.088
15	7.07E-1	3.70E-2	13.474E-2	31.088
16	7.43E-1	3.50E-2	13.596E-2	31.088
17	7.77E-1	3.29E-2	13.250E-2	30.576
18	8.09E-1	3.07E-2	13.148E-2	30.127
19	8.38E-1	2.85E-2	13.054E-2	29.7325
20	8.65E-1	2.62E-2	12.966E-2	29.3845
21	8.90E-1	2.38E-2	12.885E-2	29.077
22	9.13E-1	2.13E-2	12.813E-2	28.8085
23	9.33E-1	1.87E-2	12.749E-2	28.5745
24	9.50E-1	1.62E-2	12.694E-2	28.3705
25	9.65E-1	1.35E-2	12.646E-2	28.194
26	9.77E-1	1.09E-2	12.607E-2	28.045
27	9.87E-1	8.19E-3	12.576E-2	27.9205
28	9.94E-1	5.47E-3	12.554E-2	27.819
29	9.98E-1	2.74E-3	12.541E-2	27.7405

Bottom-Coaxial				
Sector	r_m/R	dr_m/R	c_m/R	$\frac{\beta_{0_m}}{1}$
5.966E-2	4.32E-2	13.098E-2	28.8950	
2	1.07E-1	5.08E-2	13.442E-2	28.0215
3	1.58E-1	5.12E-2	13.705E-2	27.0730
4	2.09E-1	5.09E-2	13.820E-2	26.1235
5	2.59E-1	5.04E-2	13.796E-2	25.1820
6	3.09E-1	4.97E-2	13.685E-2	24.2525
7	3.59E-1	4.88E-2	13.632E-2	23.3380
8	4.07E-1	4.77E-2	13.608E-2	22.5870
9	4.54E-1	4.66E-2	13.547E-2	22.0715
10	5.00E-1	4.53E-2	13.454E-2	21.5325
11	5.45E-1	4.39E-2	13.330E-2	20.9370
12	5.88E-1	4.23E-2	13.178E-2	20.4275
13	6.29E-1	4.06E-2	13.036E-2	19.9880
14	6.69E-1	3.89E-2	12.916E-2	19.6060
15	7.07E-1	3.70E-2	12.800E-2	19.2720
16	7.43E-1	3.50E-2	12.691E-2	18.9790
17	7.77E-1	3.29E-2	12.588E-2	18.7215
18	8.09E-1	3.07E-2	12.491E-2	18.4940
19	8.38E-1	2.85E-2	12.401E-2	18.2935
20	8.65E-1	2.62E-2	12.318E-2	18.1185
21	8.90E-1	2.38E-2	12.241E-2	17.9660
22	9.13E-1	2.13E-2	12.173E-2	17.8330
23	9.33E-1	1.87E-2	12.112E-2	17.7185
24	9.50E-1	1.62E-2	12.173E-2	17.6220
25	9.65E-1	1.35E-2	12.112E-2	17.5415
26	9.77E-1	1.09E-2	11.977E-2	17.4765
27	9.87E-1	8.19E-3	11.947E-2	17.4265
28	9.87E-1	5.47E-3	11.926E-2	17.3910
29	9.98E-1	2.74E-3	11.914E-2	17.3695

A.3 XROTOR and CROTOR Input

A.3.1 Tilt-Rotor

```

Designed blade
!      Rho      Vso      Rmu      Alt
  0.13790E-01  245.71    0.12235E-04  999.00
!      Rad      Vel      Adv      Rake
  0.50000      50.000    1.0000      0.0000
!      XIO      XIW
  0.50000E-01  0.0000
! Naero
  1
! Xisection
  0.0000
!      A0deg      dCLdA      CLmax      CLmin
 -2.0000      5.7000    1.1500    -0.30000
! dCLdAstall      dCLstall      Cmconst      Mcrit
  0.10000      0.10000    -0.10000    0.80000
!      CDmin      CLCDmin      dCDdCL^2
  0.14000E-01  0.30000    0.25000E-01
!      REref      REexp
  50000.      -0.40000
!LVDuct  LDuct  LWind
  T      F      F
! II Nbls
  30      2
    
```

A.3.2 Top Coaxial Rotor

```

E387upper
!      Rho      Vso      Rmu      Alt
  0.13790E-01  245.71    0.12235E-04  0.0000
!      Rad      Vel      Adv      Rake
  1.0000      3.0000    0.15904E-01  0.0000
!      XIO      XIW
  0.20000E-01  0.0000
! Naero
  1
! Xisection
  0.0000
!      A0deg      dCLdA      CLmax      CLmin
  -3.8310      5.8948      1.2000      -0.14000
! dCLdAstall      dCLstall      Cmconst      Mcrit
  0.10000      0.10000      -0.10000      0.80000
!      CDmin      CLCDmin      dCDdCL^2
  0.50000E-02  0.61000      0.53800E-01
!      Reref      REexp
  0.48000E+06  -0.40000
!LVDuct  LDuct  LWind
  T      F      F
! II Nbls
  30      4
    
```

A.3.3 Bottom Coaxial Rotor

```

E387aft
!      Rho      Vso      Rmu      Alt
  0.13790E-01  245.71    0.12235E-04  0.0000
!      Rad      Vel      Adv      Rake
  1.0000      3.0000    0.15904E-01  0.0000
!      XIO      XIW
  0.20000E-01  0.0000
! Naero
  1
! Xisection
  0.0000
!      A0deg      dCLdA      CLmax      CLmin
  -3.8310      5.8948      1.2000     -0.14000
! dCLdAstall    dCLstall    Cmconst    Mcrit
  0.10000      0.10000    -0.10000    0.80000
!      CDmin      CLCDmin    dCDdCL^2
  0.50000E-02  0.61000    0.53800E-01
!      Reref      REexp
  0.48000E+06 -0.40000
!LVDuct LDuct  LWind
  T      F      F
!  II Nbllds
  30     4
    
```

Appendix B

Aerobot Features

B.1 Aerobot Longitudinal Derivatives

Dimensional			
Parameters	Closed	Open	Dimension Unit
X_u	-0.0120	-0.0755	$\frac{N}{m/s}$
X_w	-0.1404	-0.009	$\frac{N}{m/s}$
X_q	0.2860	0.0459	$\frac{N}{rad/s}$
$X_{\delta_{El}}$	-2.9812	-2.355	$\frac{N}{rqd}$
M_u	0.0000	-0.061	$\frac{Nm}{m/s}$
M_w	-1.568	-2.137	$\frac{Nm}{m/s}$
M_q	-10.594	-4.898	$\frac{Nm}{rad/s}$
$M_{\delta_{El}}$	-148.688	-134.52	$\frac{Nm}{rqd}$
Z_u	-3.099	-3.100	$\frac{N}{m/s}$
Z_w	-21.903	-9.393	$\frac{N}{m/s}$
Z_q	22.8704	-10.444	$\frac{N}{rad/s}$
$Z_{\delta_{El}}$	-222.9649	-166.6036	$\frac{N}{rad}$

Nondimensional		
Parameters	Closed	Open
C_{xu}	-0.022	-0.226
$C_{x\alpha}$	0.0258	0.0003
C_q	0.0502	0.0184
$C_{x\delta_{EI}}$	-0.109	-0.0146
C_{mu}	0.0000	-0.0012
C_m	-0.1103	-0.4646
C_{mq}	-0.8453	-1.3147
$C_{m\delta_{EI}}$	-0.2614	-0.5399
C_{zu}	0.0000	0.0000
$C_{z\alpha}$	3.9794	2.8315
C_q	4.0160	4.0742
$C_{z\delta_{EI}}$	-0.8181	-0.9995

B.2 Aerobot Lateral Derivatives

Dimensional			
Parameters	Closed	Open	Dimension Unit
L_v	-4.7727	-4.4065	$\frac{Nm}{m/s}$
L_p	-70.7341	63.8823	$\frac{Nm}{rad/s}$
L_r	0.7085	4.9108	$\frac{Nm}{rad/s}$
$L_{\delta_{AI}}$	461.1082	436.2622	$\frac{Nm}{rqd}$
Y_v	0.6368	0.6406	$\frac{N}{m/s}$
Y_p	4.3070	4.3391	$\frac{N}{rad/s}$
Y_r	0.7518	0.6646	$\frac{N}{rad/s}$
$Y_{\delta_{AI}}$	22.5106	22.3343	$\frac{N}{rqd}$
N_v	0.6217	0.6465	$\frac{Nm}{m/s}$
N_p	1.6536	2.0725	$\frac{Nm}{rad/s}$
N_r	0.5769	0.0341	$\frac{Nm}{rad/s}$
$N_{\delta_{AI}}$	23.9057	20.9532	$\frac{Nm}{rad}$

Nondimensional		
Parameters	Closed	Open
$C_{l\beta}$	-0.0938	-0.1416
C_{lp}	-0.2979	-0.4400
C_{lr}	0.0283	0.0338
$C_{l\delta_{AI}}$	0.1813	0.2804
$C_{y\beta}$	-0.1168	-0.1921
C_{yp}	-0.1693	-0.2789
C_{yr}	0.0296	0.0427
$C_{r\delta_{AI}}$	0.0826	0.1340
$C_{n\beta}$	0.0122	0.0208
C_{np}	0.0070	0.0143
C_{nr}	-0.0024	-0.0002
$C_{n\delta_{EI}}$	-0.0094	-0.0135

B.3 Aerobot Body Geometry

Aerobot Geometry					
y (mm)	chord (mm)	offset(mm)	dihedral (deg)	twist (deg)	Airfoil
0.0	3250.0	0	0	0	MA1
85.0	3246.5	2.5	0	0.00	MA2
170.0	3235.4	10.4	0	0.00	MA3
255.0	3215.9	24.4	0	0.00	MA4
340.0	3186.8	45.4	0	0.00	MA5
425.0	3147.0	74.5	0	0.00	MA6
510.0	3095.1	113.1	0	0.00	MA7
595.0	3029.5	163.0	0	0.00	MA8
680.0	2948.4	226.4	0	0.00	MA9
765.0	2849.4	306.2	0	0.00	MA10
850.0	2729.6	405.9	0	0.00	MA11
935.0	2586.3	528.7	0	0.00	MA12
1020.0	2432.9	661.7	0	0.00	MA13
1087.5	2310.5	768.0	0	0.00	MA14
1155.1	2192.0	870.9	0	0.00	MA15
1222.6	2081.2	966.6	0	0.00	MA16
1290.1	1982.0	1051.3	0	0.00	MA17
1357.7	1899.3	1121.0	5	2.00	MA18
1886.1	1663.3	1271.8	5	1.17	MA19
2414.6	1462.1	1419.3	5	0.33	MA20
2943.1	1287.3	1562.3	5	-0.50	MA21
3471.5	1134.1	1699.2	5	-1.33	MA22
4000.0	999.7	1828.8	5	-2.17	MA23
4049.3	940.5	1888.0	18	-3.00	ZAGI10
4098.7	881.3	1947.2	36	-3.00	ZAGI10
4148.0	822.1	2006.4	54	-3.00	ZAGI10
4197.4	762.9	2065.6	72	-3.00	ZAGI10
4246.7	703.7	2124.8	90	-3.00	ZAGI10
4666.7	199.9	2628.5	90	-3.00	ZAGI10

Appendix C

State Space Matrices

C.1 Longitudinal Dynamics

$$A_{Lon} = \begin{bmatrix} a_{1,1} & a_{1,2} & a_{1,3} & a_{1,4} & 0 \\ a_{2,1} & a_{2,2} & a_{2,3} & 0 & 0 \\ a_{3,1} & a_{3,2} & a_{3,3} & a_{3,4} & 0 \\ 0 & 1 & 0 & 0 & 0 \\ a_{5,1} & 0 & a_{5,3} & a_{5,4} & 0 \end{bmatrix} \quad (C.1)$$

$$a_{1,1} = X_u/m \quad (C.2)$$

$$a_{1,2} = (X_q/m - W_{trim}) \quad (C.3)$$

$$a_{1,3} = X_w/m \quad (C.4)$$

$$a_{1,4} = -g \cos(\theta_{trim}) \quad (C.5)$$

$$a_{2,1} = M_u/I_{yy} \quad (C.6)$$

$$a_{2,2} = M_q/I_{yy} \quad (C.7)$$

$$a_{2,3} = M_w/I_{yy} \quad (C.8)$$

$$a_{3,1} = Z_u/m \quad (C.9)$$

$$a_{3,2} = (U_{trim} + Z_q/m) \quad (C.10)$$

$$a_{3,3} = Z_w/m \quad (C.11)$$

$$a_{3,4} = -g * \sin(\theta_{trim}) \quad (C.12)$$

$$a_{5,1} = \cos(\theta_{trim}) \quad (C.13)$$

$$a_{5,3} = \sin(\theta_{trim}) \quad (C.14)$$

$$a_{5,4} = \cos(\theta_{trim})W_{trim} - \sin(\theta_{trim})U_{trim} \quad (C.15)$$

$$B_{Lon} = [X_{\delta_{El}}/m, M_{\delta_{El}}/I_{yy}, Z_{\delta_{El}}/m, 0, 0, 0]^T \quad (C.16)$$

C.2 Lateral Dynamics

$$A_{Lat} = \begin{bmatrix} a_{1,1} & a_{1,2} & a_{1,3} & a_{1,4} & 0 \\ a_{2,1} & a_{2,2} & a_{2,3} & 0 & 0 \\ a_{3,1} & a_{3,2} & a_{3,3} & a_{3,4} & 0 \\ 0 & 1 & 0 & 0 & 0 \\ a_{5,1} & 0 & a_{5,3} & a_{5,4} & 0 \end{bmatrix} \quad (C.17)$$

$$a_{1,1} = Y_v/m \quad (C.18)$$

$$a_{1,2} = Y_p/m + W_{trim} \quad (C.19)$$

$$a_{1,3} = Y_r/m - U_{trim} \quad (C.20)$$

$$a_{1,4} = g\cos(\theta_{trim}) \quad (C.21)$$

$$a_{2,1} = L_v/I_{xx} + N_v/I_{xz} \quad (C.22)$$

$$a_{2,2} = L_p/I_{xx} + N_p/I_{xz} \quad (C.23)$$

$$a_{2,3} = N_r/I_{xz} + L_v r/I_{xz} \quad (C.24)$$

$$a_{3,1} = L_v/I_{xz} + N_v/I_{xx} \quad (C.25)$$

$$a_{3,2} = L_p/I_{xz} + N_p/I_{zz} \quad (C.26)$$

$$a_{3,3} = N_r/I_{zz} + L_r/I_{xz} \quad (C.27)$$

$$a_{4,3} = \sin(\theta_{trim})/\cos(\theta_{trim}) \quad (C.28)$$

$$a_{4,4} = q_{trim}\sin(\theta_{trim})/\cos(\theta_{trim}) \quad (C.29)$$

$$a_{5,3} = 1/\cos(\theta_{trim}) \quad (C.30)$$

$$a_{5,4} = q_{trim}/\cos(\theta_{trim}) \quad (C.31)$$

$$B_{Lat} = \begin{bmatrix} b_{1,1} & b_{1,2} & b_{1,3} & 0 & 0 \\ 0 & b_{2,2} & b_{2,3} & 0 & 0 \\ 0 & b_{3,2} & b_{3,3} & 0 & 0 \end{bmatrix} \quad (C.32)$$

$$b_{1,1} = Y_{\delta_{Al}}/m \quad (C.33)$$

$$b_{1,2} = L_{\delta_{Al}}/I_{xx} + N_{\delta_{Al}}/I_{xz} \quad (C.34)$$

$$b_{1,3} = L_{\delta_{Al}}/I_{xz} + N_{\delta_{Al}}/I_{zz} \quad (C.35)$$

$$b_{2,2} = (\rho R_t^2(\pi R_t^2))(C_{T_{tilt}} r_{ty}/I_{xz} - C_{Qt}/I_{xx} p) \quad (C.36)$$

$$b_{2,3} = (\rho R_t^2(\pi R_t^2))(C_{Q_{tilt}}/I_{xz} - C_{T_{tilt}} * r_{ty}/I_{xx}) \quad (C.37)$$

$$b_{3,2} = (\rho R_t^2(\pi R_t^2))(-C_{T_{tilt}} r_{ty}/I_{xz} + C_{Q_{tilt}}/I_{xx}) \quad (C.38)$$

$$b_{3,3} = (\rho R_t^2(\pi R_t^2))(-C_{Q_{tilt}}/I_{xz} + C_{T_{tilt}} r_{ty}/I_{zz}) \quad (C.39)$$

Bibliography

- [1] NASA. «Technology Roadmaps». In: *Robotics and Autonomous Systems, TA 4*. 2015 (cit. on pp. 1, 3–5, 11, 12).
- [2] A. Abdelkefi M. Hassanalian D. Rice. «Evolution of Space Drones for Planetary Exploration-A Review». In: (2018) (cit. on pp. 1–5, 9, 10, 13).
- [3] N. Collins. «System Design and Nonlinear State-Dependent Riccati Equation Control of an Autonomous Y-4 Tilt - Rotor Aerobot for Martian Exploration». In: (2016) (cit. on pp. 1–3, 5, 6, 12, 15, 17, 19, 20, 22, 29–35, 38, 40, 44, 63, 68, 69, 74, 76, 78, 86, 92, 95).
- [4] Håvard F Grip, Daniel P Scharf, Carlos Malpica, Wayne Johnson, Milan Mandic, Gurkirpal Singh, and Larry A Young. «Guidance and control for a Mars helicopter». In: *2018 AIAA Guidance, Navigation, and Control Conference*. 2018, p. 1849 (cit. on pp. 1, 13, 14, 53, 70).
- [5] L. A. Young. «Vertical Lift – Not Just For Terrestrial Flight». In: (2000) (cit. on pp. 2, 4, 5, 11–13, 15, 16).
- [6] L. A. Young. «Design Opportunities and Challenges in the Development of Vertical Lift Planetary Aerial Vehicles». In: (2000) (cit. on pp. 2–5, 11–13, 15, 30).
- [7] M. Drela. «XROTOR». In: (2011) (cit. on pp. 2, 3, 40, 43).
- [8] P. Carter. «CROTOR - XROTOR on steroids». In: (2015) (cit. on pp. 2, 3, 40, 44).
- [9] E. Branlard. «Wind Turbine Aerodynamics and Vorticity-Based Methods». In: (2017) (cit. on pp. 2, 40).
- [10] Robert C. Nelson. «Flight Stability and Automatic Control». In: (1998) (cit. on pp. 2, 81).
- [11] G. Hautaluoma. «NASA Announces Landing Site for Mars 2020 Rover». In: (2018) (cit. on pp. 2, 3, 19).
- [12] Aymeric Spiga. «Mars Climate Database - The Web Interface». In: (2018) (cit. on pp. 2, 3, 32, 78).

- [13] E. Kolawa J. A. Cutts J. L. Hall. «Exploration of Mars, Venus and Titan with Planetary Aerobots - A Pathway to Flight Readiness». In: *Fifth International Planetary Probe Workshop, Bordeaux, France*. 2007 (cit. on pp. 3, 4, 9).
- [14] N. Hall. «Mars Atmosphere Model - Imperial Unit». In: (2015) (cit. on pp. 3, 32).
- [15] National Academy of Sciences. «Vision and Voyages for Planetary Science in the Decade 2013-2022». In: (2015) (cit. on pp. 4, 5).
- [16] NASA. «Mars Helicopter/Ingenuity - NASA Facts». In: (2020) (cit. on p. 4).
- [17] T. Bourlai P. Karampelas. «Surveillance in Action - Technologies for Civilian, Military and Cyber Surveillance». In: (2017) (cit. on p. 4).
- [18] J. L. Hall. «Aerial Platform Options For Venus». In: (2018) (cit. on p. 4).
- [19] Elfes. «Autonomous Flight Control for a Planetary Exploration Aerobot». In: (2005) (cit. on p. 4).
- [20] L.A. Young. «Conceptual Design Aspects of Three General Sub-Classes of Multi-Rotor Configurations: Distributed, Modular, and Heterogeneous». In: (2015) (cit. on p. 5).
- [21] D. R. Williams. «Planetary Fact Sheet». In: (2019) (cit. on pp. 5, 13).
- [22] Ralph D. Lorenz et Al. «Dragonfly: A Rotorcraft Lander Concept for Scientific Exploration at Titan». In: 34 (2018) (cit. on pp. 5–8).
- [23] Joseph F. Gasbarre H. S. Wright and Dr. Joel S. Levine. «A Comparison of Platforms for the Aerial Exploration of Titan». In: (2005) (cit. on p. 5).
- [24] M. Pauken et all. «An Overview of Aerial Approaches to Exploring Scientific Regions at Titan». In: (2017) (cit. on pp. 5–7, 12).
- [25] L. Matthies. «Flight Power Modeling of VTOL Aircraft for Exploration of Titan». In: (2019) (cit. on p. 7).
- [26] K. Northon. «Mars Helicopter to Fly on NASA’s Next Red Planet Rover Mission». In: (2020) (cit. on p. 7).
- [27] H. L. Justh. «Neptune and Titan Global Reference Atmospheric Models». In: (2017) (cit. on p. 8).
- [28] M. P. Nagaraja. «Four Science Goals for Mars Exploration». In: (2020) (cit. on p. 11).
- [29] J. B. Balarm et al. «Mars Helicopter Technology Demonstrator». In: *AIAA, SciTech Forum*. 2018 (cit. on pp. 12–14).
- [30] U. Craigh H. Song. «A Mars VTOL Aerobot - Preliminary Design, Dynamics and Control». In: (2007) (cit. on p. 12).

- [31] H. Song. «A Hybrid Martian VTOL UAV: Design; Dynamics and Control». In: (2008) (cit. on pp. 12, 29).
- [32] R. T. Clancy et al. *The Atmosphere and Climate of Mars*. Cambridge University Press: Cambridge Planetary Science, 2017 (cit. on pp. 30, 74–76).
- [33] National Aeronautics and Space Administration. *Mars Global Surveyor Arrival*. Press Kit, 1997 (cit. on pp. 32, 75).
- [34] L.D. Reid B. Etkin. *Dynamic of Flight, Stability and Control*. John Wiley & Son, 1996 (cit. on p. 53).
- [35] C. Hirt. «W.E. Kilometer-resolution gravity field of Mars». In: (2012) (cit. on p. 76).
- [36] S. Adnan et al. «A Review on the Platform Design, Dynamic Modeling and Control of Hybrid UAVs». In: (2015) (cit. on pp. 81, 82).
- [37] T. Ostermann et al. «Control Concept of a tilt-wing UAV during low speed manoeuvring». In: (2012) (cit. on p. 82).
- [38] R. M. Murray. «Linear Quadratic Regulators». In: (2006) (cit. on pp. 83, 86).
- [39] R. M. Murray. «Control and Dynamical Systems, Lecture 2 – LQR Control». In: (2006) (cit. on p. 83).

Acknowledgements

ACKNOWLEDGMENTS

To my family

First I would like to thank my Advisor, Prof. Fabrizio Dabbene, and my Co-Advisors, Drs. Elisa Capello and Drs. Martina Mammarella, who guided me into UAVs world. They have been an inestimable source of notions and inspiration and this work would have not be possible without their support. Moreover, I would like to thank my family who with great sacrifices has allowed me to study and achieve this goal.